Report Prepared by:

Margareth Dugarte
Alberto A. Sagüés

GALVANIC POINT ANODES FOR EXTENDING THE SERVICE LIFE OF PATCHED AREAS UPON REINFORCED CONCRETE BRIDGE MEMBERS

Contract No. BD544-09
Final Report to Florida Department of Transportation

A. A. Sagüés
Principal Investigator
Department of Civil and Environmental Engineering

UNIVERSITY OF SOUTH FLORIDA
Tampa, FL 33620
September 30, 2009

Technical Report Documentation Page

1. Report No.
BD544 - 09

2. Government Accession No.

3. Recipient's Catalog No.

4. Title and Subtitle
GALVANIC POINT ANODES FOR EXTENDING THE SERVICE LIFE OF PATCHED AREAS UPON REINFORCED CONCRETE BRIDGE MEMBERS

5. Report Date
September 30, 2009

6. Performing Organization Code

7. Author(s)
M. Dugarte and A. A. Sagüés

8. Performing Organization Report No.

9. Performing Organization Name and Address
Department of Civil and Environmental Engineering
University of South Florida (USF)
Tampa, FL 33620

10. Work Unit No. (TRAIS)

11. Contract or Grant No.
BD544 - 09

12. Sponsoring Agency Name and Address
Florida Department of Transportation
605 Suwannee St. MS 30
Tallahassee, Florida 32399
(850)414-4615

Office of Infrastructure
Research and Development
Federal Highway Administration
6300 Georgetown Pike
McLean, VA 22012

13. Type of Report and Period Covered
Final Report 11/05/2003 - 9/30/2009

14. Sponsoring Agency Code

15. Supplementary Notes
Prepared in cooperation with the USDOT FHWA

16. Abstract

The polarization performance of two types of commercial galvanic point anodes for protection of rebar around patch repairs was evaluated. Experiments included measurement of the polarization history of the anode under galvanostatic load, in reinforced concrete slabs, and in field installations. The tests revealed, for both types of anodes, a potential-current function (PCF) indicating relatively little anodic polarization from an open circuit potential at low current levels, followed by an abrupt increase in potential as the current approached an apparent terminal value. Aging of the anodes was manifested by a continually decreasing current output in the concrete tests, and by increasingly more positive potentials in the galvanostatic tests. Those changes reflected an evolution of the PCF generally toward more positive open circuit potentials and, more importantly, to the onset of elevated polarized potentials at increasingly lower current levels. There was considerable variability among the performance of replicate units of a given anode type. Modest to poor steel polarization levels were achieved when coupled with point anodes both in laboratory and field tests. Modeling of a generic patch configuration was implemented with a one-dimensional approximation. The model calculated the throwing distance that could be achieved by a given number of anodes per unit perimeter of the patch, concrete thickness, concrete resistivity, amount of steel and amount of polarization needed for cathodic prevention. The model projections and aging information suggest that anode performance in likely application scenarios may seriously degrade after only a few years of operation, even if a relatively optimistic 100 mV corrosion prevention criterion were assumed. Less conservative criteria have been proposed in the literature but are yet to be substantiated. Other investigations suggest a significantly more conservative corrosion prevention may apply instead. The latter case would question the ability of the point anodes to provide adequate corrosion prevention.

17. Key Words
anodes, zinc, cathodic protection, concrete, corrosion, reinforcing steel

18. Distribution Statement
No Restriction
This report is available to the public through the NTIS, Springfield, VA 22161

19. Security Classif. (of this report)
Unclassified

20. Security Classif. (of this page)
Unclassified

21. No. of Pages
120

22. Price

DISCLAIMER

SI* (MODERN METRIC) CONVERSION FACTORS

APPROXIMATE CONVERSIONS TO SI UNITS

Symbol	When You Know	Multiply By	To Find	Symbol
		LENGTH		
in	inches	25.4	millimeters	mm
ft	feet	0.305	meters	m
yd	yards	0.914	meters	m
mi	miles	1.61	kilometers	km
		AREA		
in^2	square inches	645.2	square millimeters	mm^2
ft^2	square feet	0.093	square meters	m^2
yd^2	square yard	0.836	square meters	m^2
ac	acres	0.405	hectares	ha
mi^2	square miles	2.59	square kilometers	km^2
		VOLUME		
fl oz	fluid ounces	29.57	milliliters	mL
gal	gallons	3.785	liters	L
ft^3	cubic feet	0.028	cubic meters	m^3
yd^3	cubic yards	0.765	cubic meters	m^3
		NOTE: volumes greater than 1000 L shall be shown in m^3		
		MASS		
oz	ounces	28.35	grams	g
lb	pounds	0.454	kilograms	kg
T	short tons (2000 lb)	0.907	megagrams (or "metric ton")	Mg (or "t")
		TEMPERATURE (exact degrees)		
°F	Fahrenheit	5 (F-32)/9 or (F-32)/1.8	Celsius	°C
		ILLUMINATION		
fc	foot-candles	10.76	lux	lx
fl	foot-Lamberts	3.426	candela/m^2	cd/m^2
		FORCE and PRESSURE or STRESS		
lbf	poundforce	4.45	newtons	N
lbf/in^2	poundforce per square inch	6.89	kilopascals	kPa

APPROXIMATE CONVERSIONS FROM SI UNITS

Symbol	When You Know	Multiply By	To Find	Symbol
		LENGTH		
mm	millimeters	0.039	inches	in
m	meters	3.28	feet	ft
m	meters	1.09	yards	yd
km	kilometers	0.621	miles	mi
		AREA		
mm^2	square millimeters	0.0016	square inches	in^2
m^2	square meters	10.764	square feet	ft^2
m^2	square meters	1.195	square yards	yd^2
ha	hectares	2.47	acres	ac
km^2	square kilometers	0.386	square miles	mi^2
		VOLUME		
mL	milliliters	0.034	fluid ounces	fl oz
L	liters	0.264	gallons	gal
m^3	cubic meters	35.314	cubic feet	ft^3
m^3	cubic meters	1.307	cubic yards	yd^3
		MASS		
g	grams	0.035	ounces	oz
kg	kilograms	2.202	pounds	lb
Mg (or "t")	megagrams (or "metric ton")	1.103	short tons (2000 lb)	T
		TEMPERATURE (exact degrees)		
°C	Celsius	1.8C+32	Fahrenheit	°F
		ILLUMINATION		
lx	lux	0.0929	foot-candles	fc
cd/m^2	candela/m^2	0.2919	foot-Lamberts	fl
		FORCE and PRESSURE or STRESS		
N	newtons	0.225	poundforce	lbf
kPa	kilopascals	0.145	poundforce per square inch	lbf/in^2

*SI is the symbol for the International System of Units. Appropriate rounding should be made to comply with Section 4 of ASTM E380.

EXECUTIVE SUMMARY

Small galvanic anodes are being produced commercially or are under development to be cast in patch repairs of concrete damaged by corrosion of the reinforcement. A phenomenon that affects the durability of such repairs is the "halo effect" wherein the steel within the new repaired area serves as a cathode generating accelerated corrosion of the steel in the original concrete surrounding the patch repair. The anodes are intended to prevent the initiation of corrosion on the rebar around the patch that was still passive, but in contact with concrete which may have moderate to high chloride content. These anodes usually consist of a zinc alloy piece with connecting wires that also serve to retain the anode in place and are encapsulated in a mortar pellet. The mortar has admixtures that promote high pH or otherwise activate the zinc. The mortar may contain also humectants to further promote activity of the zinc and accommodate expansive corrosion products.

Embedded anodes of the type described above have been promoted by manufacturers for residential or parking building applications, and more recently there is increasing interest for their use in highway applications. Of special interest in highway service is the mitigation of corrosion in repaired bridge deck spalls, and patches in inland as well as in marine substructure components. The possibility of large scale applications in highway systems brings up several important performance and durability issues needing resolution. In the present investigation two types of anodes under production or development at the start of the project were evaluated to determine their effectiveness. The approach used was to establish the polarization characteristics of the anodes, and the polarization dependence on relevant service variables (e.g. anode type and environment, including mortar type and humidity condition). Anode polarization was described by a Potential-Current Function (PCF) and its evolution with anode service aging.

Laboratory tests were conducted and the performance was also evaluated at experimental bridge installations in two FDOT sites. Multiple replicate anodes were tested in each condition.

Galvanostatic anode tests were conducted in concrete in controlled humidity chambers and yard slab tests with anodes in reinforced concrete. The tests revealed, for both types of anodes, a PCF indicating relatively little anodic polarization from an open circuit potential at low current levels, followed by an abrupt increase in potential as the current approached an apparent terminal value. The curves resemble the behavior expected from a system that is approaching a diffusion-controlled limiting current density, or alternatively the presence of a sizable ohmic resistance. For a given test condition and anode service history, the PCFs showed significant variability among anodes of the same type within a given set of anodes delivered by the suppliers. For one of the

anode types, the first set tested performed notably worse as a group than the second set (delivered 3 years later) suggesting an initial manufacturing problem.

Aging of the anodes by delivering current in service was manifested by a continually decreasing current output in the yard slab tests, and by increasingly more positive potentials in the galvanostatic tests. As implied by slow cyclic polarization test results, those changes reflected an evolution of the PCF generally toward more positive open circuit potentials and, more importantly, to the onset of elevated polarized potentials at increasingly lower current levels.

Coupling of the anodes at the time of casting to rebar in concrete containing 1.5% chloride ion by weight of cement was not sufficient to prevent corrosion initiation of the steel rebars in that zone. Testing for about 480 days in yard slabs containing those corroding rebars in addition to passive rebars showed that the point anodes induced only modest to negligible polarization of the steel assembly. That effect was ascribed to the low polarizability of the actively corroding rebars. Upon disconnection of the actively corroding rebars, one of the anode types produced cathodic polarization levels exceeding 100 mV in the passive rebars that were in close proximity to the anode. The other anode type (a set suspected of deficiency) had exhausted much of its polarizing ability in the preceding interval and produced only negligible effects on the surrounding passive steel. A continuation test with a second set of anodes of each type, coupled with only passive rebar, showed substantial polarization levels (100 mV to 200 mV) of the rebar in the proximity of either type of anode. Current delivery decreased with service time but appreciable polarization levels were still achieved in nearby rebars after ~500 days of operation.

Most anode units of both types in the first set tested showed significant current delivery decrease after delivering a cumulative anodic charge that was only about 10% to 20% of the calculated amount for complete consumption based on alloy mass. Anodes in the second set tested showed less aging effects during the duration of the test, which was conducted until reaching up to about 25% of the theoretical limit. Estimates based on the extent of derating observed in the test interval suggest that in the absence of other degradation effects anodes of this type may be able to function up to about ¼ to ⅓ of the theoretical consumption limit. Quantitative polarization functions of the steel rebar were determined and found to agree with the results of previous investigations. Those functions were used as input for modeling projections of anode performance in a generic reinforced concrete system.

Results of field evaluations of anode performance were evaluated and found to be generally in keeping with those from laboratory and yard tests, with instances of increased current delivery consistent with greater moisture and a chloride rich environment. Decreased performance with aging was noted in the field for both makes of anode.

Modeling of a generic patch configuration with a one-dimensional approximation was used to calculate the throwing distance that could be achieved by a given number of anodes per unit perimeter of the patch, concrete thickness, concrete resistivity, amount of steel and amount of polarization needed for cathodic prevention. The model projections together with the aging information determined experimentally suggest that throwing distance in likely application scenarios may seriously degrade within a few years of operation, even if a relatively optimistic 100 mV corrosion prevention criterion were assumed.

Less conservative, current density-based corrosion prevention criteria have been proposed in the literature that would result in improved throwing distance projections under some conditions, but are yet to be substantiated. However, other investigations suggest that a significantly more conservative corrosion prevention criterion than 100 mV polarization may be necessary instead. The latter case would question the ability of the point anodes to provide a useful corrosion prevention effect for reinforcement around the patch.

TABLE OF CONTENTS

ACKNOWLEDGEMENT

The assistance with field inspections of many collaborators at the FDOT State Materials Office and from Concorr Florida, Inc. is greatly acknowledged, as is that of numerous student participants in the University Of South Florida College Of Engineering Research Experience for Undergraduates program. The assistance of Mr. Ivan Lasa of the FDOT State Materials Office in conducting cooperative activities for the field wok is greatly appreciated. Mr. Ezeddin Busba's assistance in evaluation of field data is thankfully acknowledged. The authors gratefully acknowledge the many valuable technical comments and suggestions provided by Dr. Y. Paul Virmani of the Federal Highway Administration.

1 INTRODUCTION

1.1 Project Scope

1.1.1 Origin of the investigation

Chloride-induced corrosion of reinforcing steel in concrete creates expansive corrosion products that crack the concrete cover. Repairs often consist of removing the cracked concrete and replacing it with chloride-free concrete. It takes only a small amount of corrosion metal loss (e.g. ~0.1 mm (0.004 in)) at the reinforcing steel bar (rebar) surface to create corrosion products sufficient to generate internal stresses that crack the concrete [Torres-Acosta 2004]. Thus, repairs often do not involve rebar replacement, as the remaining steel cross section is still adequate. However, patch repairs limited to the portions of the structure showing conspicuous cracking may have detrimental consequences. As is often the case, zones adjacent to the patch have already had substantial chloride contamination. As will be discussed in the following, corrosion can rapidly develop there promoted by the newly placed patch, and small ("point") anodes at the periphery of the new patch are often recommended as a means to alleviate that problem. This investigation evaluated the performance of those anodes.

1.1.2 Corrosion of steel in concrete

Steel in concrete is normally in the passive condition (protected by a nanoscale-thick oxide film) due to the highly alkaline nature of the pore water. However, the film is disrupted by events such as a decrease in the pH of the pore water due to carbonation, or intrusion of chloride ions from the external environment. The latter modality tends to result in earlier distress in bridge applications and will be considered here. Corrosion starts when the chloride concentration at the rebar surface exceeds a critical value known as the chloride corrosion threshold (C_T). Much of the information available on the value of C_T concerns atmospherically exposed concrete. In that case the potential E between an isolated plain rebar steel segment and the immediately surrounding concrete tends to be, when passive, in the range -100 to -200 mV in the Copper/Copper Sulfate Electrode (CSE). In those conditions C_T is typically >~0.4% of the mass of cement per unit value in the concrete [Li 2001]. The value of C_T depends on many variables such as the rebar material [Hurley 2006], the pH of the concrete pore water [Li 2001, Gouda 1970, Hausmann 1967] and the presence or voids [Glass 2007]. Of importance to the present work, C_T has been found to depend also on the value of E for the passive steel in a manner that reflects the well known dependence between pitting potential and chloride content in other systems [Szklarska-Smialowska 1986]. The evidence available to date for steel in concrete is limited, but it suggests that if all other factors remain the same, C_T tends to increase manifold when E decreases from ~-150 to ~-600mV CSE.

There is uncertainty as to the precise amount o polarization needed for a given effect [Presuel-Moreno 2005A, Alonso 2000, 2002; Izquierdo 2004, Pedeferri 1996].

The value of E for an isolated rebar segment is determined by the interplay between cathodic electron-consuming reactions (principally reduction of dissolved oxygen in the pore water) and anodic electron-producing reactions (such as the dissolution of iron from the rebar in the corrosion process). In the passive condition the rate of iron dissolution, or passive corrosion rate, is very small [Sagüés 2003] and the resulting mixed potential [Fontana 1986] for the system is in the relatively high value range indicated above. After C_T is exceeded, the rate of the anodic reaction increases dramatically. The resulting mixed potential of steel that is corroding actively in atmospherically exposed chloride-contaminated concrete drops, typically to values E_{ACT} in the ~-300 mV to -600 mV SCE range [Bentur 1997, Broomfield 1997, Li 2001].

1.1.3 Cathodic Protection and Cathodic Prevention

These modes of corrosion control and their differences and associated terminology are briefly reviewed here as they pertain to the scope of this project.

Cathodic protection in concrete is a method for decreasing the corrosion rate of steel that is already in the actively corroding stage. The decrease is achieved by lowering the steel potential to a value below that which existed in the freely corroding condition. The rate of corrosion is that of the net anodic reaction, which decreases strongly as the potential becomes more negative following usual electrochemical kinetic laws [Fontana 1986]. Assuming on first approximation Tafel kinetics and neglecting the effect of the metal deposition reaction, a decrease in potential by an amount equal to one Tafel slope (typically in the order of 0.1V [Jones 1996] would lower the corrosion rate by about 90%. It is then not surprising that practical criteria for achieving cathodic protection, based on operating experience, specify a polarization level of 100 mV below the freely corroding potential as a criterion for effective application of cathodic protection [Funahashi 1991]. In addition to direct action on anodic kinetics, the electric field driving the cathodic polarization current tends over time to respectively decrease and increase the concentrations of chloride and hydroxide ions at the rebar surface. Depending on the electric field strength [Glass 1997], those changes may actually restore passivity on the rebar surface.

Cathodic prevention is based on the entirely different concept from that of cathodic protection. In cathodic prevention the potential of the passive steel is shifted from its natural value in the negative direction *before* the onset of active corrosion, to substantially delay or prevent the initiation of such corrosion. The change to a more negative potential has the effect, noted above, of increasing the value of C_T so that the steel can withstand significantly greater chloride content in the surrounding concrete before sustained passivity breakdown takes place. The mechanism responsible for this effect is not precisely known, but it may involve phenomena observed in other systems such as improved resistance of the passive film to chloride ions [Macdonald 1992], or destabilization of incipient pits [Frankel 1998] as the polarization becomes less anodic. Such processes involve conditions quite different from those present on fully active rebar, so criteria such as the 100 mV shift for cathodic protection do not necessarily apply to cathodic prevention cases. As indicated earlier, there is uncertainty as to the value of the potential at which the passive rebar needs to be held to achieve a given increase in C_T, an issue that will be addressed later in this report. There is agreement however that the current density needed to cathodically shift the potential by a given amount from the freely corroding condition is significantly less for passive than for active rebar [Glass 1997, Pedeferri 1996]. Thus, if the required potential shifts were comparable, cathodic prevention would be comparatively easier to implement than cathodic protection. For example, the lesser driving potential of a galvanic system may suffice in a cathodic prevention application, while an impressed current system may be needed for cathodic protection.

The polarization needed for cathodic protection or prevention may be achieved either with impressed current or galvanic systems [Broomfield 1997]. In either case an anode or system of anodes in contact with the concrete is the physical source of the polarizing current, which travels through the concrete to the rebar assembly. Given a certain polarization criterion value, the effectiveness of both cathodic protection and prevention depends also on how far away from the anode the polarization criterion is satisfied. That reach is called the throwing distance. The throwing distance and its decrease with age are important descriptors of the capability of a protection or prevention system.

1.1.4 Corrosion macrocells and effect of patch repairs

If a rebar segment is not isolated but is instead part of a larger rebar assembly, then because of electrochemical coupling the local value of E at the rebar segment is elevated or decreased if the potential in the surrounding zones is higher or lower respectively than that of the segment if it were isolated. This *macrocell* coupling effect is stronger if the electrical conductivity of the concrete is high (low resistivity) [Sagüés 1990, 2003, Broomfield 1997, Kranc 1994, Kranc 2001, Raupach 1996].

An important consequence of macrocell coupling is that any passive steel surrounding an actively corroding rebar zone may develop E values significantly more negative than if the rebar assembly were discontinuous. As a result, the corroding zone is effectively acting as a galvanic anode providing a degree of cathodic prevention to the surrounding passive steel. Thus, C_T in that surrounding steel is increased and active corrosion would not take place there for some time, even if chloride contamination at the rebar depth were already substantial. Such situation takes place in reinforced concrete structures, such as for example a bridge deck in deicing salt service, where chloride contamination was more or less widely distributed and increased with service time. Eventually active corrosion starts at a location where chloride buildup was fastest. The steel surrounding that zone, while still in the passive condition, may be nevertheless in contact with concrete with high chloride content. Corrosion there could have started soon afterwards without the prevention effect mentioned. Models providing visualizations of this effect have been presented elsewhere [Sagüés 1998, 2009A, 2009B].

The zone experiencing corrosion may be patch-repaired by removing the chloride contaminated concrete there and replacing it with fresh, chloride-free concrete. As a result the previously active steel in the patch becomes passive and corrosion stops there. However, that transition to the passive condition also elevates the potential of the steel in the patch from its former highly negative value to one that can be several hundred mV more positive. Consequently, the cathodic prevention effect on the surrounding zone is lost. The newly lowered value of C_T in the surrounding zone then may be less than the existing local chloride concentration, and active corrosion could promptly start. This detrimental consequence is called a *ring* or *halo* damage around the patch [Broomfield 1997].

1.1.5 Anodes for controlling corrosion around patch repairs

Small galvanic anodes (“point anodes”) are available commercially for casting in patch repairs, for the intended purpose of forestalling the halo damage effect [Bennett 2002, Sergi 2001,Whitmore 2003,Bennett 2006]. The anodes usually consist of a zinc alloy piece with steel connecting wires, and embedded in a mortar disk. Electronic connection to the rebar is necessary for these anodes to work, and it is made by tying the wires to the rebar in the patch. The mortar around the zinc alloy is formulated to obtain high pore water pH, increase water retention, or otherwise promote a regime where the formation of a passive film on the alloy is hindered and the alloy stays in an active condition. The mortar may also be engineered to mitigate the effect of expansive anode corrosion products. The alloy composition itself may also be adjusted to promote activity. In such condition the isolated (open circuit) value of E for Zn alloys is highly negative (e.g. ~-1,000 mV CSE). Macrocell coupling with the rebar in both the patch and the surrounding zone then could allow for appreciable lowering of E and restoration of a cathodic prevention regime to a condition comparable to or greater than that existing before the repair. Proprietary patch concrete mixtures are also marketed to increase the conductivity around the anode and maximize macrocell coupling with the ring zone.

Point anodes as described above were the subject of developmental work and commercial production in Europe during the previous decade [Sergi 2001] followed by introduction in North America by two different companies. Typical production units are illustrated in Fig. 1. Much of the marketing of those units has been aimed at residential or parking building applications, but recently there is increasing consideration for highway applications. Of special interest is the mitigation of corrosion around repaired bridge deck spalls patches in inland as well as marine substructure components.

1.1.6 Open questions

The possibility of large scale applications in highway systems brings up several important performance and durability issues needing resolution. Among those, at the beginning of this investigation there was little documented information on the quantitative relationship between the operating potential of point anodes and the amount of current delivered as function of that potential.

There was also a need to know how the ability of the anode to provide protective current would be degraded with service time and the total amount of protective charge that could be delivered. It was also unknown over how long of a distance away from the repair patch the corrosion prevention effect may be obtained for a given potential-current anode function, anode age, and especially anode placement density so that a means of assessing the number of anodes needed (and hence cost) for a given desired effect could be assessed by the potential user.

1.2 Objectives

Based on the needs indicated in the previous section, the present investigation was conducted with the following main objectives:

1) Determine for selected commercially available point anodes the operating potential/current delivery function, and its dependence on relevant service variables.

2) Establish anode cumulative capacity (total usable charge delivered) and associated ultimate service life capability.

3) Assess the anode ability to achieve cathodic prevention over a usable distance (throwing distance) under realistic service conditions and as a function of the number of anodes needed, so as to establish the means of conducting cost/benefits analyses by potential users.

1.3 Approach

To achieve the project objectives the following three tasks were performed:

Task 1. Laboratory experiments. Two types of anodes were selected for evaluation. A set of experiments (Subtask 1A) assessed the current/potential behavior of the anodes as function of time and surrounding concrete parameters. These tests used constant current application by galvanostatic circuits in controlled humidity chambers. Another set of experiments (Subtask 1B) included tests of combined anode-rebar performance in outdoor exposure test yard slabs.

Task 2. Field installations. Suitable locations in Florida were selected in parallel work by FDOT for implementation of actual bridge repairs fitted with embedded anodes. The performance of these anodes was monitored periodically by FDOT. The results to date were interpreted under this project alongside those of the laboratory experiments.

Task 3. Overall assessment and modeling. The findings of the experimental and modeling effort were interpreted and a predictive model was developed to determine applicability of the anodes for their intended use.

2 INVESTIGATION METHODOLOGY

2.1 Products selected for evaluation

In this research program two types of point anodes, each from a different manufacturer, were evaluated. These products are designated by the code names C and W. The manufacturers provided the anodes used for the laboratory tests directly to the University of South Florida, identifying those anodes as regular production units. Two sets of anodes from each manufacturer were evaluated. The first set was provided in 2004 and the second set in 2007. The anode model name for each manufacturer was the same for both sets.

For C anodes the mortar pellet surrounding the anode proper was circular (Figure 1) and had an external diameter ~63 mm and thickness ~27 mm. The mortar mass was ~100 g. The zinc alloy anode proper met ASTM B 418-95a Type I requirements according to the manufacturer. The pellet was of highly alkaline mortar, reported by the manufacturer to have pH=14 or greater. The product Material Safety Data Sheet for this product model name identifies cement (no type specified) and lithium hydroxide as major constituents. Destructive examination of a unit of the 1st set revealed an internal solid zinc alloy disk (Figure 2a) 44 mm in diameter and 12 mm thick. The zinc alloy mass (after subtracting that estimated for internal steel wires) was 103 g. The steel wires for external connection (~1.5 mm diameter) were embedded in the zinc alloy medallion and extending outwards. Examination of a unit of the 2nd set revealed a ribbed zinc alloy disk (Figure 2a) 43 mm in diameter, 19 mm maximum thickness and 115 g alloy mass, with external connection wires as those in the 1st set.

For W anodes the mortar pellet surrounding the anode proper was roughly rectangular (Figure 1), 77 by 60 mm on the sides and 33 mm thick. The mortar mass was ~ 170 g. The zinc alloy met ASTM B418-01 requirements according to the manufacturer. The pellet was of mortar reported by the manufacturer to contain humectants and proprietary zinc activators. The product Material Safety Data Sheet for this product model name identifies Portland cement and lithium bromide among major constituents, and calcium salt (a synonym for calcium hypochlorite but no clarification given), calcium nitrate and lithium nitrate among minor constituents. Destructive examination of one unit from the 1st set revealed an internal zinc alloy element consisting of four piled rectangular expanded metal mesh squares, 34 mm on the side, with a combined height of 18 mm. A plastic sponge separated the squares into two pairs (Figure 2b). The total zinc alloy mass was 48 g. Two steel wires (~1.5 mm diameter) for external connection were wrapped tightly against the expanded metal squares. Examination of three units from the 2nd set (Figure 2b) revealed in all cases an internal zinc alloy element consisting of three piled rectangular expanded mesh squares, 34 mm on the side, with a combined height of 14 mm. There was no plastic sponge separating the squares. The total zinc alloy mass averaged over the 3 units was 40 g. Two steel wires (~1.5 mm diameter) for external connection were wrapped tightly against the expanded metal squares.

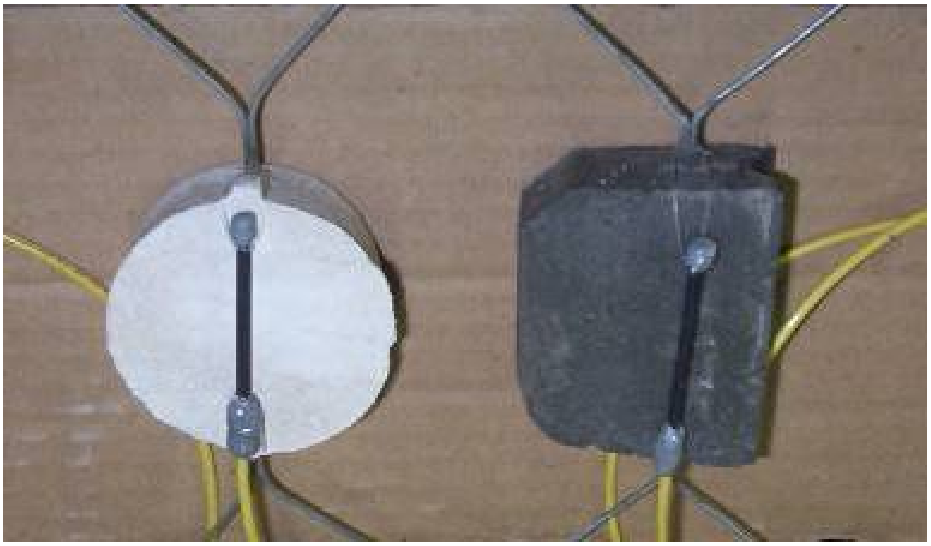

Figure 1 - External appearance of the anode types evaluated (C on left, W on right) with dual steel wires for connection to rebar emerging at top and bottom. See text for pellet dimensions. (The activated titanium rod electrodes with yellow connecting wires were placed to prepare these specimens for Subtask 1A tests).

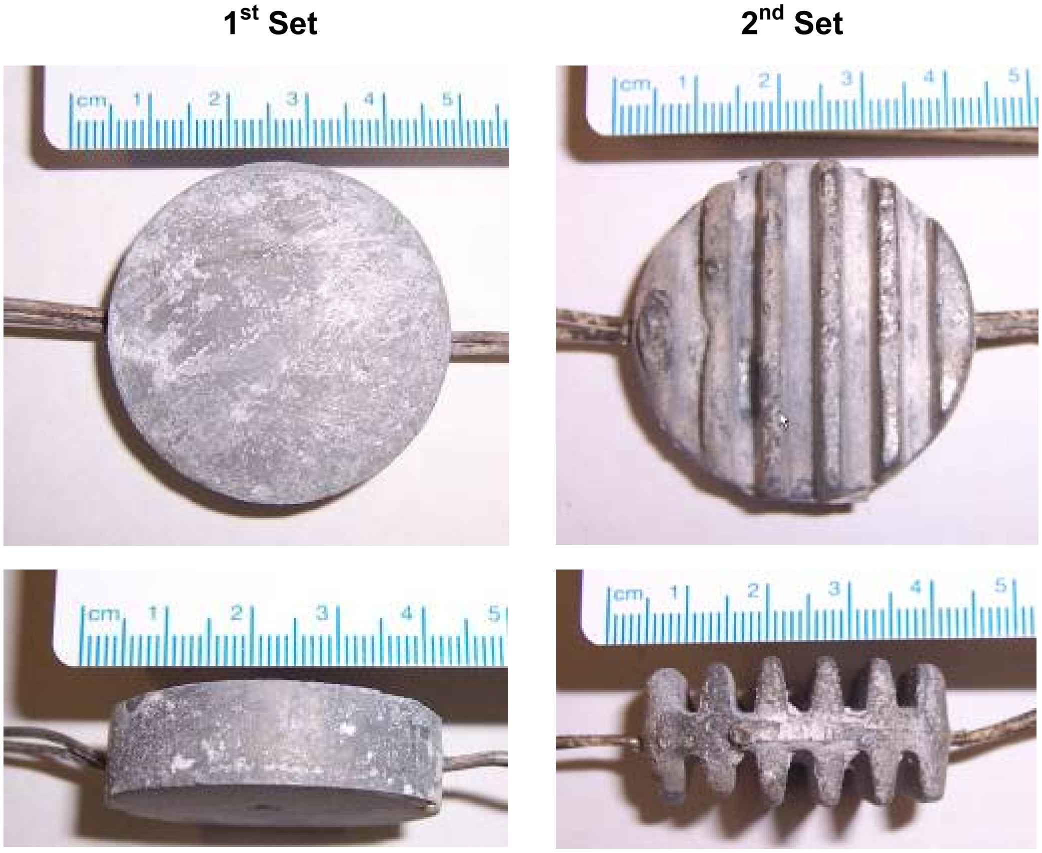

1^{st} Set **2^{nd} Set**

Figure 2a - Type C anode specimens. Zinc alloy anode appearance after embedded mortar was stripped; otherwise as-received. Left, 1st set; Right, 2nd set.

1st Set

2nd Set

Figure 2b - Type W anode specimens. Zinc alloy anode appearance after embedded mortar was stripped. Top group of pictures, 1st set. Bottom group, 2nd set (mortar only partially stripped).

2.2 General Aspects of the Anode Evaluation Approach

The investigation aims in large part to characterize anode performance by determining the potential/current delivery function (PCF) of the anode, and its dependence on relevant service variables (e.g. moisture content and alkaline content of surrounding concrete) and on service time. Implicit in this approach is determining the ability of the anode metal to remain in the active condition over long periods of time, as well as the cumulative capacity of the anode (total usable charge delivered) and associated ultimate service life capability.

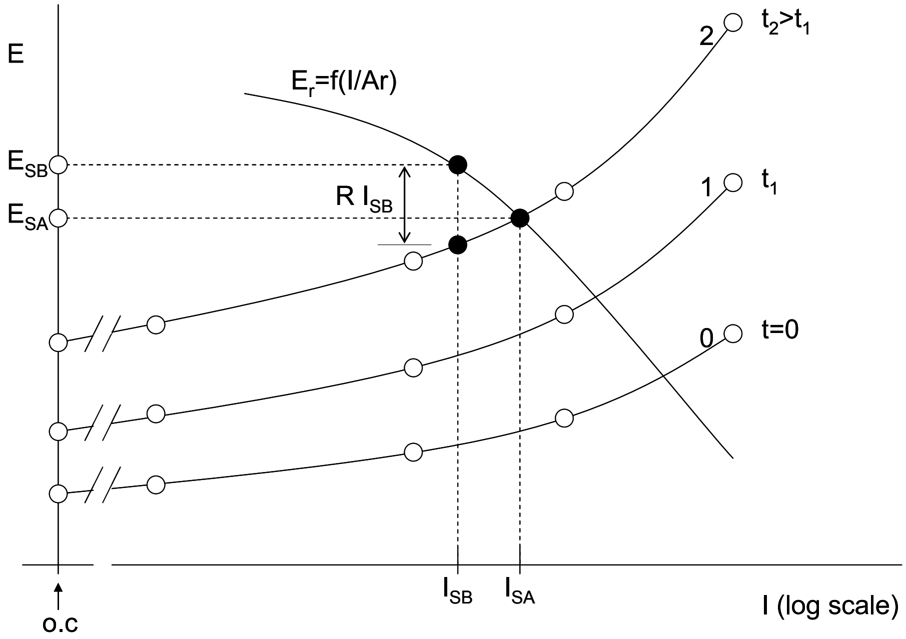

Figure 3 - Idealized potential-current diagram of the evaluation approach.

Figure 3 shows the concepts involved and their application [Sagüés 2005]. Consider an anode being evaluated when initially placed in service. The anode is expected to develop under open circuit (OC) condition, a potential in the order of -1V CSE. If connected with a passive rebar assembly, the anode delivers current and polarization causes the anode potential (as measured against a reference electrode placed in close proximity to the anode) to become less negative than in the OC condition. The polarization increases with larger current demand, as described by Curve 0 which is effectively the PCF of the anode at the beginning of its service life. Curve 0 would also result from joining the locus of separate points corresponding to a number of similar newly placed anodes acting independently at different current demands. If current delivery of each anode were kept constant for a long time, the anode performance is expected to degrade somewhat from causes such as zinc consumption (with consequent decrease in effective surface area) and accumulation of corrosion products that may impede the passage of ionic current or even promote passivation of the anode surface. The manifestation of such degradation would be a shift to more positive values in the anode potential, likely to a greater extent at longer services times and higher currents, as illustrated by PCF Curves 1 (time = t_1) and 2 (time = $t_2 > t_1$) . Those curves can be obtained experimentally by operating the anodes while connected to an external galvanostatic control circuit. Both the ability of the anode to remain active and the cumulative capacity of the anode can then be characterized from the curves at each current regime.

A diagram thus obtained (family of PCF curves as function of time) for a given anode type and environment, including mortar type and humidity condition, can serve as a standardized descriptor of the anode performance for those conditions. If a galvanic control circuit is used, this procedure eliminates the variability that appears when evaluating anodes, as it is often done [Sergi 2001], by coupling to a passive rebar assembly embedded in the same mortar or concrete. The variability in such cases stems from the current demand by the rebar assembly, which may sometimes be sustained at high levels for long periods of time, or drop rapidly early in the life of the test depending on the initial condition of the steel surface or small variations in the pore water composition or concrete moisture.

Subtask 1A addressed tests conducted using the above principles, where anode specimens were evaluated under various galvanostatic regimes in controlled humidity chambers.

Subtask 1B involved outdoor yard exposure of reinforced concrete specimens in which the combined action of the anode and the rebar was allowed to proceed. These tests were intended to supplement the information provided by the galvanostatic experiments by examining an anode aging trajectory closer to that expected in actual applications, and to have an opportunity to reveal possible effects of diurnal and seasonal variations in temperature and humidity that would have not been experienced in the laboratory tests. In addition, the reinforced concrete tests would serve to provide information on steel polarization data, and to offer a means to validate modeling predictions such as those described in the next paragraph. The outdoor tests served also to compare the behavior of the first and second sets of anodes from each manufacturer. For these tests and for the reasons indicated earlier, additional test strategies were needed to separate the information that pertains solely to the anode performance. One of those strategies was to insert resistors of various sizes between the anode and the rebar assembly in a test system and monitor the resulting potential/current trajectory of the anode, thus yielding an alternative way of obtaining a PCF diagram at various stages of anode aging.

The curves in a PCF diagram may be used to obtain a bounding indication of how much protective action may be expected from a rebar assembly for which there is information on its polarization characteristics. As an illustration, the polarization information can take the form of the long term potential-cathodic current density polarization curve E_r=f(i) for the reinforcing steel, determined by prior measurements. Thus if the anode placement density is such that each anode is to protect an area A_r of rebar surface area, the curve E_r=f(I/A_r) describing the polarization characteristics of that area [Sagüés 2003] can be superimposed directly on the PCF diagram to determine how much rebar polarization may be achieved at different aging conditions (Figure 3). If the resistivity of the concrete path between anode and rebar is very small, the rebar receives a current I_{SA} and is polarized down to potential E_{SA}, which may then be compared with the minimum requirements for corrosion prevention in the specific application considered. E_{SA} is the best polarization level to be expected; if concrete resistivity is finite so an effective circuit resistance R applies, the current is less (I_{SB}) and the rebar polarization is only down to E_{SB}. The amount of polarization is proportionally less if the area to be polarized is greater, as the effect is the same as moving the rebar polarization curve to the right. This type of analysis, to project the extent of useful anode action based on the results of the test, can be extended to more complex system geometries by appropriate current distribution modeling [Presuel-Moreno 2005B, Sagüés 2003]. Those concepts have been applied in more detail in Task 3 of the present investigation, dealing with performance modeling.

2.3 Subtask 1A, Galvanostatic Potential-Current Function Tests

These tests involved the two anodes types to be evaluated (1st set only), in two different embedding media, two relative humidity (RH) regimes, four galvanostatic regimes, and were conducted in triplicate for each condition for a total of 96 specimens. These specimens were exposed for approximately 4 years.

The basic test specimen arrangement (Figure 4) consisted of a prism 20 cm x 20 cm x 10 cm) with a test anode placed near the center. An embedded activated titanium rod (ATR) reference electrode [Castro 1996] (periodically calibrated against a Copper Sulfate Electrode (CSE)) was placed against one of the external mortar faces of the anode. Alternatively, an externally placed CSE is used with appropriate compensation for electrolyte resistance if potential measurements are done with current on. An activated titanium mesh of the type used for impressed current cathodic protection of steel in concrete was cast underneath one of the main faces of the prism. The specimens were kept in controlled containers at the desired relative humidity. Connecting wires from anode and mesh led to a galvanostatic system capable of handling multiple independent channels. A summary of materials and test conditions is given in

Table 1. A picture of the 95% RH chamber with test specimens is shown in Figure 5.

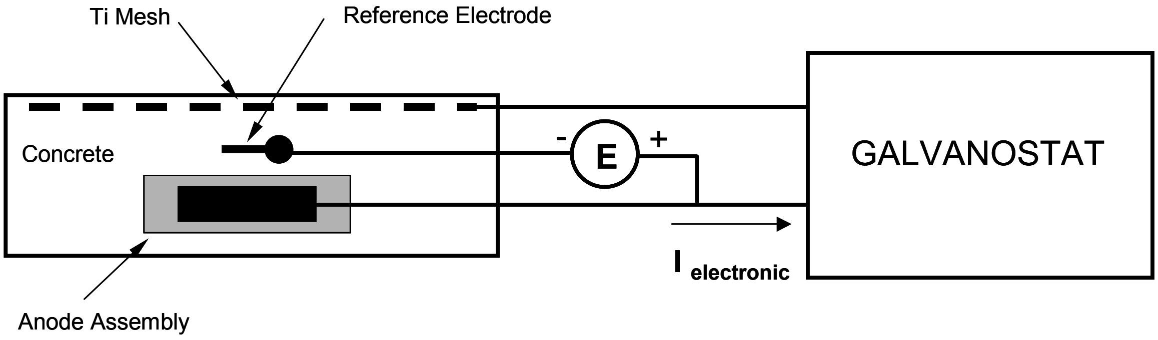

Figure 4 - Anode Test Arrangement (Sketch). Anode was placed centrally in specimen.

The potential E_{IO} of the anodes is reported in the CSE scale in the instant-Off condition (~ 1 sec after current interruption) either measured directly against a CSE electrode placed on the block side, or against the internal activated Titanium rod calibrated against a CSE. Potential is reported as function of time t, with t=0 chosen to correspond to the moment of energizing of the anodes subject to galvanostatic control, which was 48 days after casting for the 95% R.H. tests and 81 days after casting for the 60% tests.

Table 1. Materials and test conditions - Subtask 1 A specimens

Anodes evaluated	C and W.
Embedding media	• A Portland-cement with polymers commercial product marketed for patch repairs(EC). Mixed per manufacturer's instructions, using 2 liter water per 50 lb bag of product plus 15 lb 3/8” Aggregate. • Ordinary Repair Concrete (ORC), 0.41 w/c, 658 lb per cubic yard. Type II cement, 3/8” Aggregate.
Test environments	95% R.H. and 60% R.H. – target values; typically controlled to +-5%
Galvanostatic regime	0, 30, 100 and 300 μA anodic current
Replication	Triplicate
Total test blocks	96

The instant-Off potential, E_{IO}, values of triplicate specimens were averaged. If the power-on potential of any specimen reached ~0V (i.e., clearly incapable of any protective action) at a given test time, testing of that specimen was discontinued and the E_{IO} average value from that time on was computed only for the remaining specimens of that trio.

Figure 5 - The 95% RH test chamber.

2.4 Subtask 1B, Test Yard Slab tests.

2.4.1 Test configuration and preparation

Figure 6 shows the test slab configuration. The steel rebars were regular production No.7 (nominal diameter 7/8 in (22mm)) bars complying to ASTM A-615 Grade 60, with dark gray mill scale on the surface. Each rebar had a nominal 293 cm^2 surface area, resulting in a 0.80 nominal ratio of steel area to concrete footprint area. The yard slabs were built using the same Ordinary Repair Concrete formulation as for the Subtask 1A test blocks, except that the shaded portion near the center contained admixed sodium chloride to obtain 5.9 Kg/m^3 (10 pounds per cubic yard (pcy)) chloride ion. Each slab contained two anodes of the first set provided by the manufacturers, placed as shown. Rebars were numbered from 1 to 12, starting from the left on Figure 6. Both anodes were of either Type C in triplicate slabs numbered 1, 3 and 5 or Type W in triplicate slabs numbered 2,4 and 6. The anode on the slab centerline (Main) was normally always connected to the rest of the rebar assembly. The other anode (Auxiliary) was disconnected except when indicated. After 1045 days of operation of the first set of anodes an additional pair of externally wired duplicate anodes, from the second set provided by the manufacturers, was placed in each slab as shown and keeping the same slab assignment for each type of anode. The second set of anodes was placed by first drilling two partially overlapping 2-in (5 cm) diameter core holes in the space indicated, inserting the anode in the opening and filling it with a proprietary mortar compound for placing point anodes as a retrofit in hardened concrete, applied per manufacturer's instructions. The connection to the previous Main anode was then switched to the Main anode of the second set; all other anodes remained normally disconnected.

Externally wired switches permitted performing instant-Off potential measurements and measurements of current delivery to individual rebars. All rebars and the main anode were normally interconnected. ATR electrodes were placed 12 mm away from the surface of each of the rebars. Figure 7 shows an installed slab.

The slabs were cured in the molds for one week and then demolded and placed horizontally, elevated 1 ft above ground, in the outdoor test yard at USF. The demolding date was designated as the start of the exposure period (t=0). While curing, the main anode was kept provisionally wired to the four rebars in the Cl^- rich zone. Since placement in the yard and until connections boxes were in place, the entire rebar assembly and the main anode were kept interconnected with provisional wiring. Due to casting difficulties the concrete in the chloride-rich zone was at places poorly consolidated and exhibited some honeycombing. After placement in the yard the affected slabs were fitted with partial forms and a cement-water grout was poured as needed to fill in the voids in the honeycombed spots.

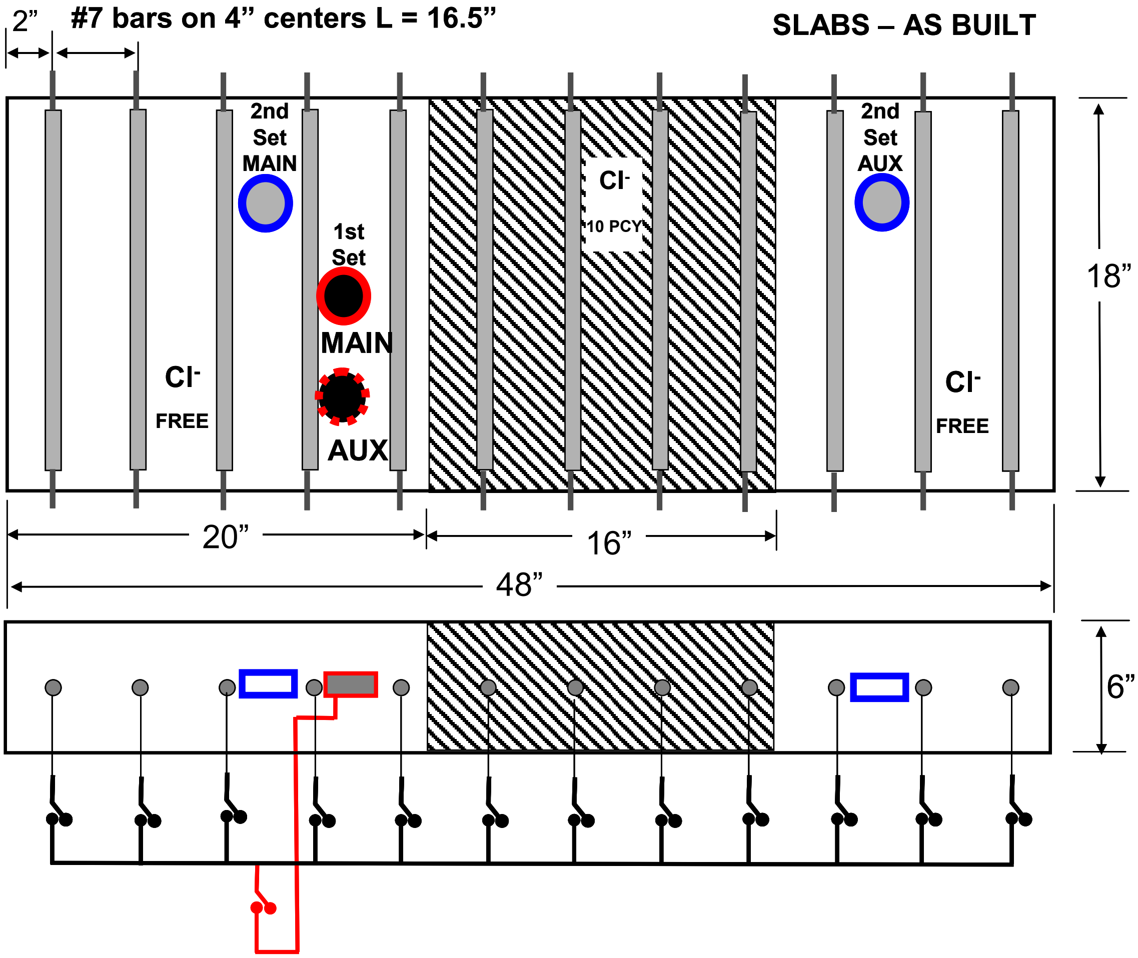

Figure 6 - Yard slab test configuration showing 1st and 2nd set anode positions. Dimensions in inches. Rebars are numbered starting with No. 1 at left.

Figure 7 - Installed yard slab with connection box.

2.4.2 Measurements

Measurements conducted typically on a weekly schedule included (a) anode and individual rebar currents; (b) potential of the anode-rebar assembly with anode energized (" Current-On" potential) with respect to a CSE placed on the concrete on top of each individual rebar as well as over the anode position, and also with respect to each of the embedded ATR electrodes; and (c) potential measured 1 s after disconnection ("Instant-Off potential) and immediate reconnection afterwards of each individual rebar as well as the anode, using both the CSE and the ATR electrodes. Air temperature (and internal concrete temperature after the second set of anodes was installed) was measured each time those tests were performed.

The following measurements and calibration tests were conducted typically on a monthly or less frequent schedule.

Concrete resistivity: A Nilsson Model 400 Soil resistivity meter (square wave alternating current (*ac*), 97 Hz). In this meter current is applied with current terminals designated C1 and C2, and potential is measured between terminals P1 and P2. The meter was employed with a 4-point configuration that determined the concrete resistivity as function of distance along the main axis of the slab. All slab switches were temporarily placed in the open position. The rebars at each end of the assembly (No. 1 and 12) were connected to the meter terminals C1 and C2 respectively. The potential connections were made consecutively to pairs of rebars starting with meter terminal P1 to rebar No.1 and terminal P2 to rebar No.2, then P1 to rebar No. 2 and P2 to rebar No.2 and so on. The resulting resistance for each of the other measurements was multiplied by a cell factor (68.6 cm, equal to the cross sectional area of the slab divided by the center-to-center rebar distance) to obtain the concrete resistivity for the concrete between each the pair of rebars. The raw measurement for the rebar pairs 1-2 and 11-12 were divided by a correction factor of 1.2 to account for uneven current distribution at the injection current rebars[A]. The *ac* current path was uneven due to the presence of the main and auxiliary anodes between rebars No.4 and 5 for the 1st set of anodes, and in addition between rebars No. 2 and 3 and 10 and 11 for the second set. Thus, the resistivity of the chloride-free concrete is reported as the average of that obtained for rebar pairs 1-2 (corrected), 2-3, 3-4, 10-11 and 11-12 (corrected). After the introduction of the 2nd set of anodes, the values for pair 3-4 and 10-11 were not used for that calculation. The resistivity for the concrete in the chloride-containing concrete is reported as the average for rebar pairs 5-6, 7-8 and 8-9.

[A] The cell factor was obtained as the average, for all slabs and for all test times up to the introduction of the 2nd set of anodes, of the raw resistivity value for rebar pair 1-2 divided by that for pair 2-3, and similarly for pairs 11-2 and 10-11.

Anode to rebar resistance: These measurements were conducted at irregular intervals. The anode was temporarily disconnected from the rebar assembly to which it was normally connected. The soil resistivity meter was then used as a 2-point resistance measuring device, with one terminal connected to the anode and the other to the rebar assembly to which the anode was normally connected.

Steel depolarization: This test started with an instant-Off potential determination, after which the anode was left disconnected and remained so while the potentials of the anode and individual rebars ("Off potential) were measured 1h, 4h and 24h following disconnection. The anode was reconnected afterwards. The result of the depolarization test was normally reported as the difference between the 4h Off potentials and the Instant-Off potentials at the beginning of the test. Results for the other intervals were archived and discussed when appropriate.

Slow anode cyclic polarization: This test was conducted to obtain an approximation of the anode PCF at various stages of aging. The tests were conducted as slowly as practical to approximate stabilization of the anode at each of the potential/current points determined. Moreover, the tests were conducted first changing conditions in one direction and then again in the return direction. The extent to which any hysteresis effects appeared was an indication of how much the results obtained deviated from long term steady conditions. The test began after a regular set of Instant-Off measurements was conducted and is exemplified by the following sequence. The connection between the anode and the rebar assembly was then opened and restored after introducing a 500 ohm resistor in the current path. After a typically 24 h wait period the current and Instant-Off potential of the anode was determined and the resistor was replaced by another about 2 times greater in value. The procedure was repeated in subsequent days. When a resistor value >=30 kohm was reached, the next daily step was in the open circuit condition so as to document the unpolarized potential of the anode. The subsequent daily steps were conducted with the same series of resistors but in reverse order, until reaching the direct connection condition. The test typically was completed over a period of 1-2 weeks. The Instant-Off potential vs current data with the forward and reverser data were reported as the PCF curve of the anode at the aging condition corresponding to the beginning of the test.

2.4.3 Other corrections and adjustments

This section concerns corrections to measured variables in the yard slab experiments.

Potential measurements conducted with a CSE on aged concrete surfaces are subject to artifacts including junction potentials induced by the gradient in

OH^- concentration due to carbonation or leachout of pore water [Myrdal 1996]. To correct for those effects small (typically 1 cm^2) portions of the upper slab surface of each slab were periodically chipped off or abraded to expose a fresh concrete surface next to each of the positions used for regular measurements. Potential measurements taken with the CSE tip on the fresh surface were compared with measurements performed on an adjacent undisturbed surface. The difference was tallied as function of time and prorated accordingly to build a potential correction (averaged for all slabs) that was globally applied to the raw potential data. Cross-checks against the internal ATR electrodes (not subject to the surface effects) validated that approach. All reported anode potential values in this document have been corrected accordingly.

In addition to the systematic deviations noted above, potential measurements conducted on the concrete surface even in the absence of appreciable temperature variations (discussed below) were subject to scatter from e.g. surface moisture variations and degree of contact with the electrode sensing tip. Rebar potential measurements spanned a narrower range than that of anode potentials, so the obscuring effects of random scatter were considerable when attempting to construct a global steel polarization curve as shown in Section 3.2.2. In contrast, potential measurements of steel against the embedded ATR electrodes were found to be appreciably more stable. Consequently, the potentials reported in this document for constructing the steel polarization function were based on the measurements against the embedded ATR, corrected by calibration performed at selected times against an external CSE. The calibration was conducted by carefully controlling surface conditions and performing repeated measurements to minimize random error in the average of those measurements. As the steel potential measurements were instant-Off values with only the current to a single rebar interrupted at a time, a compensation procedure was developed to account in the calibration for residual ohmic drop between the respective potential measuring points of the CSE and the corresponding ATR.

Temperature of the test yard slabs spanned a wide range, from ~5 to ~35 ^oC. Measured values of galvanic currents, concrete resistivity and potentials showed appreciable day to day and seasonal fluctuations that correlated well with variations in temperature. Those fluctuations obscured long term trends due solely to anode aging and other system evolution, and added scatter to determinations of anode PCFs. Consequently, the data were analyzed to extract parameters that could serve to approximately compensate for the temperature variation effects. Following prior approaches documented in the literature [Virmani 1983, Pour-Ghaz 2009] the anode current, I, was assumed to follow an apparent Arrhenius relationship

$$I(T_1) = I(T_2) \exp [- H_A R^{-1} (T_1^{-1}-T_2^{-1})] \qquad \text{(a)}$$

Where T_1 is the temperature for which all measurements are to be reported (chosen to be 298°K, 25°C which was the approximate average temperature of the yard slabs at the time of the day measurements were conducted), T_2 is the temperature at the moment the measurement was performed, H_A is the apparent activation energy and R is the gas constant.

The value of H_A was obtained from the best fit slope of a modified Arrhenius plot of the current-temperature data for each anode type of the 2nd set of anodes. The modification consisted of plotting the value $(\Delta \ln I)/R$ as function of ΔT^{-1}, where the differences are the change in measurement results for each slab of a given type of anode from the previous test date. The slope of the straight line best fitting the combined results for that anode was reported as the average effective activation energy. This approach emphasizes the changes due to temperature variations, which are relatively short-term, and minimizes error in estimating H_A introduced otherwise by the longer-term changes due to system aging and not related to temperature. Values of H_A=53 kJ/mole and 32 kJ/mole were thus obtained for the C and W anodes respectively. Accurate concrete temperature records were kept only during the last half of the evaluation of the 1st set of anodes, when anode current values were generally small which tended to result in larger relative experimental scatter. Trial calculations showed that the resulting uncertainty in H_A determination was considerably greater than that for the 2nd set of anodes. Consequently, it was decided instead to apply globally the H_A values obtained for the 2nd set of anodes to the 1st set as well, recognizing that its correction is only roughly evaluated due to reduced confidence in both temperature and activation energy values.

The temperature compensation described above for the anode current is only a rough approximation that ignores the complex interaction of the combined electrochemical processes at the anode and the rebar assembly, plus the effect of variation of electrolyte resistance with temperature. For example, the correction did not take into account the value of the potential at the time the current was measured. This simplified approach was adopted as it was felt that the uncertainty inherent in the instant-Off anode potential (where a relatively large ohmic potential drop is eliminated but never exactly) did not merit further precision.

A more sophisticated approach was used for temperature correction of the (mostly) cathodic current on the rebar, for which the instant-Off potential can be determined more accurately. Following a simplified absolute reaction rate kinetics approach (see for example Kaesche 2003 and observations by Tanaka (1964)), the cathodic rebar current density was corrected for temperature taking into account the potential E as well by:

$$I(T_1, E) = I(T_2,E) \exp [- (H'_A+P E) R^{-1} (T_1^{-1}-T_2^{-1})] \qquad (b)$$

Where H'_A is a nominal corrected activation energy term, and P is a parameter that adjusts for the value of the steel potential when the current measurement was made. The approach neglects also the complicating effect of any anodic reaction that took place on the rebar surface.

The values of H'_A and P were obtained by a best fit procedure to be presented elsewhere [Dugarte 2009] that takes into account the cathodic current density, temperature and potential changes between measurements performed at consecutive test dates. The resulting average values of H'_A and P were 40 kJ/mole and 10.4 kCoul/mole respectively, with no significantly different results from steel in the slabs that contained C or W anodes. Because of the small value of the products PE compared with H'A, the final correction is not much different that what would have been obtained with a simpler relationship such as Eq.(a) with only the nominal activation energy term.

A procedure similar to that used for the anodic current temperature correction was used to obtain the apparent activation energies for the concrete resistivity, with a resulting value of 24 kJ/mole for the concrete in the chloride-free zone. These apparent activation energy values and Eq.(a) were then applied to the entire data set. All anode current and concrete resistivity results reported in the following are temperature-compensated by that procedure.

It is noted that the temperature corrections were intended primarily for data smoothing to assist in revealing trends in other system variables. Further analysis of this issue, including mechanistic interpretation of the apparent activation energies values obtained is left for future continuation work (Dugarte 2009).

2.5 Field Installations

Field tests with both anode types C and W with same manufacturer model designations as those evaluated in the laboratory and the yard slabs were conducted by FDOT in a parallel investigation at two Florida bridge sites. Detailed reports on those sites are archived by FDOT; the text below includes brief excerpts from those reports. Parts of this activity are still in progress with further findings to be reported in the future.

2.5.1 Test Site1

This Site had test anodes installed in substructure components of Bridge Nos. 700028 and 700115 (parallel bridges on S.R. 528 over the Banana River), Brevard County. The anodes were installed in four spall repair areas at the experimental test locations shown in Table 2. At those locations the anodes were connected to the rebars via external wires to allow for circuit interruption and testing. Two other locations where patches were made without any anodes installed served as controls. All reinforcing steel in each test area was electrically continuous and two ground connections were installed in each test area. Additional test stations at this site evaluated other types of anodes but those fall outside the scope of this report.

A proprietary concrete repair material containing polymers was used by Contractor's option as the patch repair material for all test areas. The same material was also used to repair all other spalls in bents 10 and 11 on both bridges.

Potentials were monitored periodically at positions 3, 6 and 12 inches away from the patch perimeter. Anode currents were monitored as well. Depolarization tests (~22 hours duration) were conducted at various intervals. Extended testing took place over a 1200 day period.

It is noted that at this site the anodes were not connected to the rebar assembly until a time ranging from 53 days to 111 days from the day of patching. The anodes for this field site were acquired at about the same time the manufacturers supplied the 1st set of anodes for the laboratory and test yard slabs.

Figures 8 and 9 illustrate the repair locations and anode installations at Site 1.

Table 2. Site 1 test area locations and material installation information.

Bridge	Pier	Component	Location Number	Anode Type (No anode)	Date Anodes Installed	Date Patch Material Placed	Date Anode Energized	Approx. Patch Area m^2 (sq.ft)	Physical Survey 1			Physical Survey 2		
									Age (Days)	C cm (in)	D m^2 (sq.ft.)	Age (Days)	C cm (in)	D m^2 (sq.ft.)
700028	10	Strut (E Face & NE Corner)	10-1	W (7)	10/7/05	10/7/05	11/23/05	1.2 (13)	349	X	X 0.07 (0.73)	587	X	X 0.13 (1.35)
	10	Column (N Face & NW Corner)	10-6	None (Control)	N/A	8/18/05	N/A	0.5 (6)				587	X	
700115	10	Column (W Face & SW Corner)	10-3	C (10)	9/13/05	9/14/05	11/23/05	1.6 (18)	188	X		587	X	
	10	Strut (W Face & Top Corner)	10-4	W (6)	8/24/05	8/24/05	11/23/05	1.1 (12)	148, 188	X 18 (7)		587	X	
	11	Strut (W Face)	11-5	C (10)	8/4/05	8/4/05	11/23/05	1.1 (12)						
	10	Strut (W Face)	10-7	None (Control)	N/A	8/23/05	N/A	0.9 (9)	188	X		587	X	

* Location 2 is not listed as it involves a type of anode not covered in this investigation

C: X indicates crack observed, length given if available.

D: X indicates delamination observed, surface area given when available.

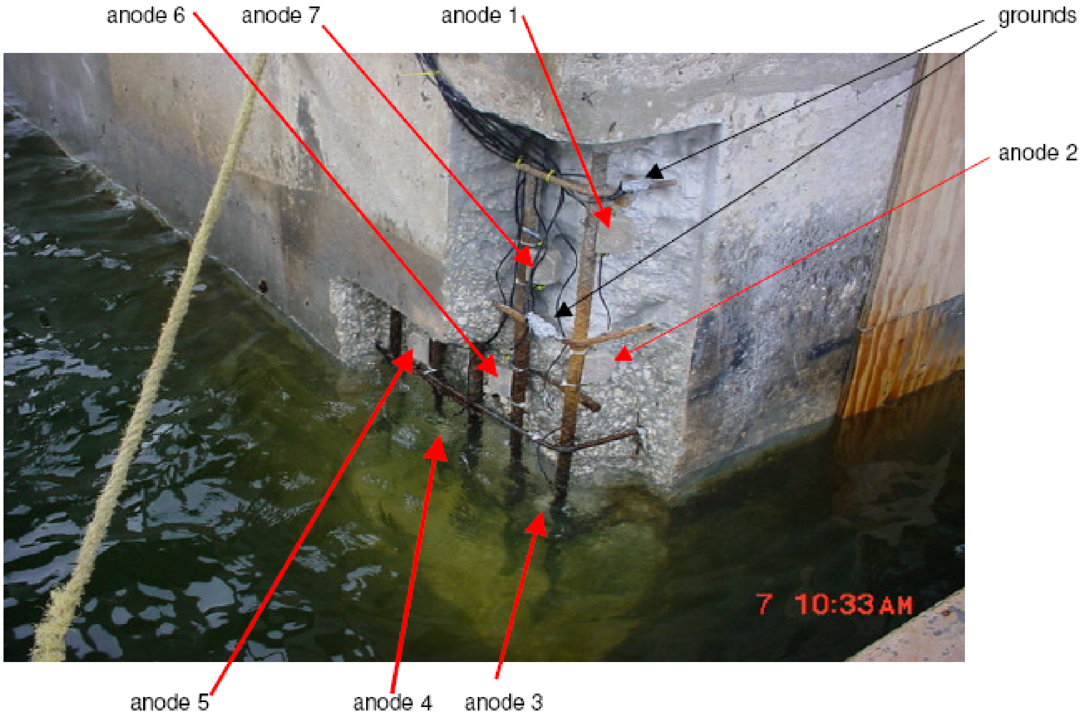

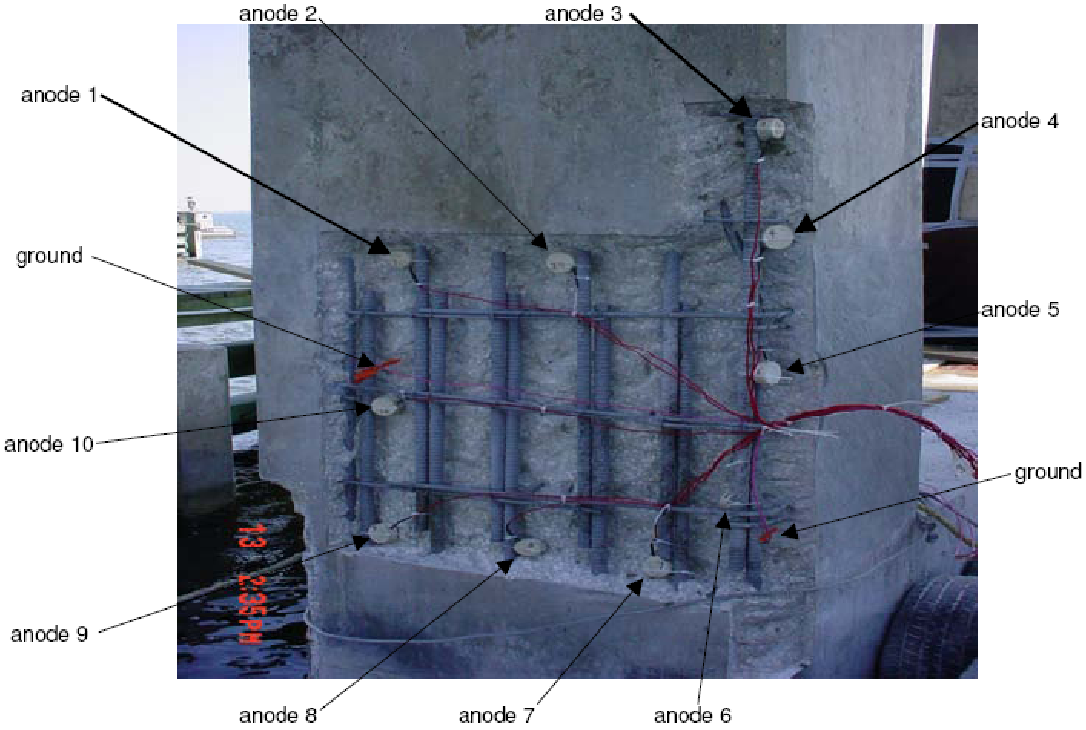

Figure 8 - Field Test Site 1, Locations No.1 (top) and No.2

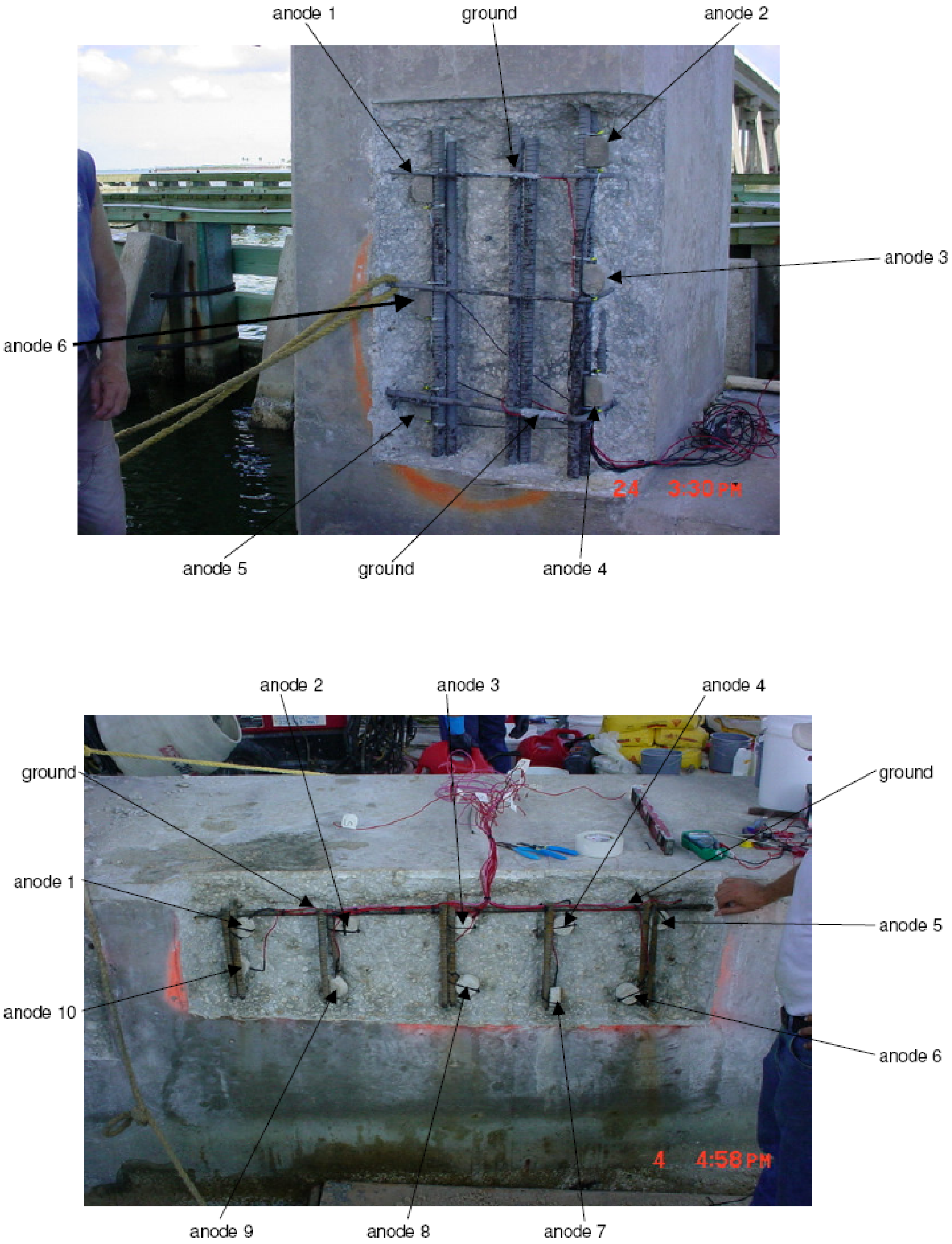

Figure 9 - Field Test Site 1, Locations No. 4 (top) and No. 5

2.5.2 Test Site 2

This site is at the Julia Tuttle Bridge, No.870301 in Dade County, Miami area. Installation details are given in Table 3, and Figures 10 and 11 show typical installations. Locations 10-3 and 2-3 had 33 Type C and 42 Type W anodes installed respectively, and were wired to allow for measuring individual and combined anode potentials and currents. The anodes at locations 2-2, 2-4 and 2-5 (all type W) were not externally wired locations so the anodes were permanently connected to the steel; only closed circuit ("Current-On") potentials were measured there. Locations 5-2 to 5-5 had patches made without any anodes installed and served as controls. Additional test stations at this site evaluated other types of anodes and test conditions that fall outside the scope of this report.

All patching was performed with a repair material supplied by the manufacturer of the W anodes, with a specified minimum strength of 34.5 MPa (5,000 psi). The C anodes were first embedded each in smaller patches of a proprietary compound supplied the manufacturer of the C anodes as shown in Figure 11. That patch material was of lower resistivity and strength than that used for the rest of the repairs. The footers are 1.2 m (48 in) tall, with the mean high tide elevation approximately at mid-height. All the patches are located at approximately the same elevations, repairing the lower half of the footer, so the upper edge of the patch is approximately at high tide. Potential and current measurements were performed following procedures similar to those for Test Site 1. Thus, the potential test points start nominally 7.5 cm (3 in) above high tide.

The anodes for this field site were acquired at about the same time the manufacturers supplied the 2nd set of anodes for the test yard slabs.

Table 3. Site 2 test area locations and material installation information

Bridge	Pier	Component	Location number	Anode Type (No anode)	Date Anodes Installed	Date Patch Material Placed	Date Anode Energized	Approx. Patch Area m^2 (sq.ft)	Physical Survey		
									Age (Days)	C cm (in)	D m^2 (sq.ft.)
870301	2 East	Pile Cap 2	2-2	W	6/6/07	6/6/07	6/6/07	6.7 (72)	91	X 107 (42)	-
		Pile Cap 3	2-3	W*(42)	6/7/07	6/7/07	6/14/07	6 (64)		-	-
		Pile Cap 4	2-4	W	6/8/07	6/8/07	6/8/07	6.6 (71)		-	-
		Pile Cap 5	2-5	W	6/11/07	6/11/07	6/11/07	7.9 (86)	86	X 25 (10)	-
	10 East	Pile Cap 3	10-3	C*(33)	9/6/07	9/6/07	9/11/07	5.4 (58)			
	5 East	Pile Cap 2	5-2	None (Control)	N/A	6/13/07	N/A	5.2 (56)		-	-
		Pile Cap 3	5-3			6/14/07		11.2 (121)	75	X 137 (54)	X 0.04 (0.41)
		Pile Cap 4	5-4			6/15/07		10.3 (111)		-	-
		Pile Cap 5	5-5			6/18/07		7.1 (76)	71	X 25 (10)	X 0.23 (2.5)

* Location with externally wired anode connections.
C: X indicates crack observed, length given if available.
D: X indicates delamination observed, surface area given when available.

Figure 10 - Field Test Site 2, view of an instrumented Type C anode location before (top) and after placing grout on anodes (examples arrowed).

Figure 11 - Field Test Site 2, view of an instrumented Type W anode location before placing grout on anodes. Arrow shows position of an embedded reference electrode.

3 EXPERIMENTAL AND FIELD RESULTS AND DISCUSSION

3.1 Results, Subtask 1A, Galvanostatic Potential-Current Function Tests.

For the following, it is recalled these experiments were performed only with the first set of anodes provided by the manufacturers.

The average Instant-Off potentials E_{IO} from individual anodes of a given replicate trio were again averaged over 200 day periods from 0-200 days to 800-1200 days, and the results are illustrated in Figures 12 and 13 for the 95% and 60% RH humidity conditions respectively. The 0 mV vs CSE condition was reached in the high RH chamber for only a few of the specimens, most in the 300 μA regime and then relatively late in the test. In contrast, in the low RH chamber the condition was reached relatively soon in more specimens and at lower current levels, effectively terminating the test early for those cases.

The initial open circuit potentials (OCP) of the anodes ranged from values approaching that commonly expected for active zinc (~-1V vs CSE) to sometimes markedly more positive values. In general both C and W anodes showed a more negative OCP in the proprietary mix medium than in the ordinary repair concrete, in both the high and low RH chambers. At 95% RH and for both embedding media the C anodes had more negative initial OCP than the W anodes. In contrast, at low RH the initial OCP of both anodes were comparable and not so negative. Scatter in the OCP values was significant, obscuring determination by these measurements of a possible variation of OCP with time such as the increasing trend suggested in the introduction.

The results for tests with galvanostatic current control typically showed clear increases in E_{IO} with increasing current and time, culminating often in reaching the test-termination condition as noted above. At 95% RH the C anodes tended to polarize more, and faster with time, than the W anodes thus offsetting much of the difference in OCP between both types of anodes. At 60% RH both types of anodes (but more so the C anodes) tended to reach the test-termination condition faster than at 95% RH. By 1200 days of exposure at 60% RH a majority of the anodes of both types had reached the test termination condition at all three impressed current levels.

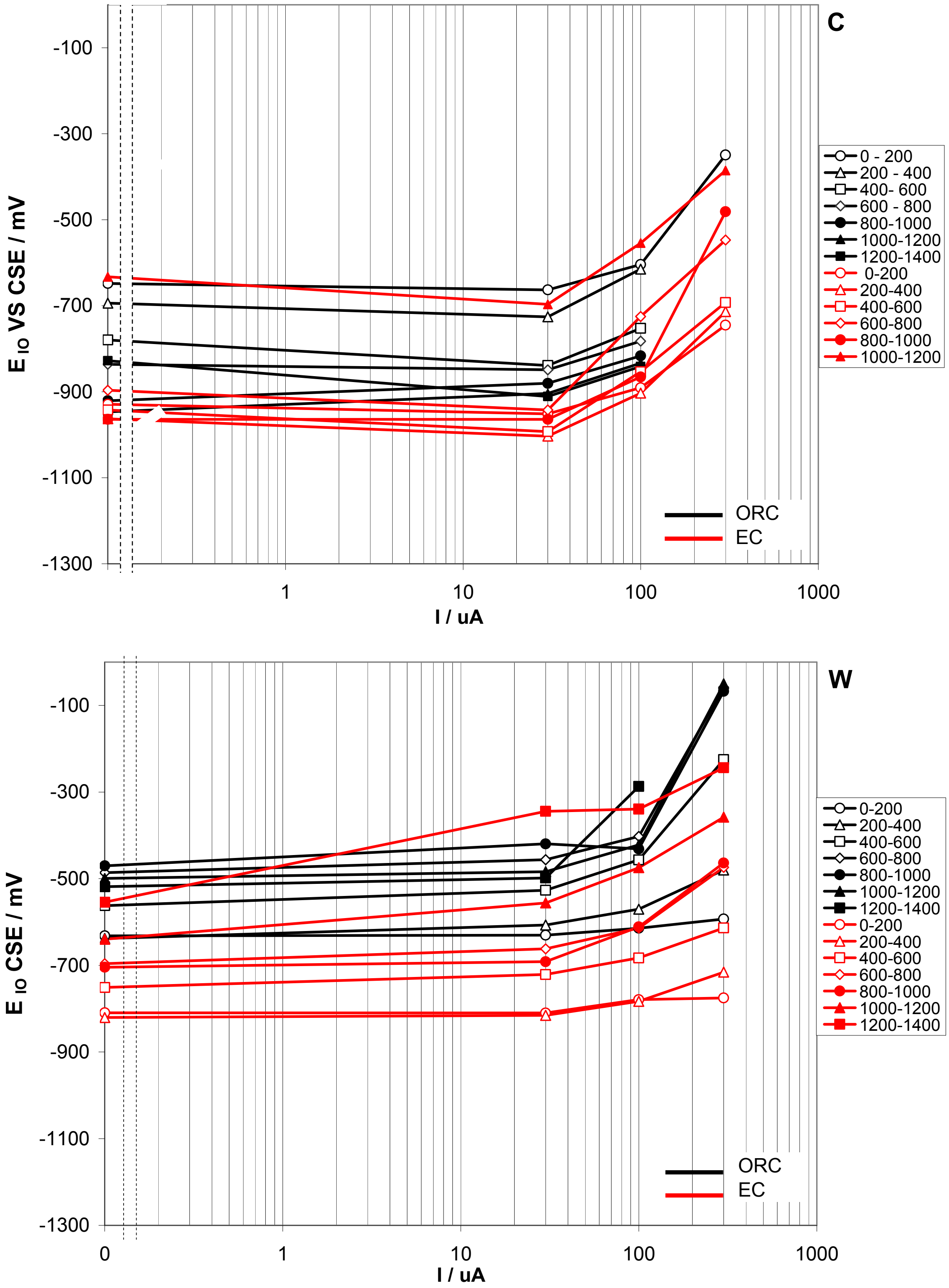

Figure 12 - EIO evolution for both test media and anode types exposed in the 95% RH chamber. Average results from multiple replicate anodes over each period (in days of exposure) indicated in the legend.

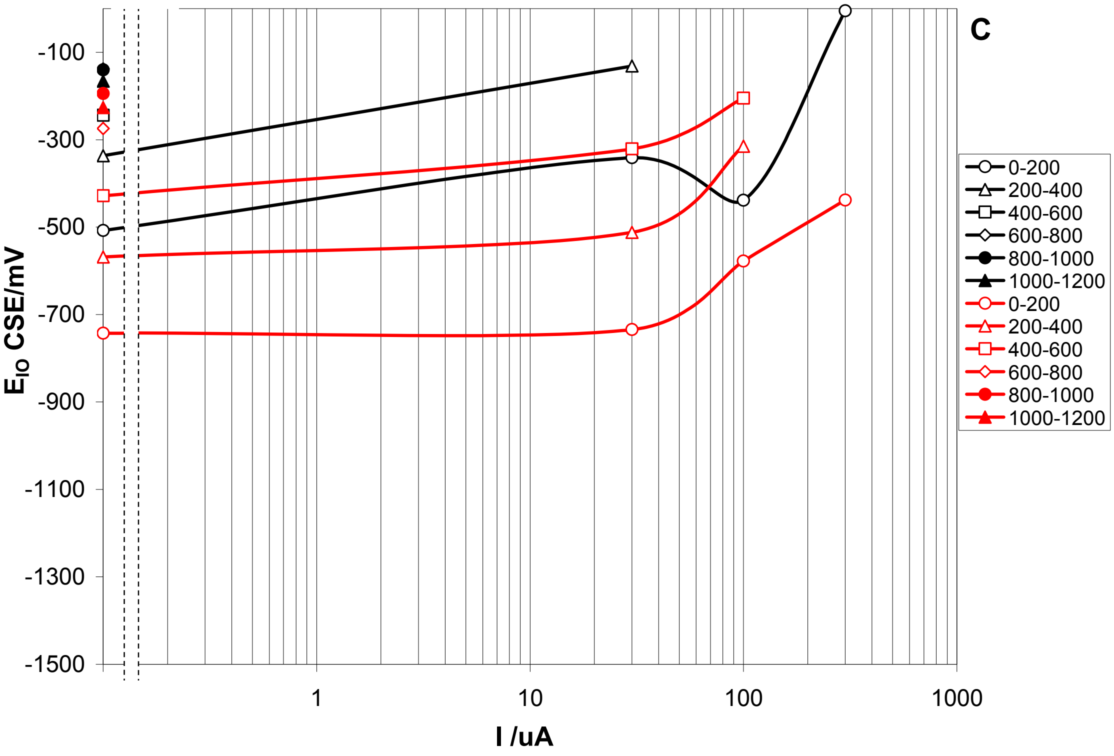

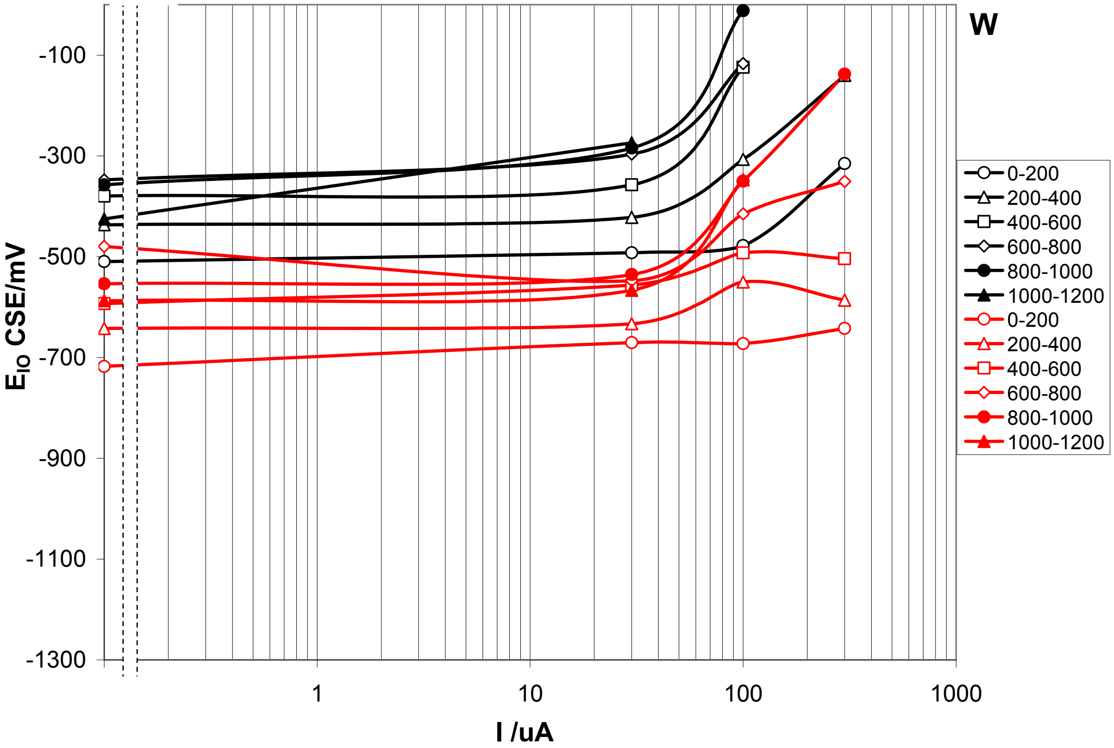

Figure 13 - EIO evolution for both test media and anode types exposed in the 60% RH chamber. Average results from multiple replicate anodes over each period (in days of exposure) indicated in the legend.

3.2 Results, Subtask 1B, Test Yard Slab tests.

3.2.1 Anode Polarization

For the following, it is recalled that these experiments were performed with anodes from both the 1st and the 2nd sets provided by the manufacturers. The products were nominally the same in each case. The test schedule differed between both sets of anodes in that for the 1st the 4 rebars in the chloride-contaminated region were connected from day 0 to day 477 and disconnected from thereon until day 1045 when testing of the 1st set ended. For the 2nd set tests, that started immediately afterwards, those rebars were never connected. Unless otherwise indicated, time reported in the following corresponds to the period starting at the beginning of the placement of the respective set of anodes. This report covers the evolution of the 1st and 2nd set of anodes through their first 1045 and 590 days respectively.

The current delivered by the anodes to the entire rebar assembly as a function of exposure time is shown in Figure 14 for both sets tested. In both instances there were high initial currents (sometimes > 3 mA) that decayed generally steadily to values in the range of 200-500 μA after about 1.5 years for the C anodes of either set, and for the W anodes of the 2nd set. Notably, the performance of the 1st set of W anodes deteriorated much faster than the rest, to values about one order of magnitude lower than those of the C anodes (e.g. 20-90 μA) at the end of the same period. For the 1st set of anodes of both types, there was a momentary lull in the long term decreasing trend after the active rebars were disconnected, but the trend was resumed afterwards. It is noted that for much of the test period the current delivered by anode C1 or the1st set was consistently significantly greater than that of its peers in the same set.

The evolution of Instant-Off potentials with time for both sets of anodes is shown in Figure 15. Initially potentials for all anodes in both sets were quite negative, ~-700 mV. For the 1st set the potential rapidly increased early on for both anodes, to reach a roughly steady regime at ~-400 mV CSE. Disconnection of the active rebars was followed by an increase of ~100 mV for the W anodes but little change for the C anodes. Of the latter, anode C1, which had the highest currents as noted above had also the more negative potential, which began to drift toward even lower values later in the exposure period. Both anode types in the 2nd set showed a relatively slow increasing potential trend with time, reaching average potentials of ~-450 mV CSE by the end of the test period.

The trends of potential evolution with time of the auxiliary anodes, which were normally in an open circuit condition, are shown in Figure 16. For the 1st set, with one exception, the auxiliary anode potentials of both types started at values ~100 to 200 mV lower than those of the energized anodes, but increased at a much slower rate, reaching on average a plateau at ~-600 mV after about 1.5 years. The auxiliary anode in Slab 1 stayed however at more negative potentials over much of the test period. The 2nd set of anodes showed also a slow increasing potential trend, but with starting values that were markedly more negative than those of the 1st set.

The current and potential evolution of the energized anodes is shown in Figures 17 and 18 as function of the cumulative amount of galvanic charge, Q, delivered by each anode up to the moment of each measurement. The value of Q was obtained by summation of the product of anode current-duration of all the previous test intervals up to the moment of measurement. The larger the value of Q, the larger is the amount of anode metal consumption due to the galvanic current, so Q serves as one descriptor for the extent of anode aging. For the 1st set of anodes there was a striking decrease in current output of the W anodes Q reached ~10 k Cuol to 20 k Coul. Two of the C anodes in the 1st set showed markedly decreased current delivery at Q ~10 k Coul to 20 k Coul, but anode C1 was delivering ~500 μA even at Q ~ 60 k Coul.

Anodes in the 2nd set showed a more uniform decrease in current delivery with increasing Q, up to ~ 35 k Coul by the end of the test period. Unlike in the 1st set, performance of the W anodes did not show early deterioration and was comparable up to the end of the test interval to that of the type C anodes in both sets. Potential evolution trends as function of Q were obscured in the 1st set, especially for the C anodes. The 2nd set showed a clearer trend, with potentials of both types of anodes increasing somewhat uniformly as Q increased.

The potential-current trajectory of the anodes in the test yard slabs is shown in Figures 19-20. Each symbol correspond to the average Instant-Off potential and corresponding current reading for each anode, over a 100-day period starting with anode placement. The smallest symbol indicates the 0-100 day interval with increasingly large symbols for the subsequent intervals. With the exception of data for anode C1 near the end of the test period, the trajectories correspond roughly to lines with a negative slope, small for the 1st set of anodes and steep for the 2nd set. The general direction of the trajectories (C1 for 1st set excepted) is indicated by arrows.

Results from the slow cyclic polarization tests for the 1st set of anodes are illustrated in Figures 21 and 22. For this set the tests were conducted only near the end of the exposure period, so the curves reflect significant performance derating due to aging. The curves for the C anodes show little hysteresis, with the forward and return curves nearly overlapping, while the results for the W anodes tended to some hysteresis. The results show significant unit-to-unit variability, but the shape of the curves generally resembles that of the galvanostatic test results, with a relatively abrupt increase in anodic polarization once a given current level is reached.

.

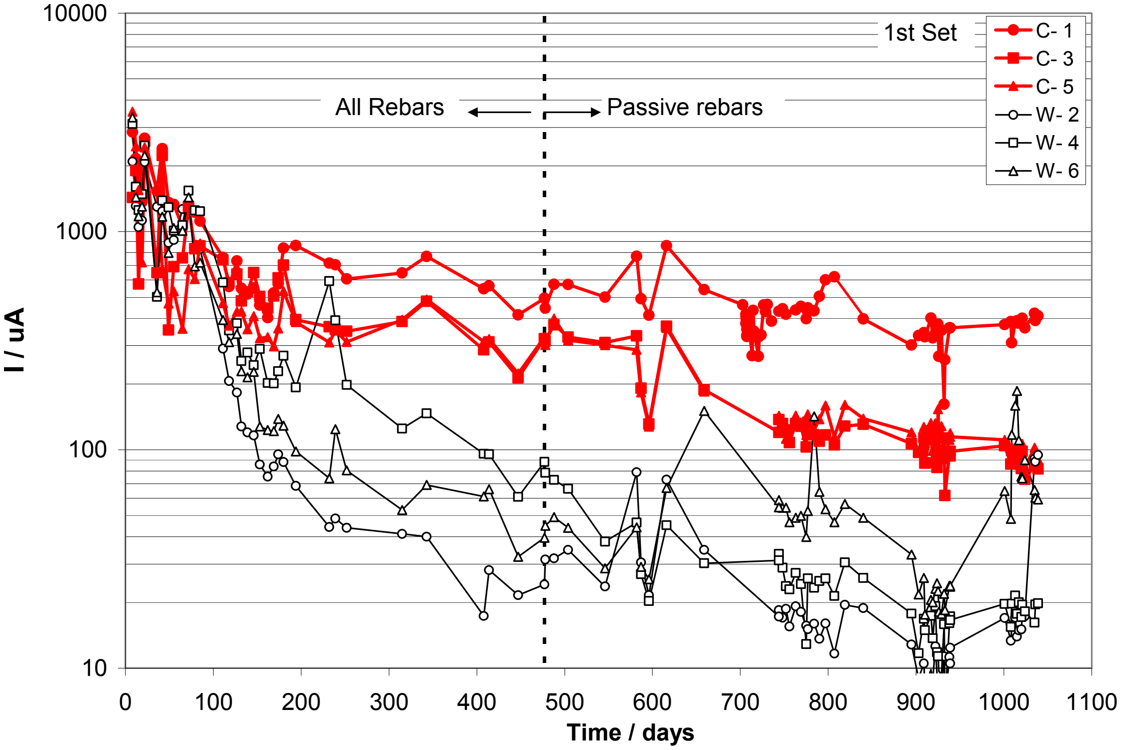

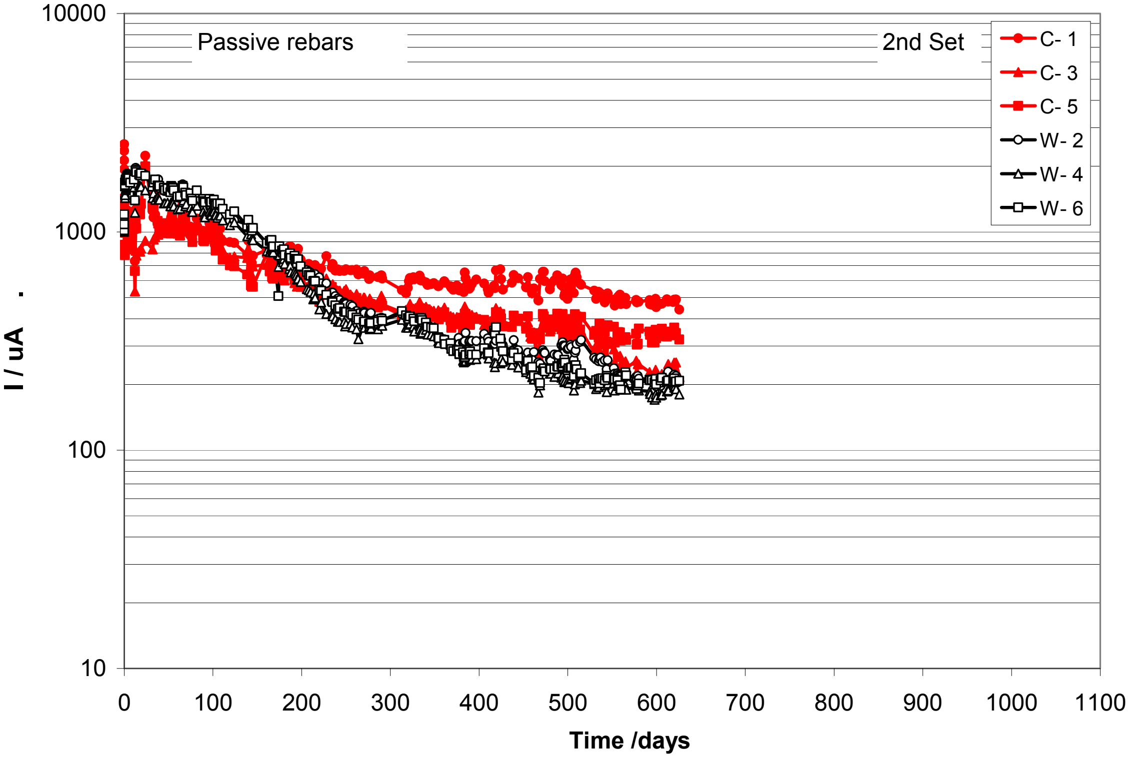

Figure 14 - Anode current evolution with time for both sets of anodes. Results of anodes in individual test yard slabs.

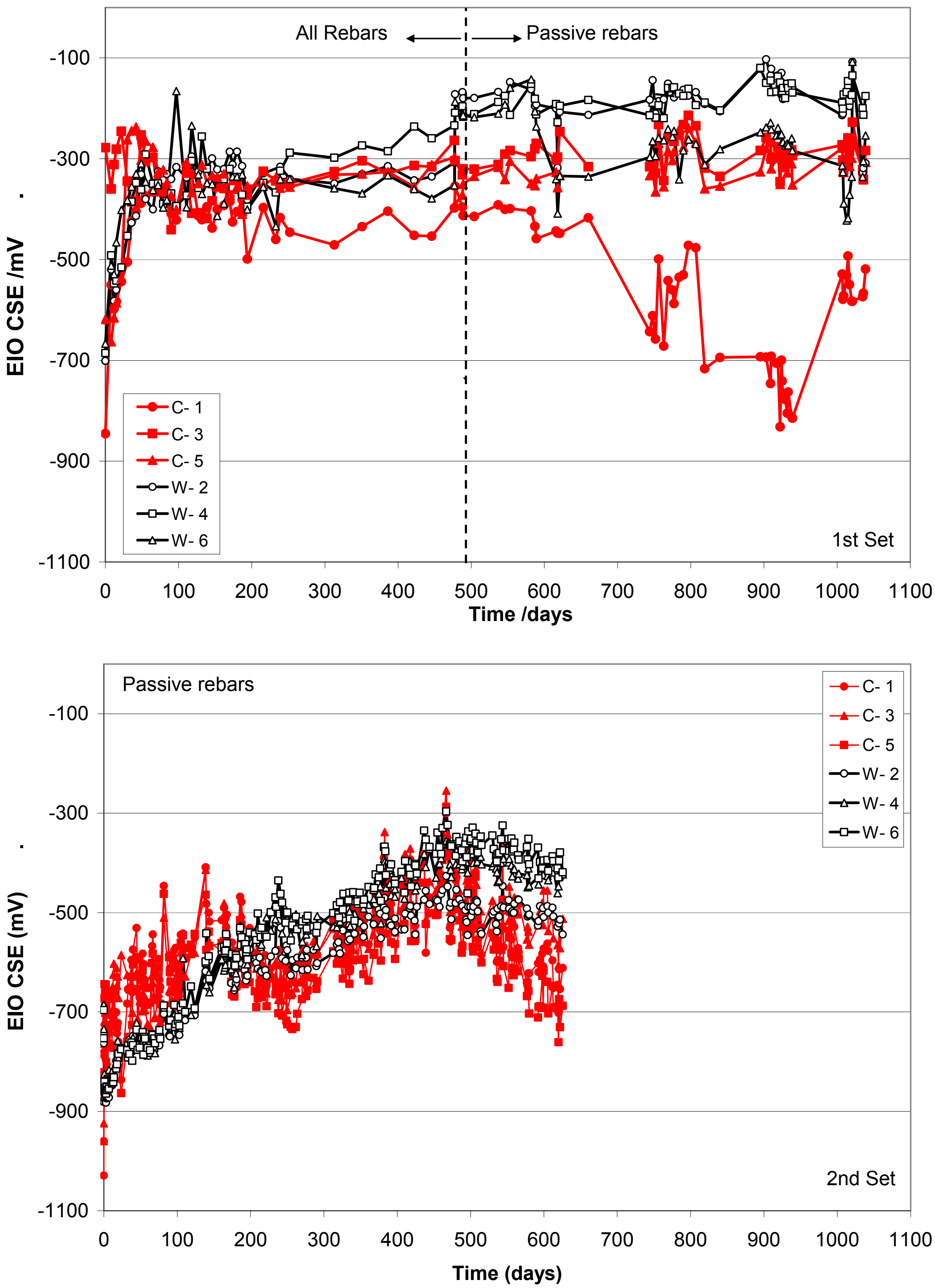

Figure 15 - Anode potential (Instant-Off) evolution with time for both sets of anodes. Results of anodes in individual test yard slabs.

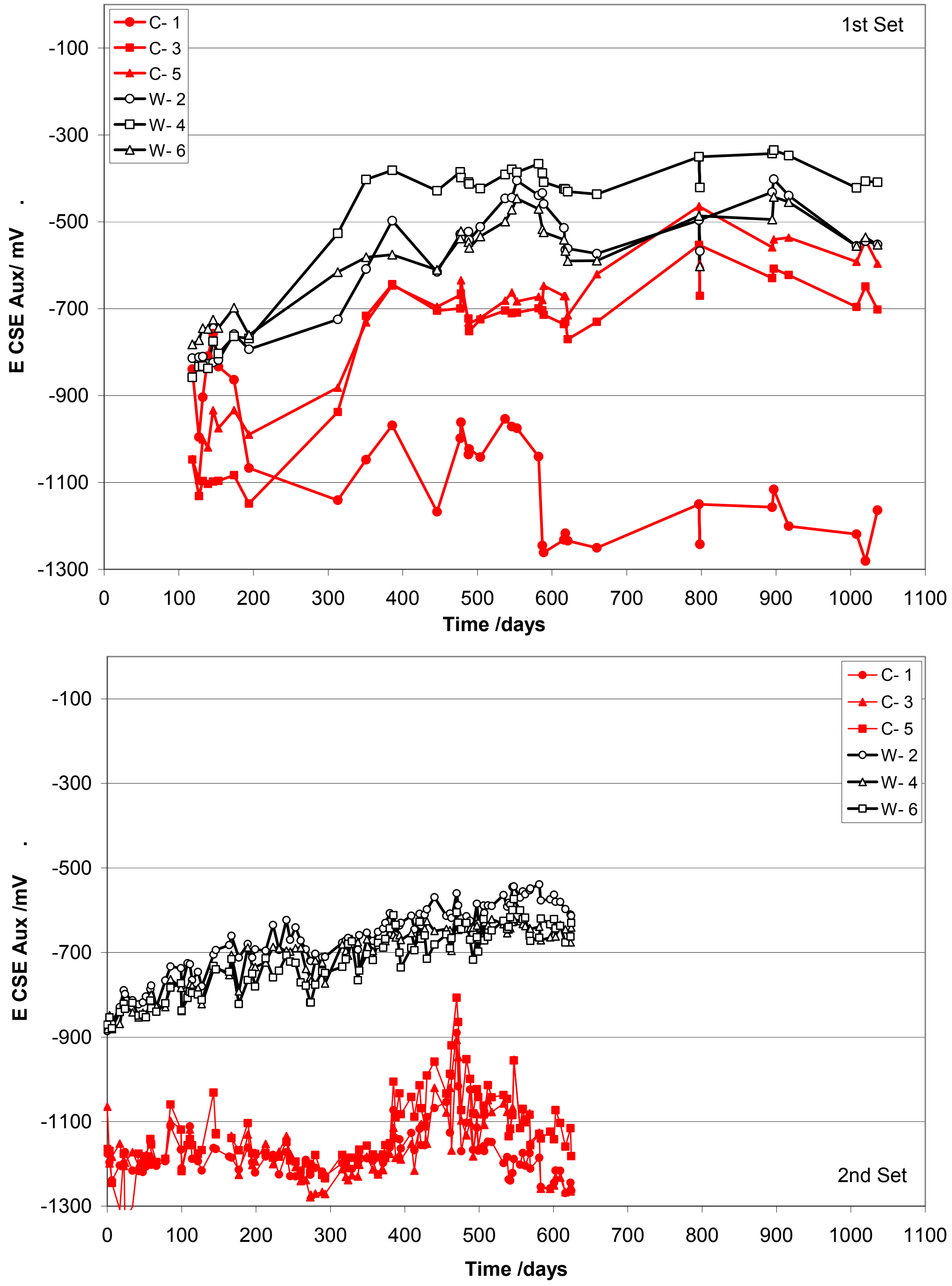

Figure 16 – Auxiliary anode potential evolution with time for both sets of anodes. Results of anodes in individual test yard slabs.

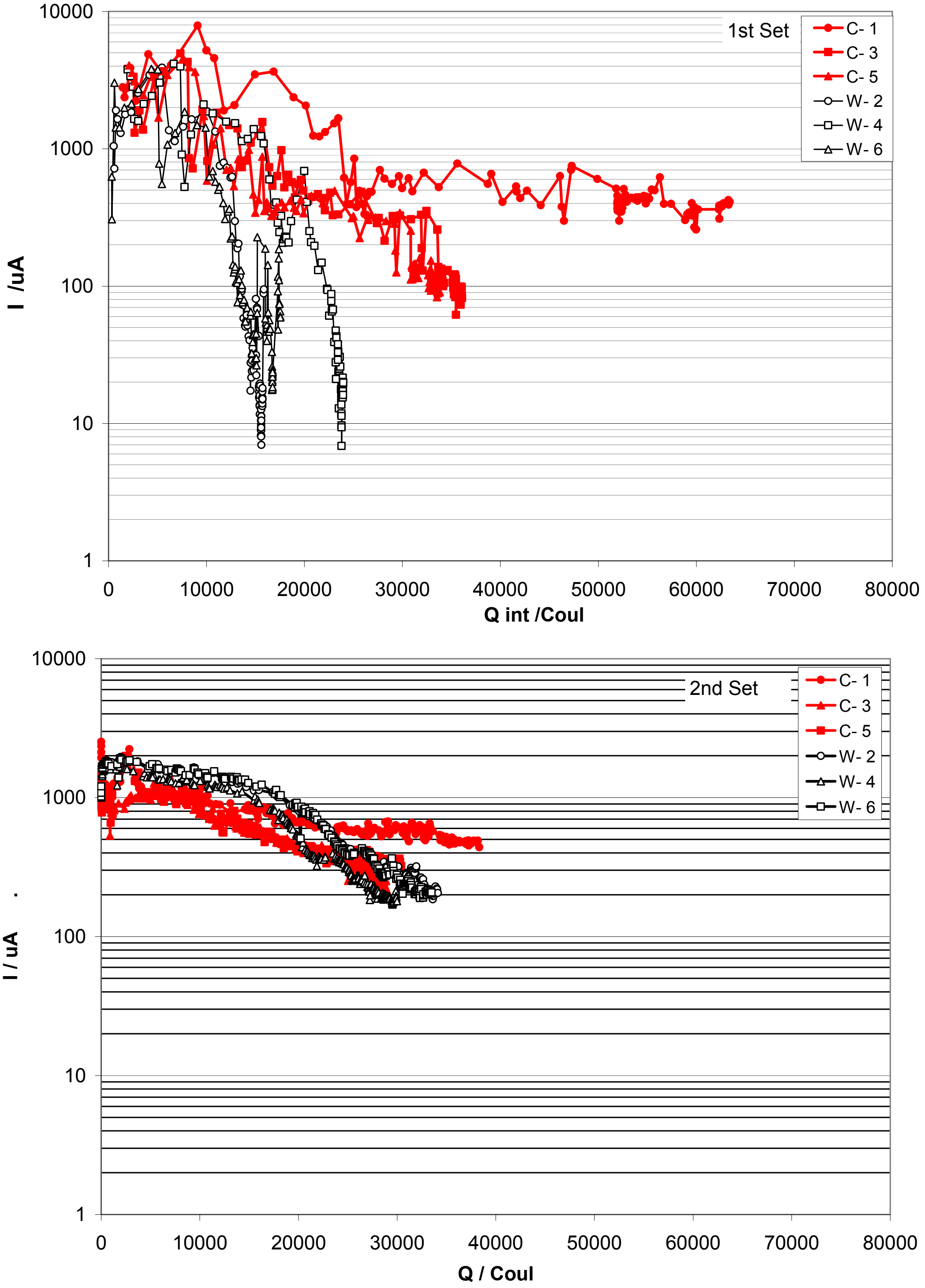

Figure 17 - Anode current as function of integrated anodic charge delivered for both sets of anodes

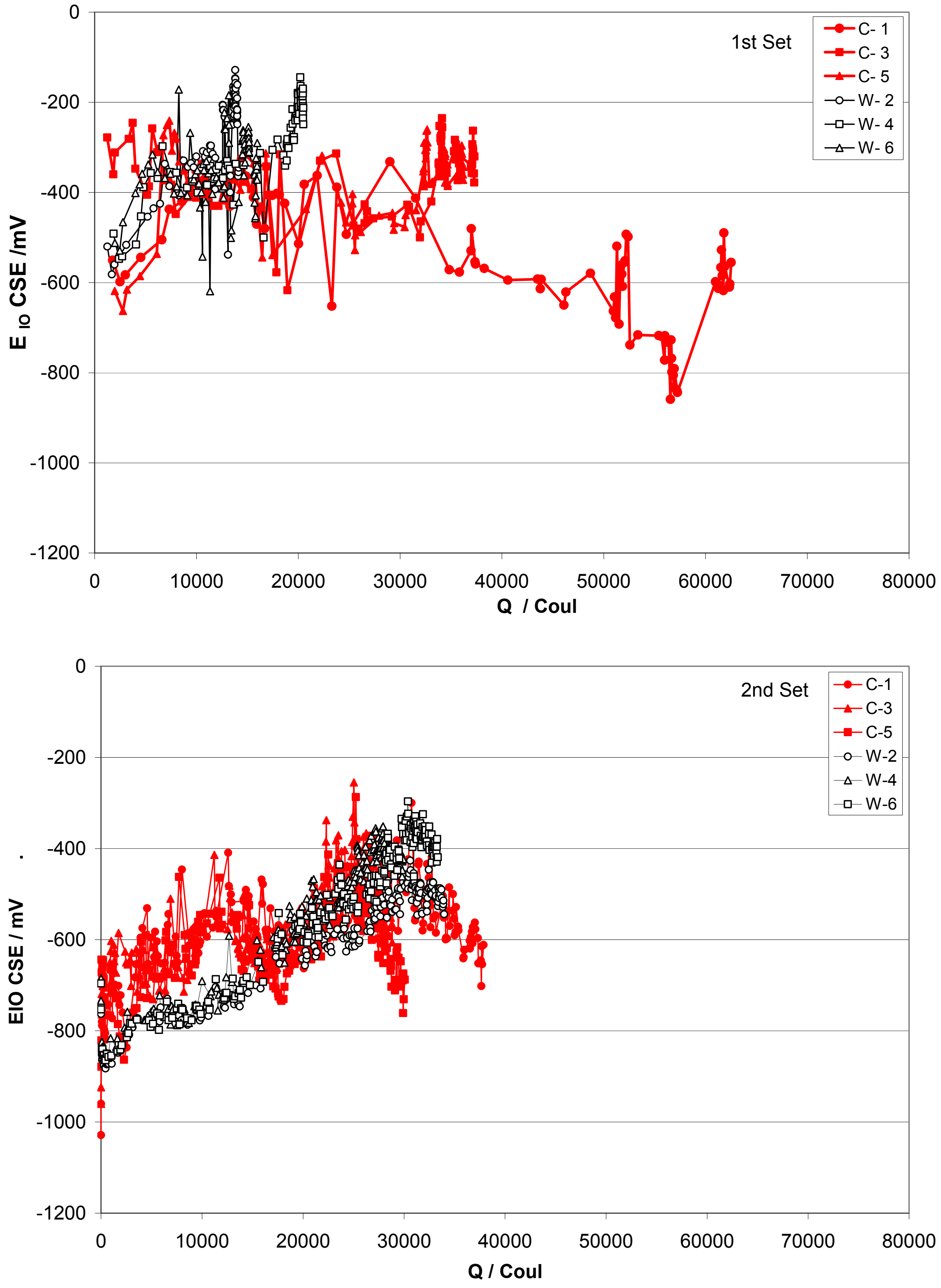

Figure 18 - Anode Potential as function of integrated anodic charge delivered for both sets of anodes

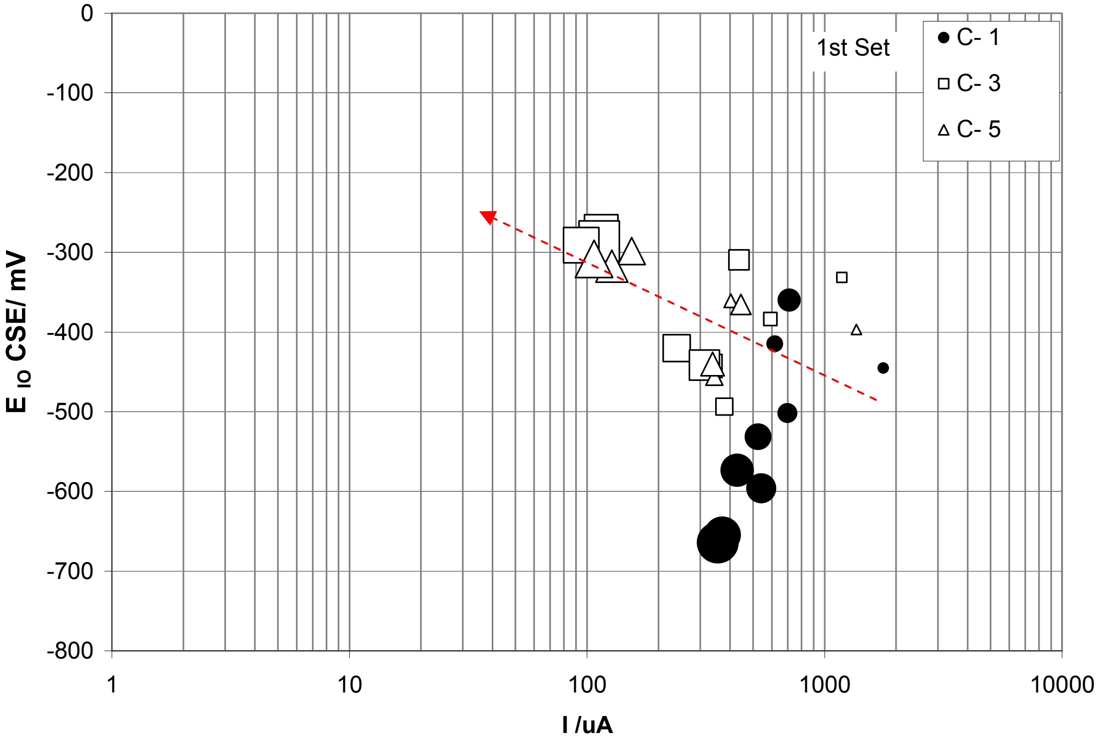

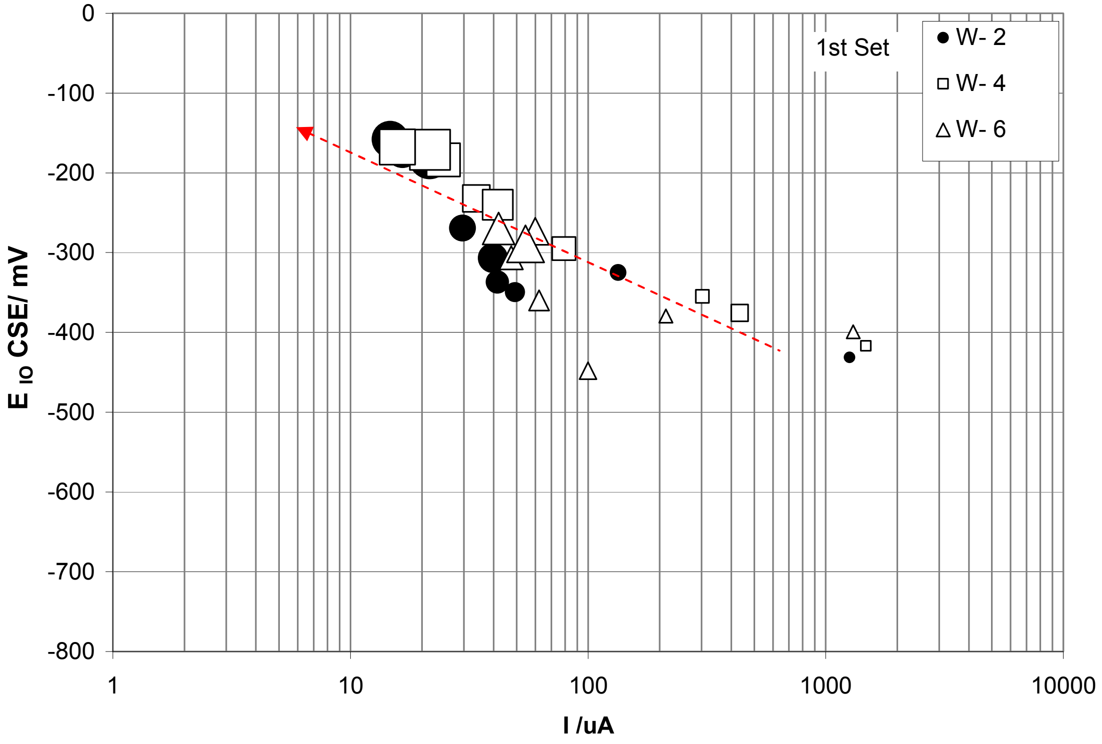

Figure 19 - Potential-Current trajectory for 1st set of anodes in test yard slabs. Largest symbols indicate greater age. See text for explanation of other symbols and on behavior of anode C-1.

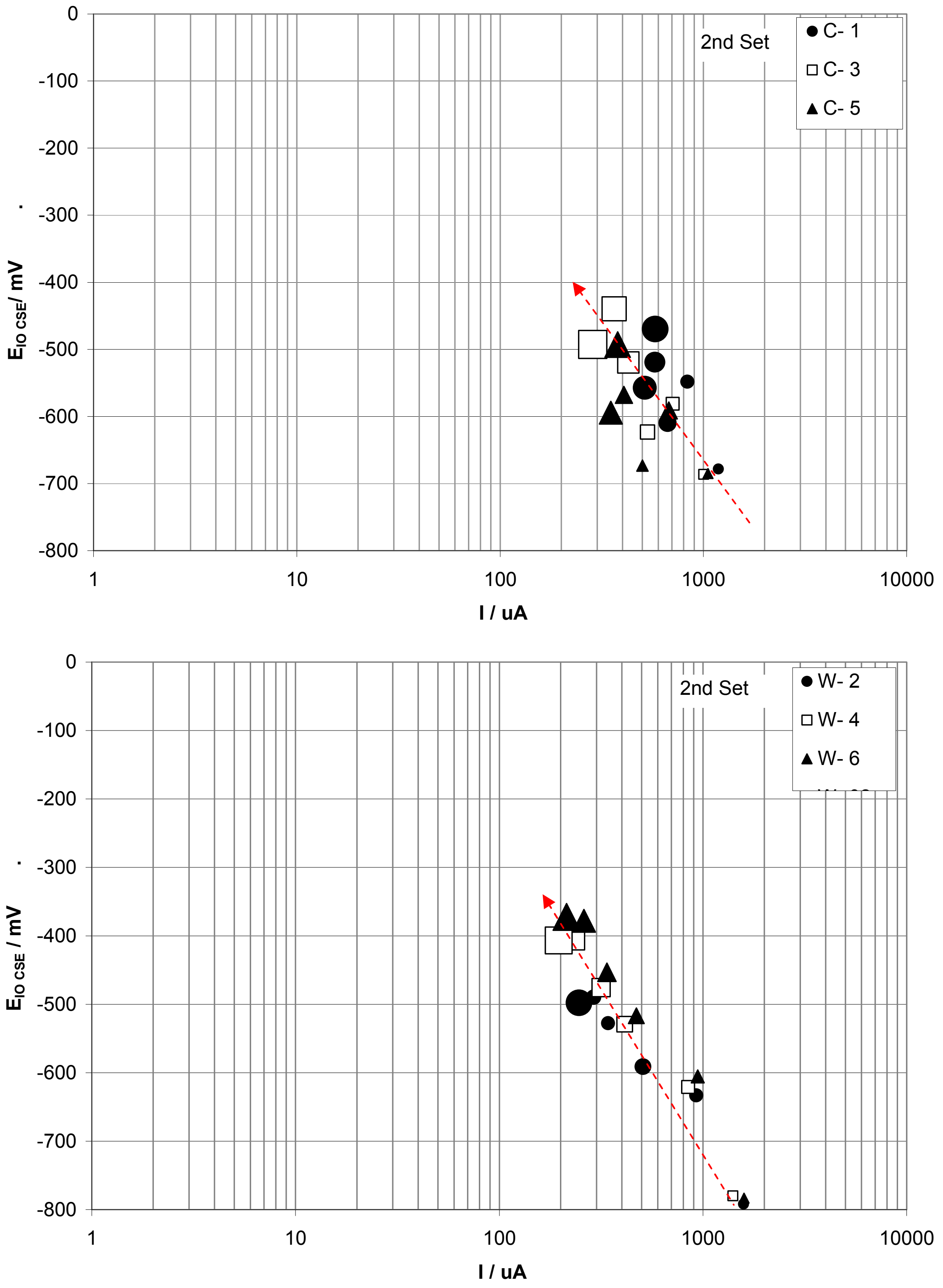

Figure 20 - Potential-Current trajectory for 2nd set of anodes in test yard slabs. Largest symbols indicate greater age. See text for explanation of other symbols.

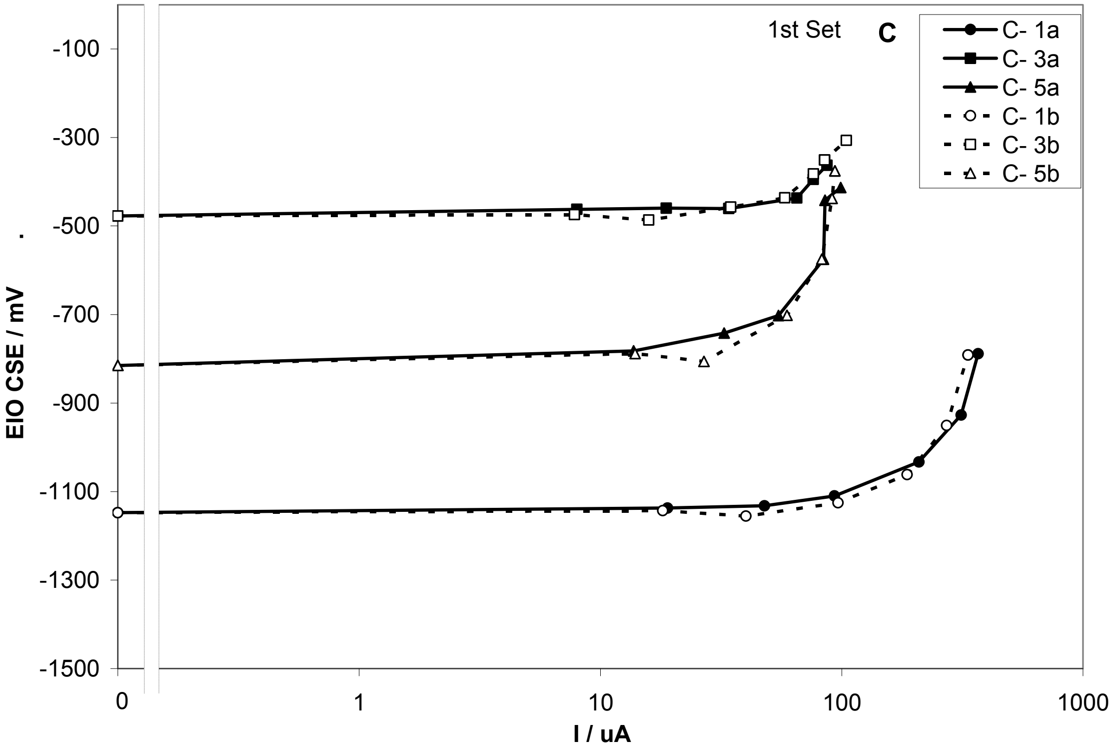

Figure 21 - E_{IO}-log I curves of the 1st set of C anodes in test yard slabs. Polarization curves in the forward (a) and return directions (b).

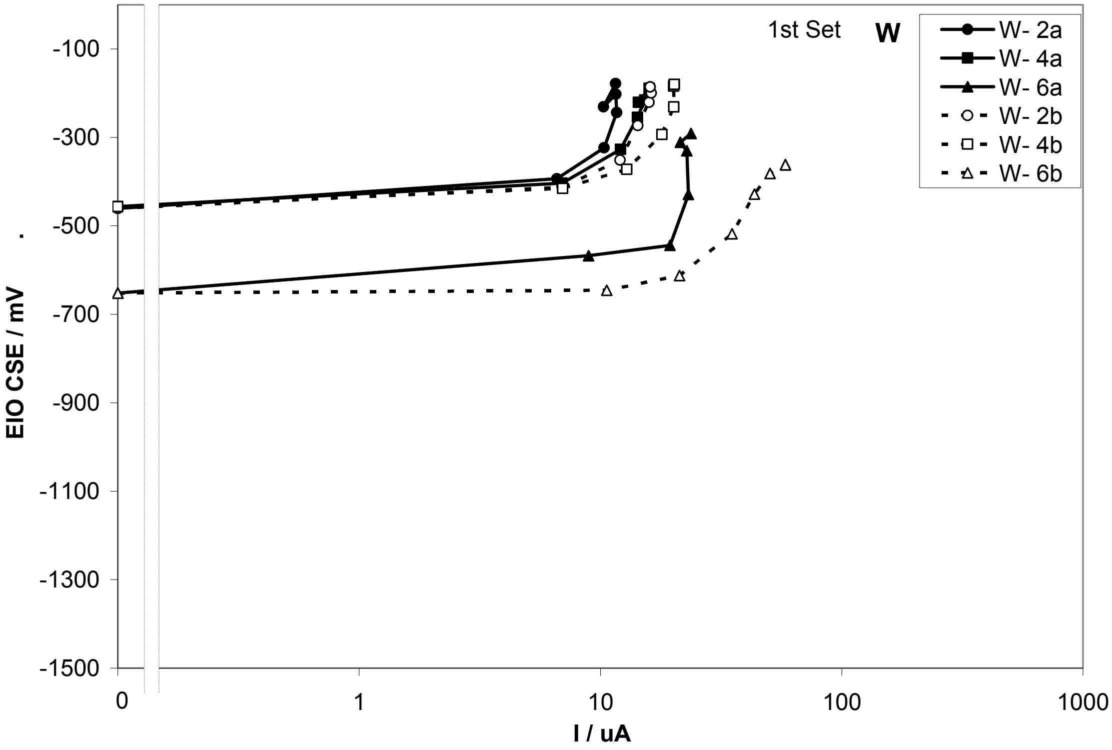

Figure 22 - E_{IO}-log I curves of the 1st set of W anodes in test yard slabs. Polarization curves in the forward (a) and return directions (b).

The slow cyclic polarization test results for the 2nd set of anodes are given in Figure 23. The 2nd set tests but tests of both C and W anodes tended to have as a whole small hysteresis, comparable to that observed for the C anodes in the 1st set tests. Therefore, for graphic simplicity only the average values of the forward and reverse parts of the test are presented. Tests were conducted at anode ages of 1, 4 and 13 months. The starting point of each curve generally matched the corresponding position in the potential-current trajectory (Figure 20) for the respective anode type. The results show increasing anodic polarization with anode age, with the C anodes having a more negative OCP (the zero current condition) than the W anodes, but with a more abrupt polarization increase with increasing anodic current. Unlike the case of the 1st set, the results from replicate anodes of a given type and aging condition showed relatively little variability.

3.2.2 Rebar Polarization

The amount of current delivered by the 1st set of anodes to the rebars at different positions in the slab at various times is shown in Figures 24 and 25, for stages early and late respectively during the period when all bars were connected. Cathodic (protective/preventive condition) current is assigned a positive sign. Currents values are the average of the three slabs of each type of anode. Both types of anode delivered about the same level of current at that time. All the passive rebars were subject to a net cathodic current, and it was greatest for the bars immediately next to the anode. In contrast, some of the active bars in the chloride contaminated zone had negative current indicating that they were acting as net anodes. That effect persisted until the time in which the active bars were disconnected. After disconnection of the active bars (Figure 26) the current to the remaining bars, all-passive, was always cathodic. The bars closest to the anode received the highest current, which decayed for rebars further away. A corresponding pattern was observed at the far end of the slab.

Four-hour depolarization test results of the rebars performed during the evaluation for the 1st set of anodes, while all rebars were connected, are shown in Figures 27-29. The depolarization level achieved was poor or nil on much of the rebar assembly both early on (Figure 27) and after 14 months (Figure 28). Depolarization levels improved somewhat for the C anode yard slabs when both the main and the auxiliary anode were temporarily connected together (Figure 29), but only on the side of the slab containing the anodes and still yielding modest to poor results there. After disconnection of the active rebars (Figure 30, top) the extent of depolarization increased markedly for the C anode yard slabs, exceeding 100 mV on average for the slabs closest to the anodes. By that time the performance of the 1st set of W anodes had degraded dramatically and only poor depolarization levels were reached in those slabs even with an all-passive connected assembly. Later on, (Figure 30, bottom, for day 1000) the average performance of the C anodes had degraded significantly and average depolarization levels did not reach 100 mV even next to the anode.

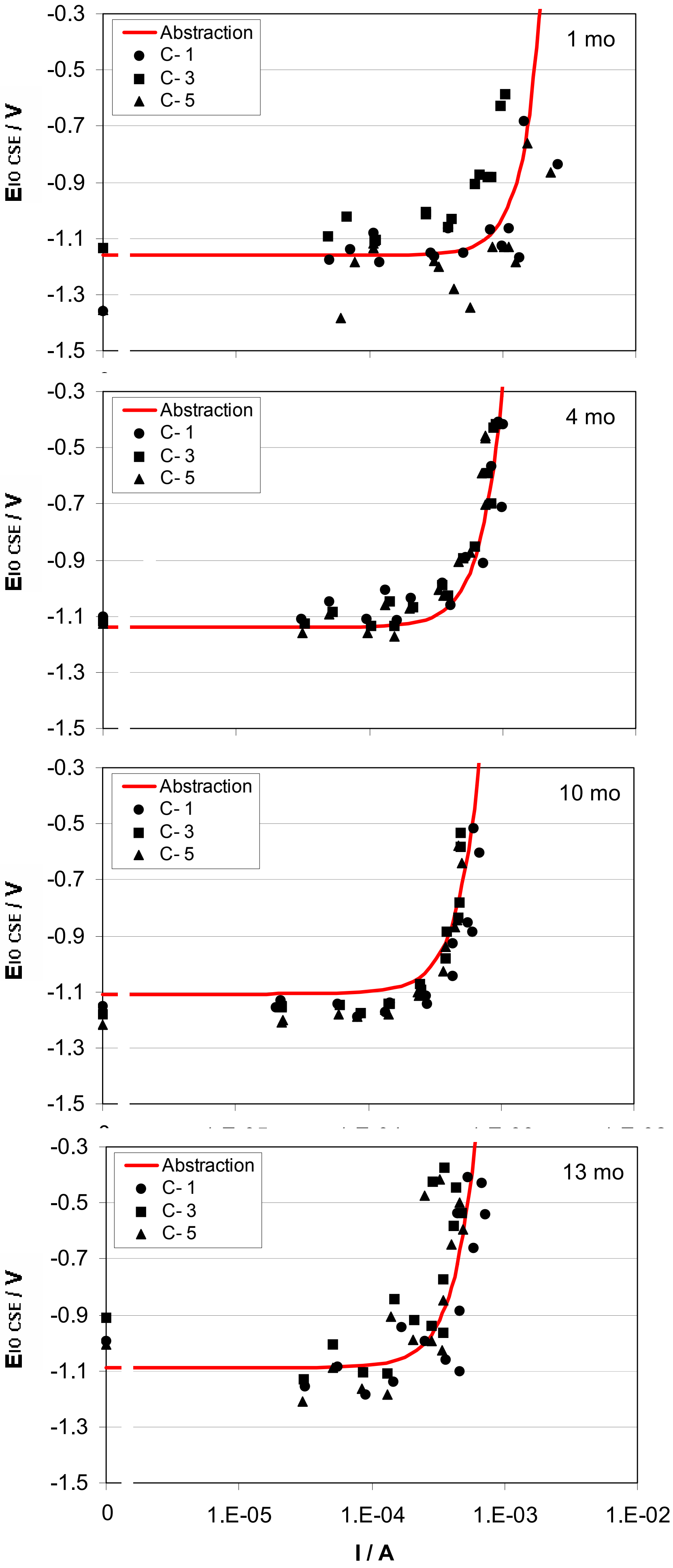

Figure 23a - E_{IO}-log I slow cyclic polarization data for 2nd set of Type C anodes in each of the corresponding test yard slabs (1,3,5), at approximate indicated anode age. Both forward and return data are displayed for each symbol. The abstraction function values for each age resulted from the global fit procedure described in the Modeling section.

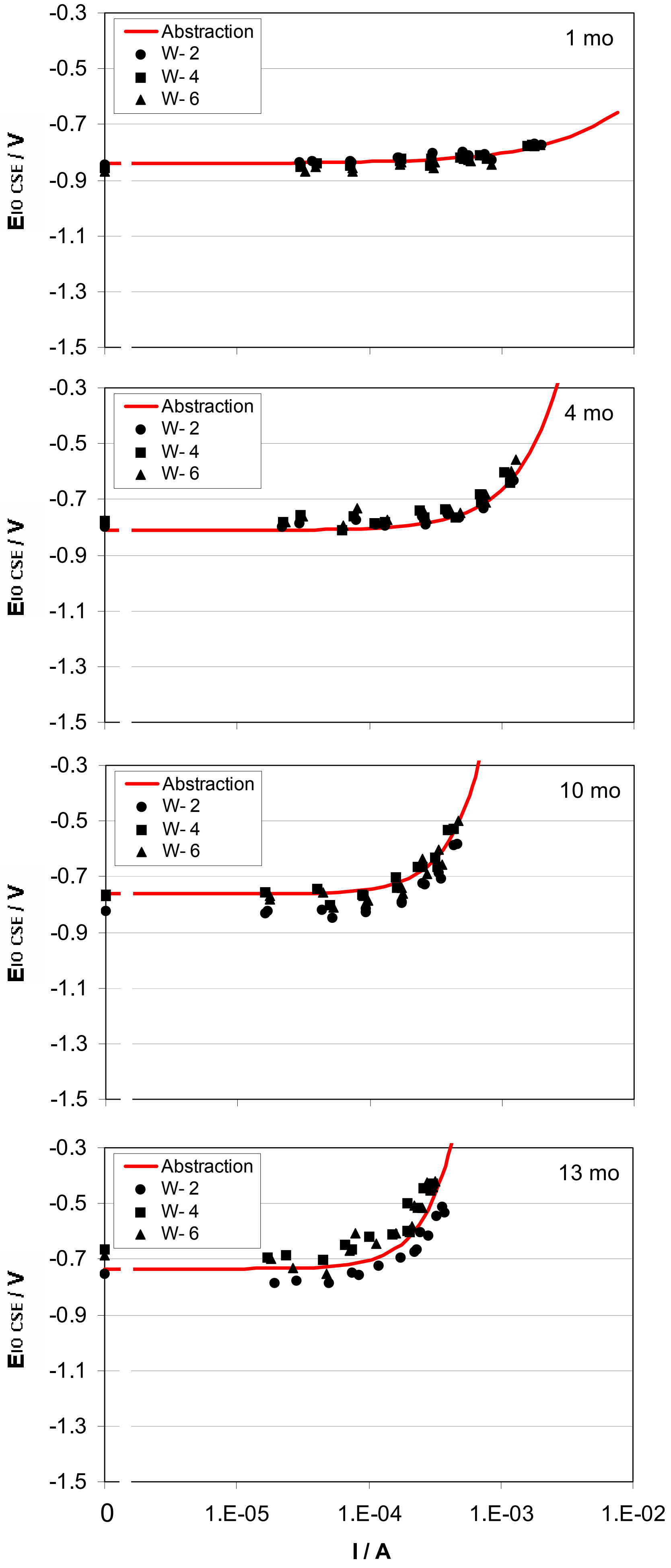

Figure 23b - E_{IO}-log I slow cyclic polarization data for 2nd set of Type W anodes in each of the corresponding test yard slabs (2,4,6), at approximate indicated anode age. Both forward and return data are displayed for each symbol. The abstraction function values for each age resulted from the global fit procedure described in the Modeling section.

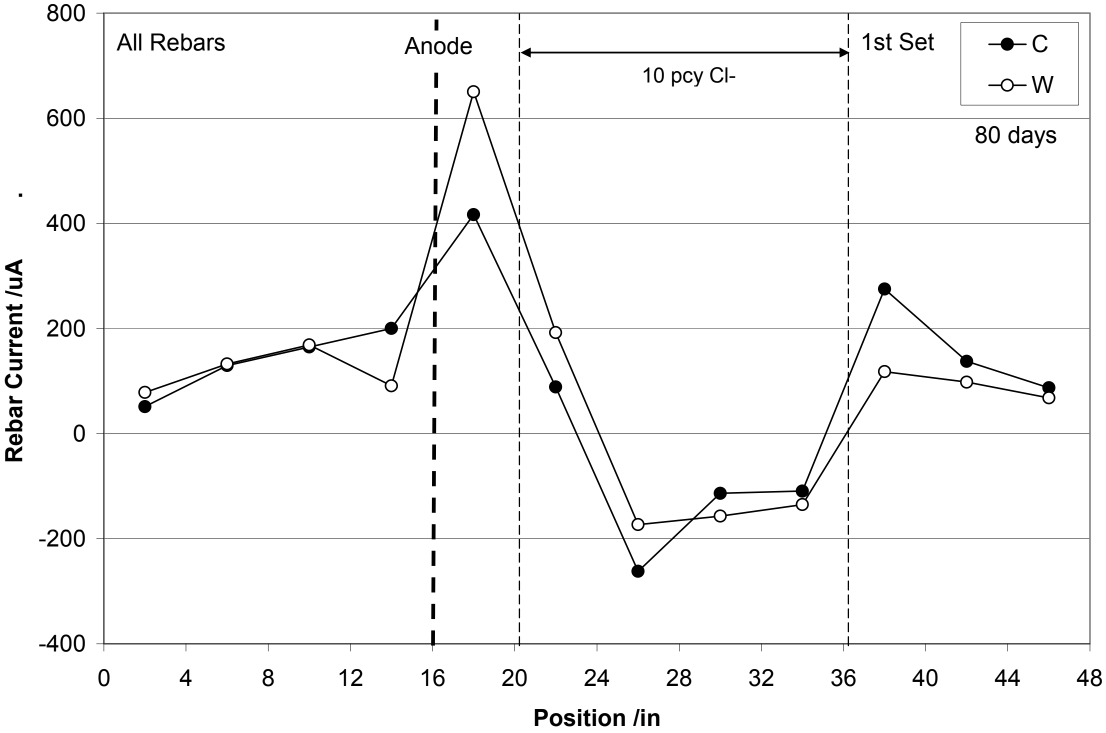

Figure 24 -1st set of anodes. Rebar current along the yard slab main direction (average of triplicate slabs) early in the exposure period (80 days). All rebars connected.

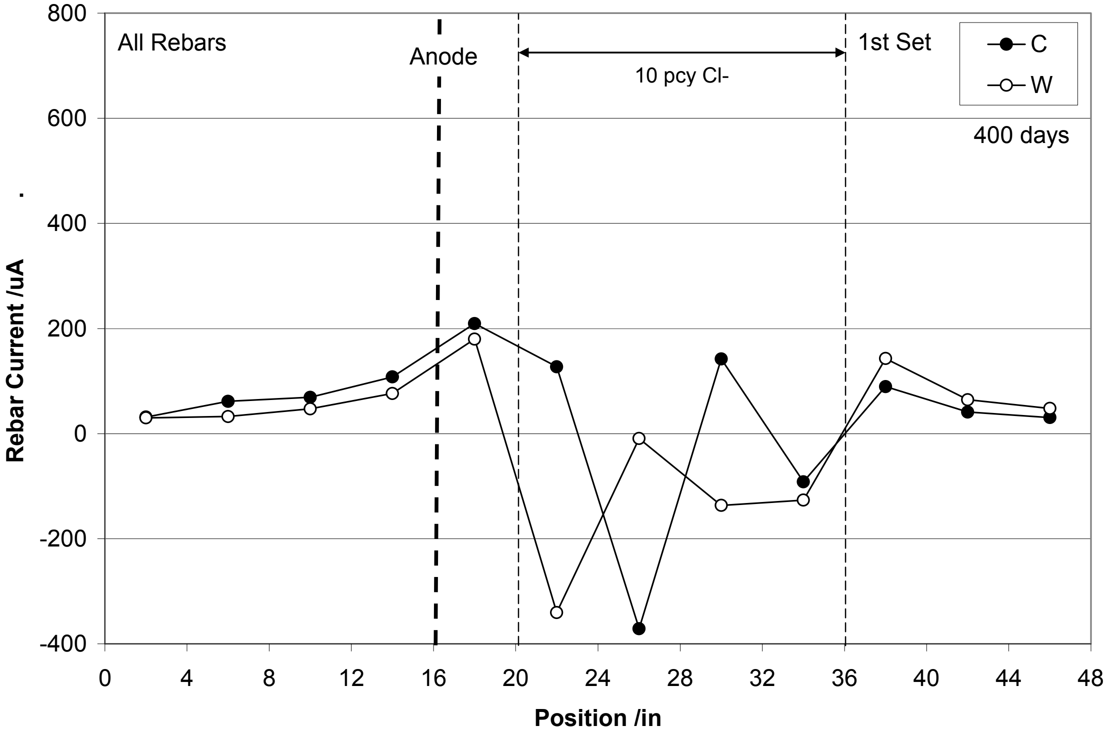

Figure 25 - 1st set of anodes. Rebar current along the yard slab main direction (average of triplicate slabs) later in the exposure period (400 days). All rebars connected.

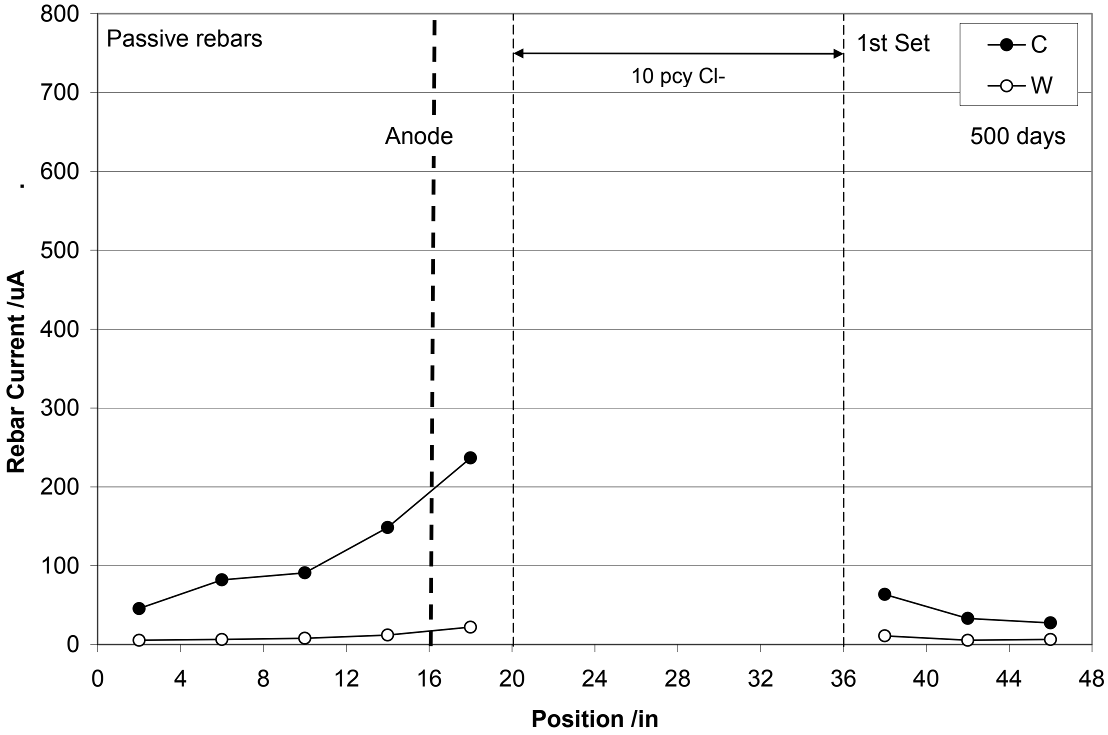

Figure 26 - 1st set of anodes. Rebar current along the yard slab main direction (average of triplicate slabs) shortly after the 4 rebars in the chloride-contaminated zone were disconnected, leaving only passive rebars connected.

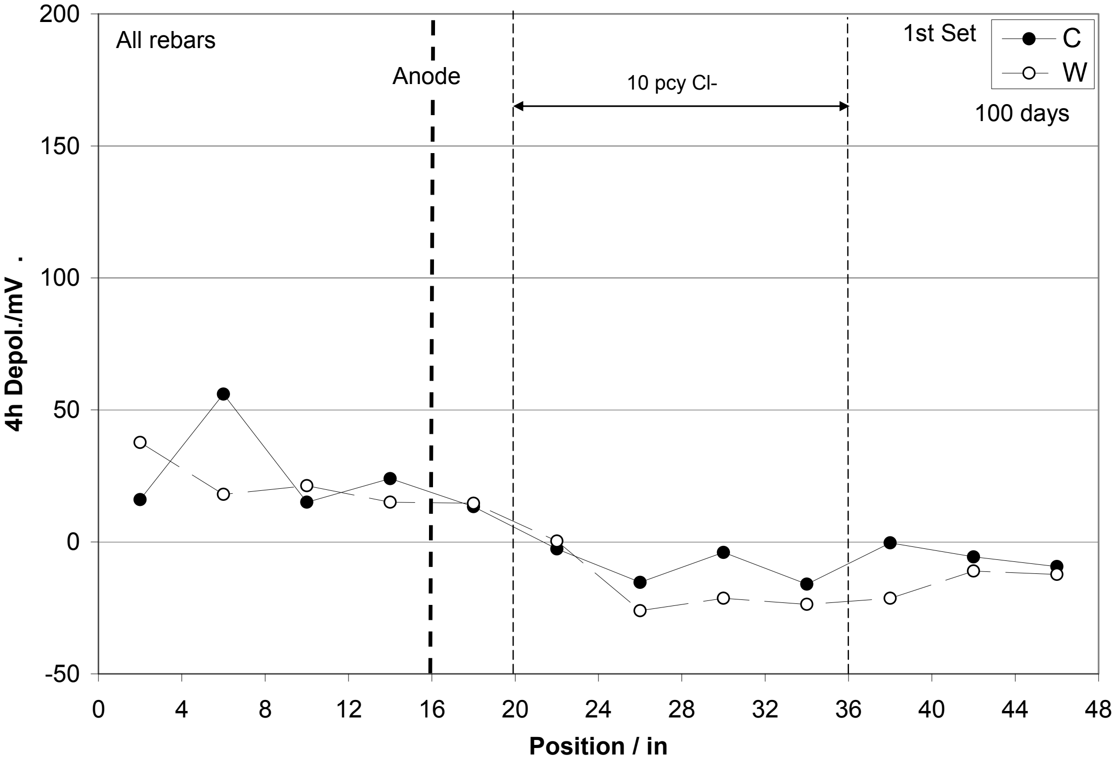

Figure 27 - 1st set of anodes. Four-hour rebar depolarization after 4 months of normal exposure. Average results of triplicate slabs.

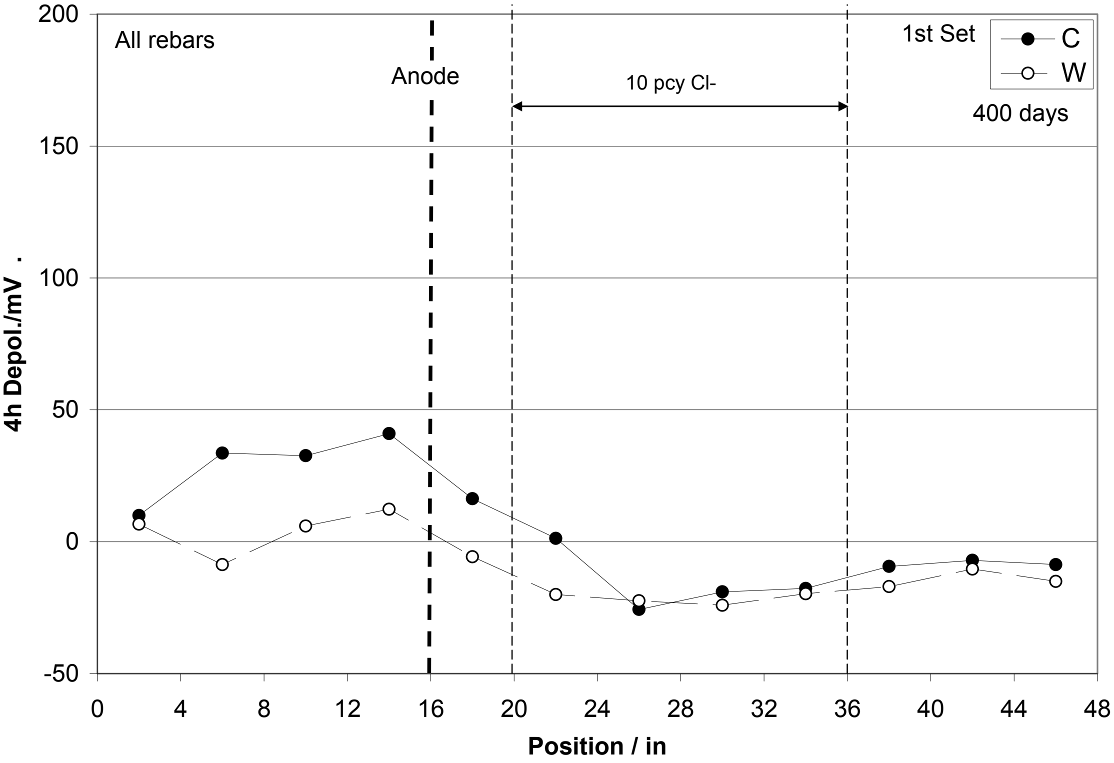

Figure 28 - First set of anodes. Four-hour rebar depolarization after 14 months of normal exposure. Average results of triplicate slabs.

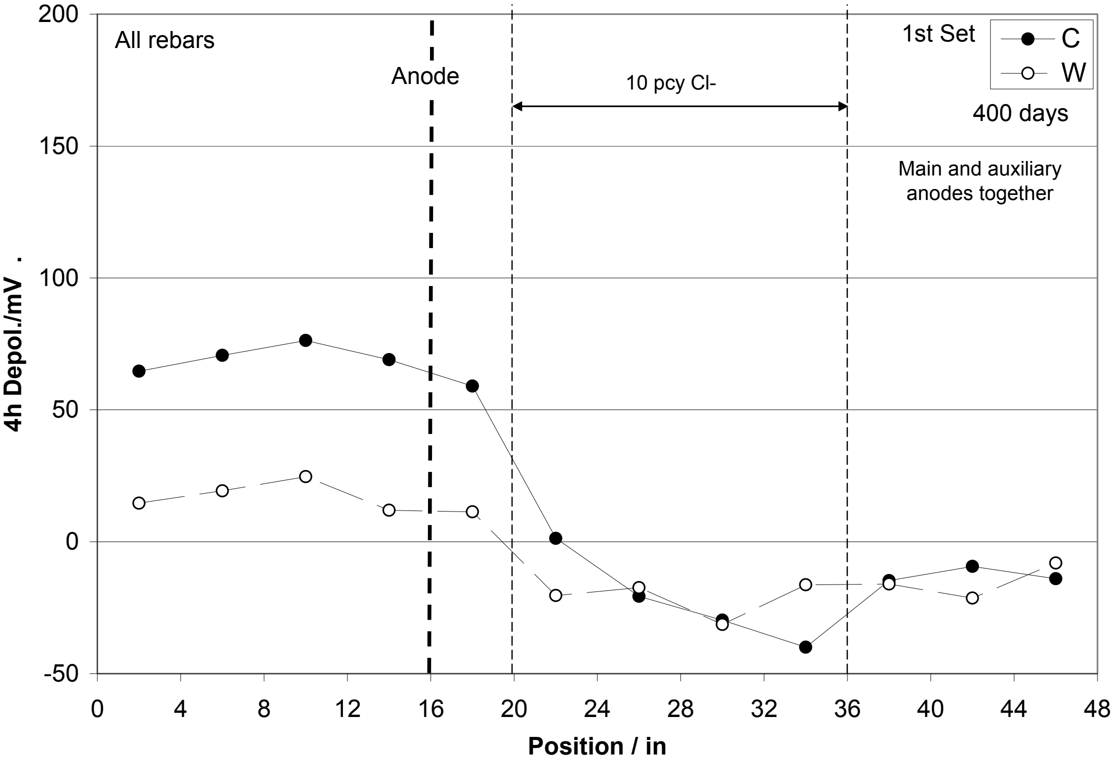

Figure 29 - 1st set of anodes. Four-hour rebar depolarization after 14 months of normal exposure plus several days of jointly connecting the Main and Auxiliary anodes. Average results of triplicate slabs.

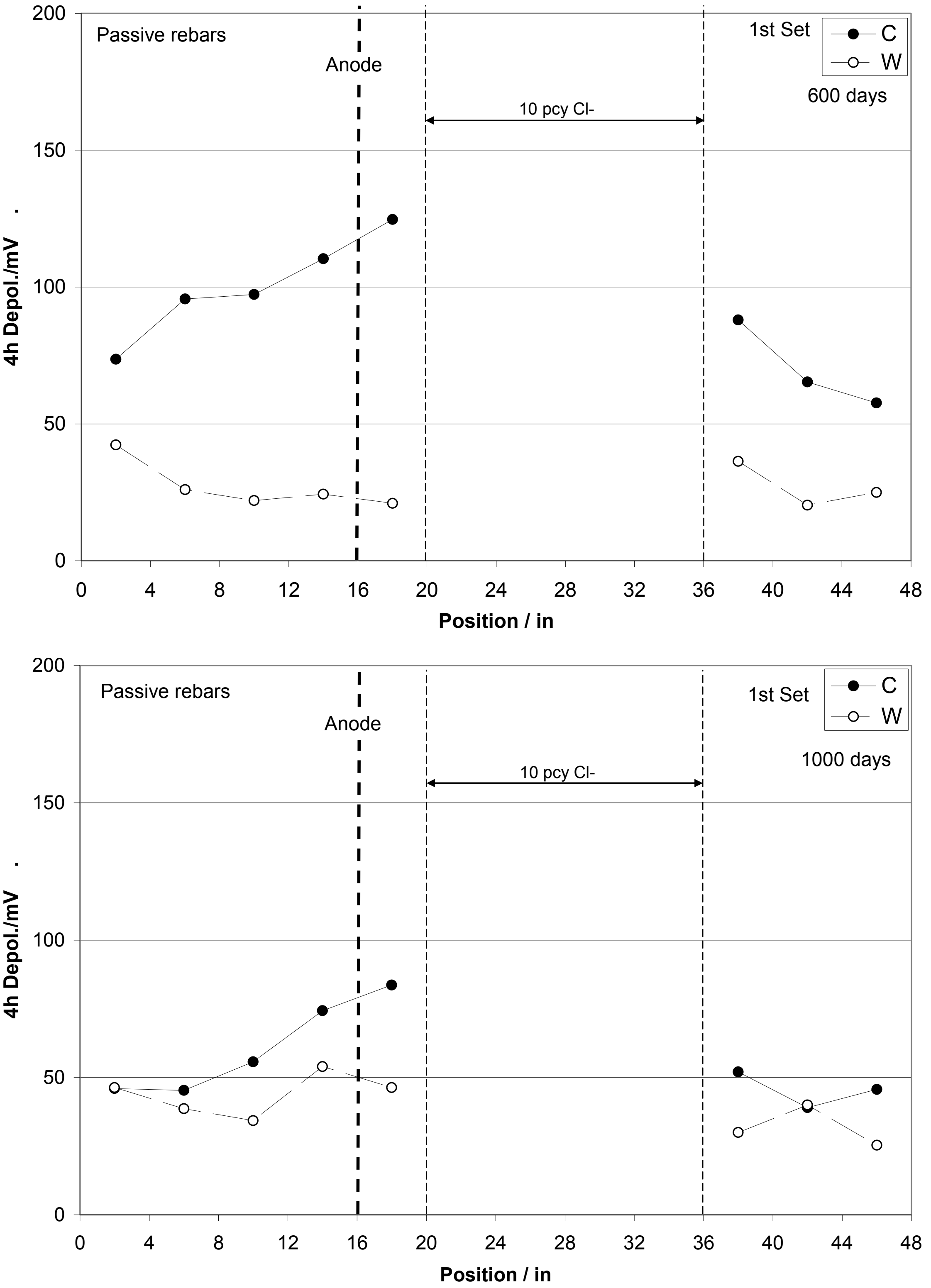

Figure 30 - 1st set of anodes. Four-hour depolarization of passive rebars after disconnection of the rebars in the chloride contaminated zone. Average results of triplicate slabs.

Figure 31 summarizes the depolarization measurement results for the 1st set of anodes for the different conditions and aging times evaluated. Rebar numbering starts at number 1 for the leftmost rebar as shown in the plan view of Figure 6.

Cathodic rebar currents and 4-h depolarization levels increased substantially when energizing the 2nd set of anodes, which always acted only on the passive rebars. The effect decreased moderately with time over the ~500 days test period. Both types of anodes performed comparably although the performance of the W anodes appears to have degraded somewhat faster (relative to the initial levels) than that of the C anodes. Figures 32-34 document these trends.

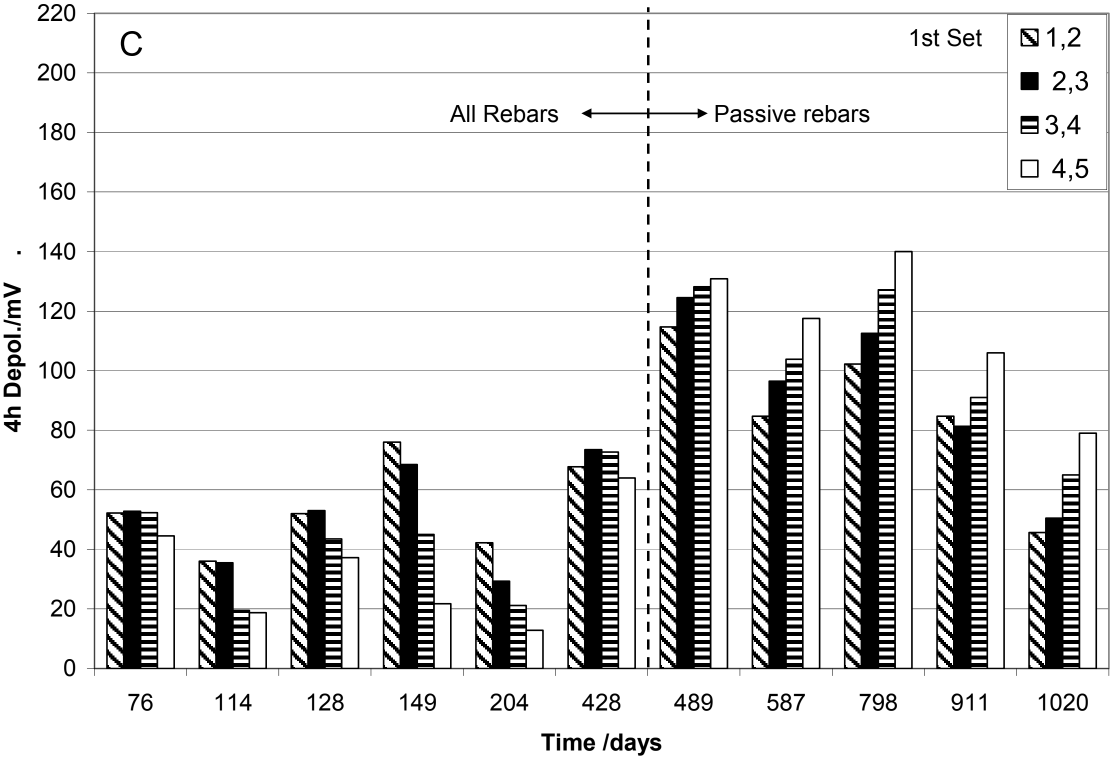

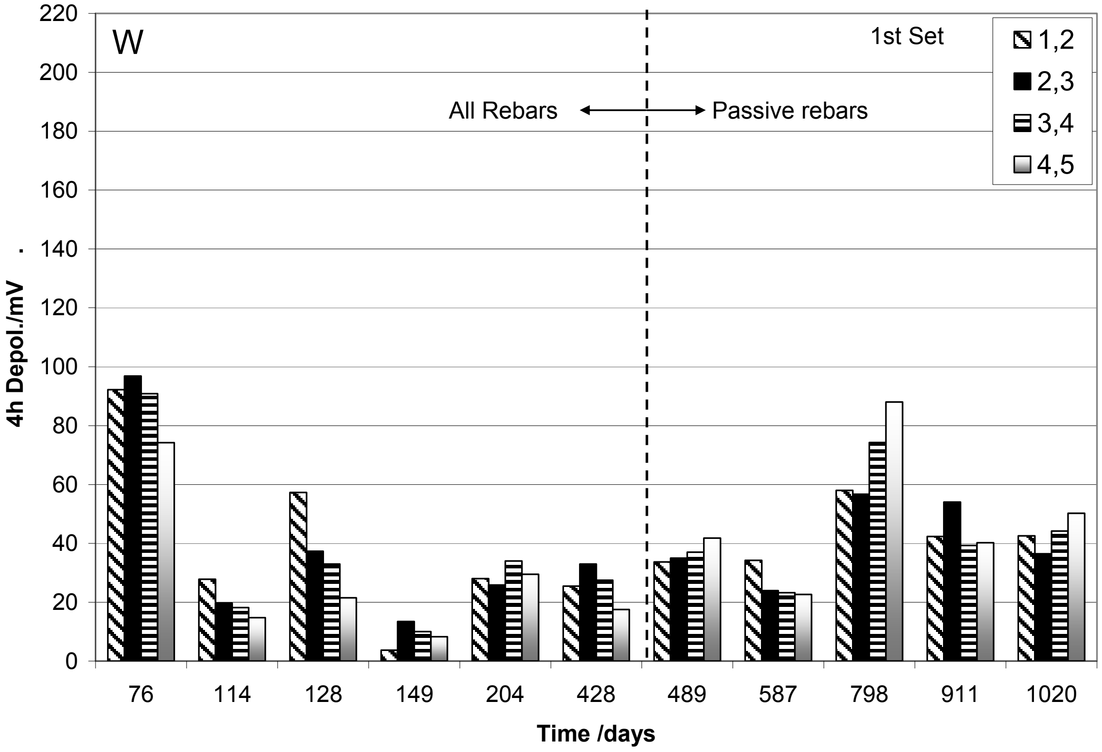

Figure 31 - 1st set of anodes. Summary of 4-h depolarization test results. Columns indicate average value for rebar pair indicated by numbers. Anode was located between rebars 4 and 5. Time indicates period since anode placement.

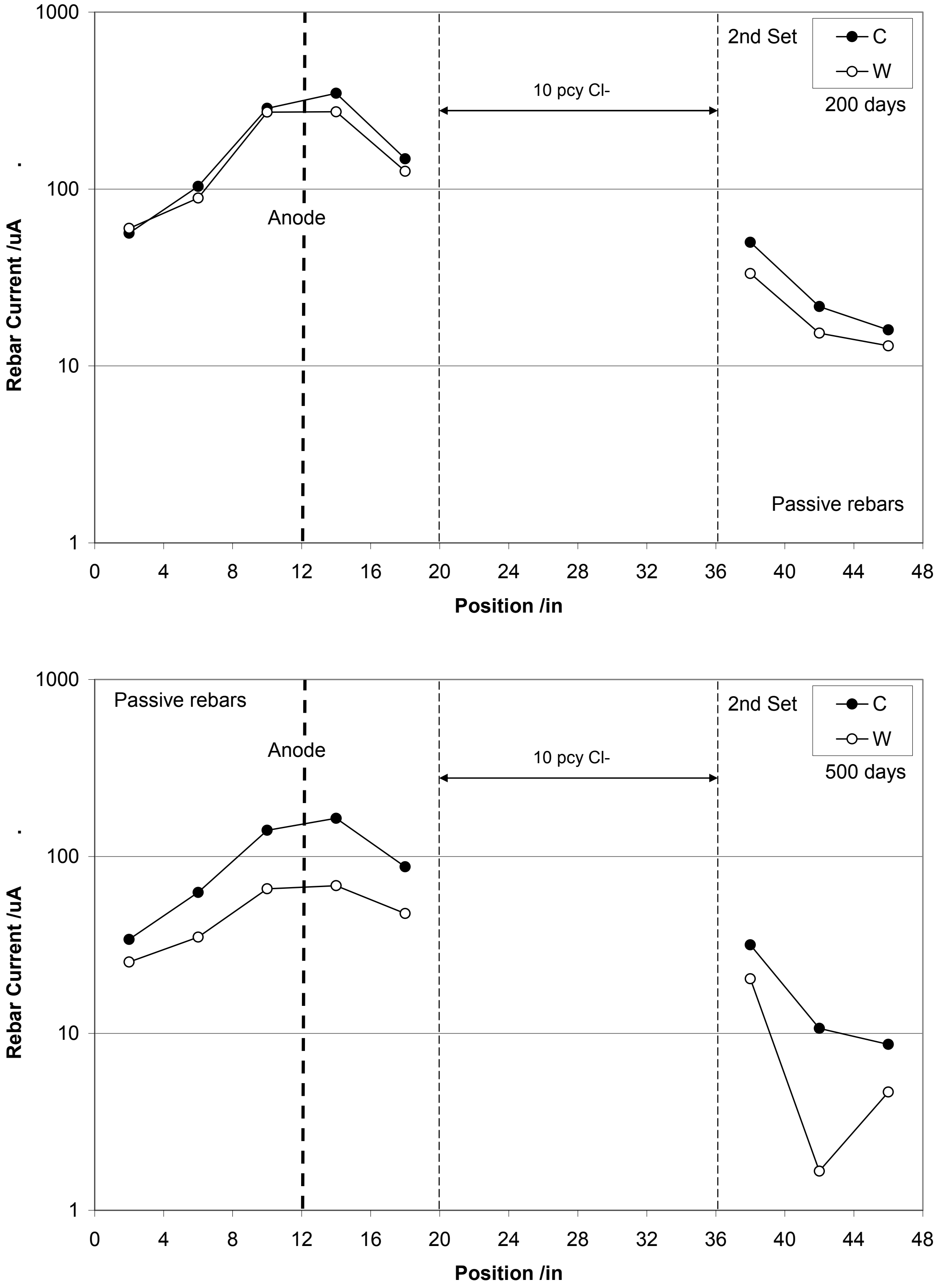

Figure 32 - 2nd set of anodes. Rebar current along the yard slab main direction at two different anode ages. Average of triplicate slabs. Only passive rebars connected. Time indicates period since placement of 2nd set anodes.

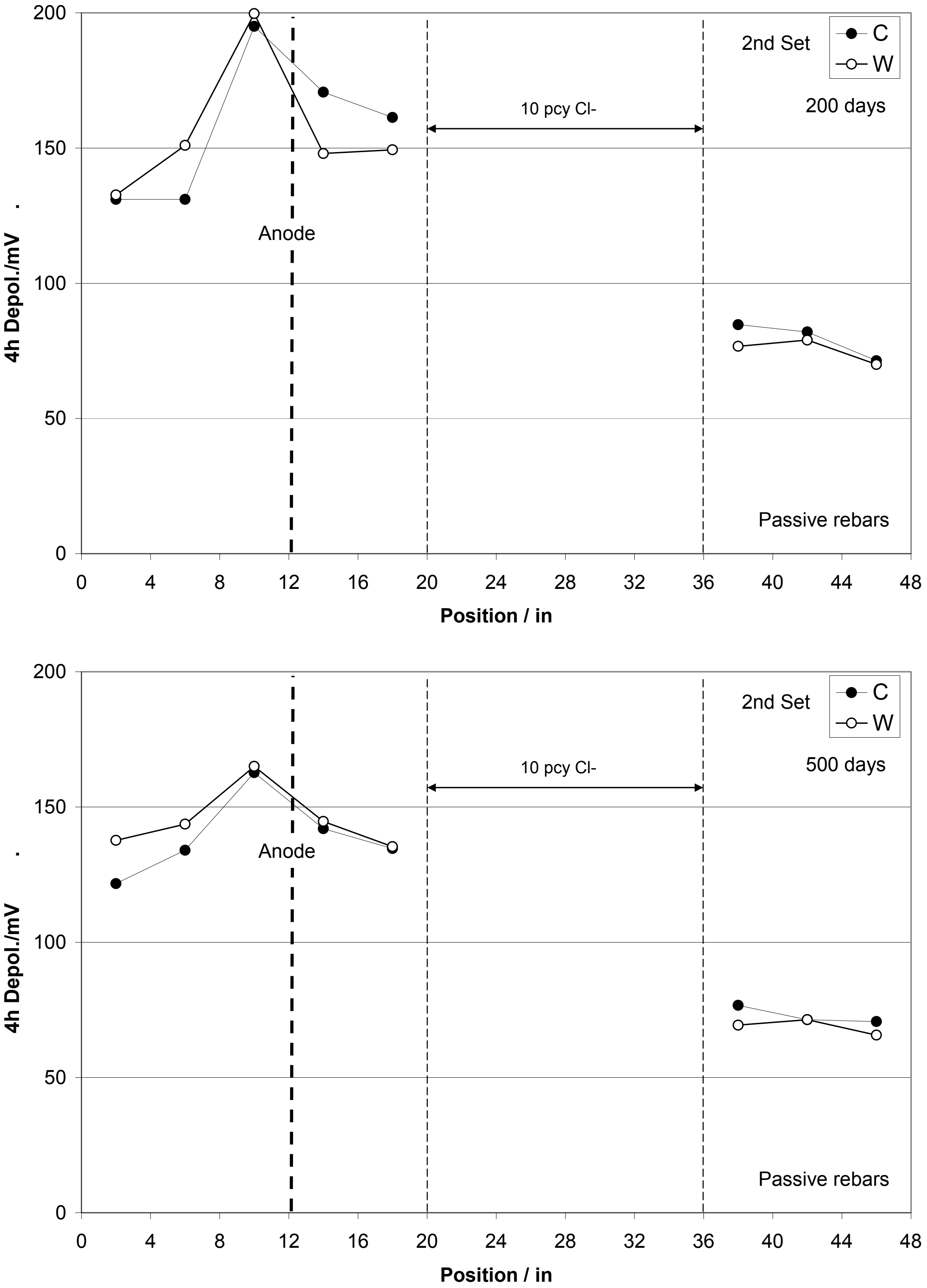

Figure 33 -Figure 20. 2nd set of anodes. Four-hour rebar depolarization after 14 months of normal exposure. Average results of triplicate slabs. Only passive rebars connected. Time indicates period since placement of 2nd set anodes.

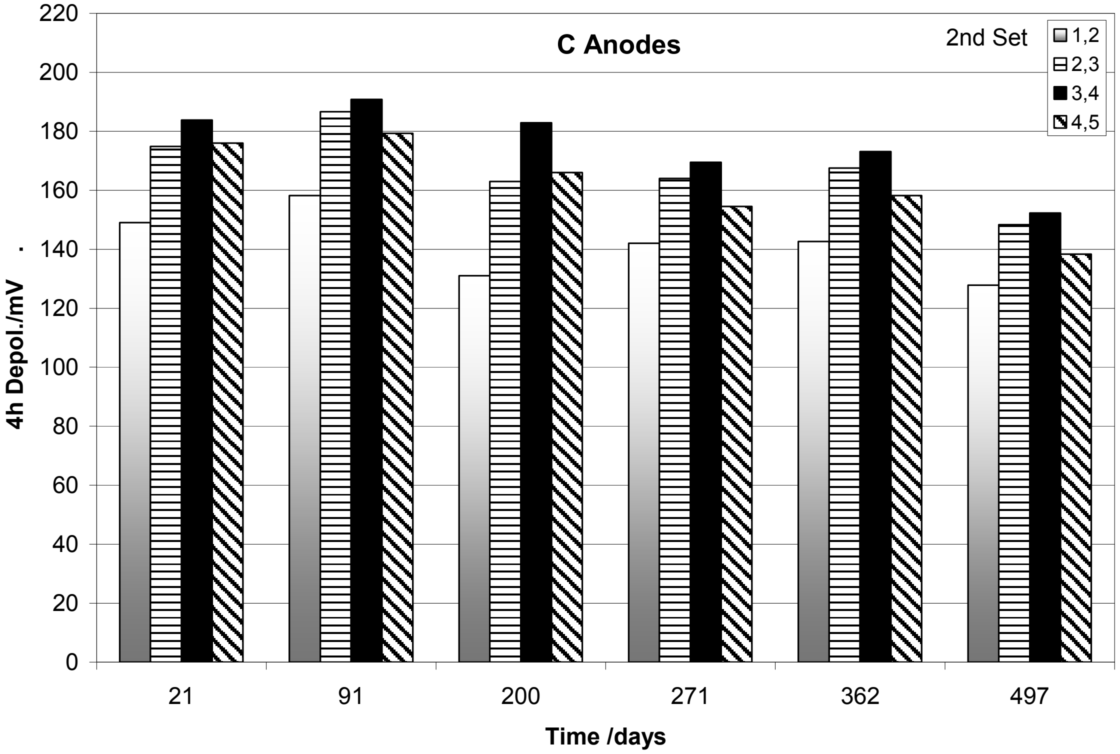

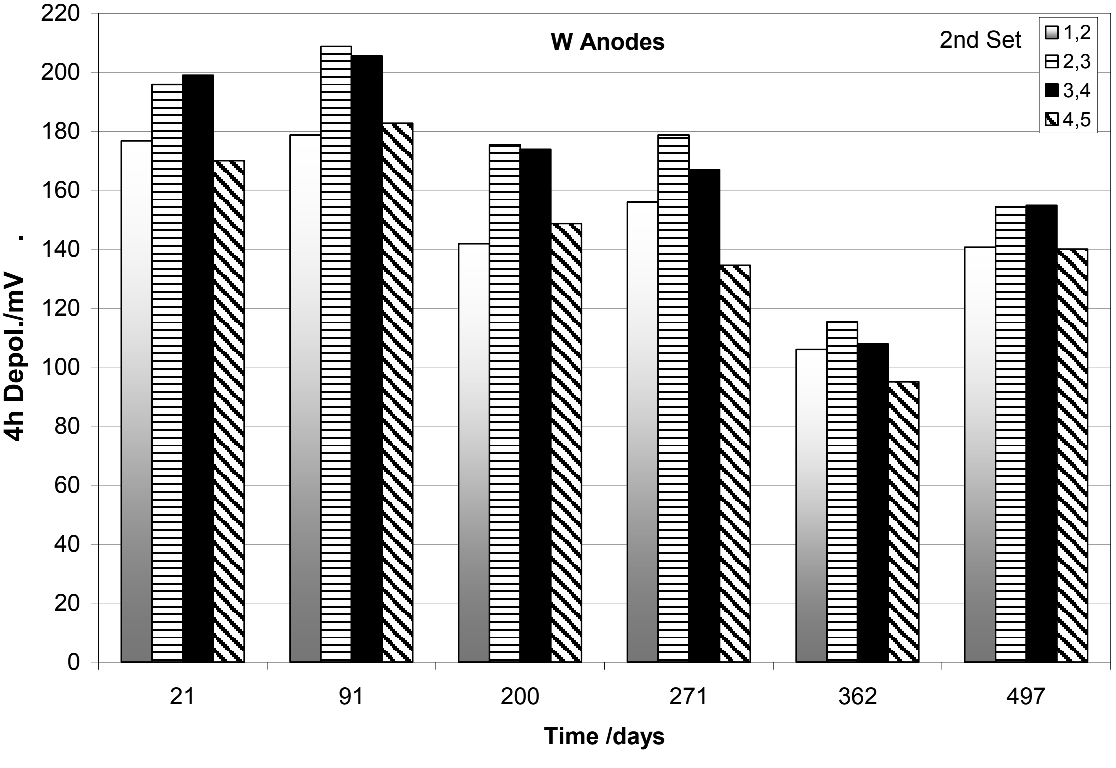

Figure 34 - Summary of 4-h depolarization test results, 2nd set of anodes. Columns indicate average value for rebar pair indicated by numbers. Anode was located between rebars 3 and 4. Time indicates period since placement of 2nd set anodes. Only passive rebars connected.

Each periodic measurement series of the test yard slabs yielded individual Instant-Off potential and current values for each of the passive rebars in every slab. At any given time those values covered a broad range depending on proximity of the rebar to the anode and condition of the anode, and the range varied further as the anodes aged. Since the rebar material was the same throughout and the concrete surrounding the rebar had (with exceptions noted below) the same composition, the combined results are expected to reflect the overall polarization behavior of the steel surface under those conditions. The graph in Figure 35, with results expressed as current densities by dividing current by the nominal rebar surface area confirms that expectation. There the data obtained from separate rebars in the six slabs, spanning a wide time period, generally delineate a cathodic polarization curve. The data in Figure 35 include results for rebars No. 1-5 and 10-12 for the 1st set of anodes, and rebars No. 1-4 and 11-12 for the 2nd set of anodes. Data for rebars No.5 and 10 while evaluating the 2nd. set of anodes are not included since, as discussed elsewhere, there was some evidence of chloride levels having increased there significantly by that time , causing incipient rebar activation in some cases. As expected, the large majority of the recorded net rebar currents were cathodic. The data reflect the typical scatter of test yard slab measurements, of which uncertainty in the potential value is expected to be a major contributor. The solid line represents a fit to the results based on an abstraction consisting of an activation-limited cathodic reaction current density and a potential-invariant passive dissolution anodic current density, as described in the Modeling section.

3.2.3 Concrete resistivity and anode resistance.

Average values of concrete resistivity of the zones with and without admixed chloride of all slabs as function of time since casting the concrete are shown in Figure 36. The resistivity increased with age toward a long term average value approaching 25 $\kappa\Omega$-cm for the zone without chloride, and about half as much for the zone with admixed chloride. There was modest variability from slab to slab (standard deviation typically <20% of the average).

Anode to rebar assembly resistance measurements for the 2nd set of anodes, averaged for a period between ~1 and ~1.5 years after placement were ~240 and 290 Ω for the Type C and Type W anodes respectively. From calculations performed in the Modeling section, it is estimated that ~2/3 of the anode to rebar assembly resistance is due to the anode-concrete current spread resistance.

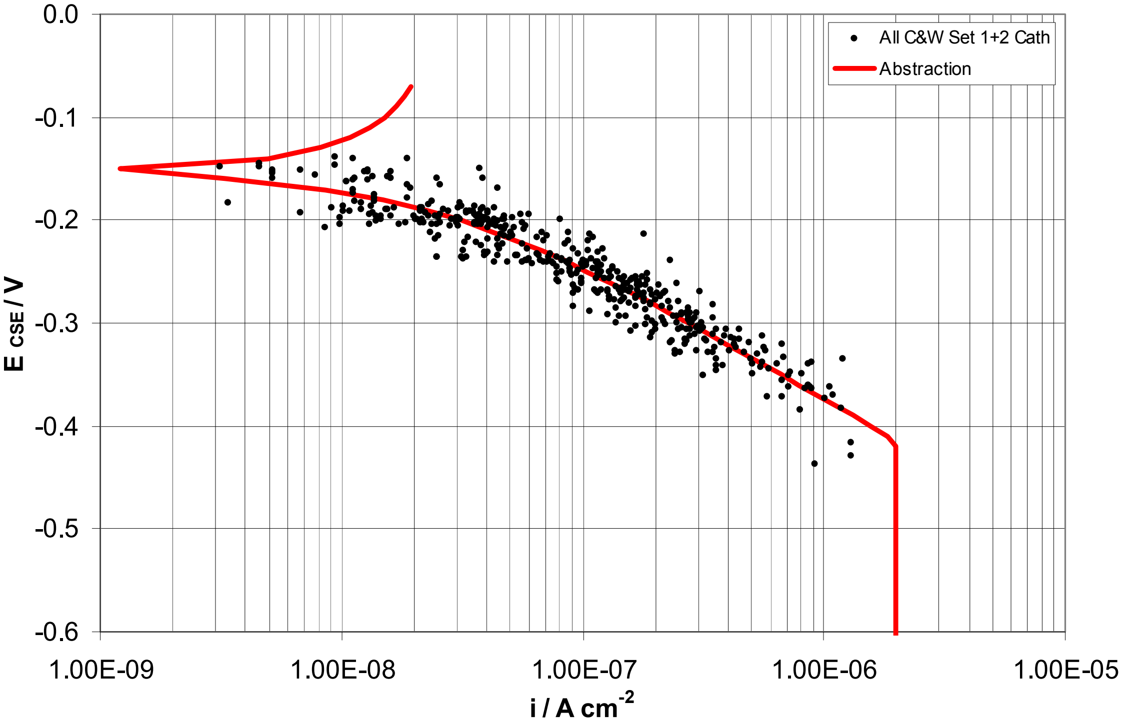

Figure 35 - Combined E_{IO}-log i representation of the individual Instant-Off potential and current density values for passive rebars recorded during evaluation of both sets of anodes. Filled symbols indicate cathodic current; open symbols indicate rare instances of anodic currents. The abstraction function is discussed in the Modeling section.

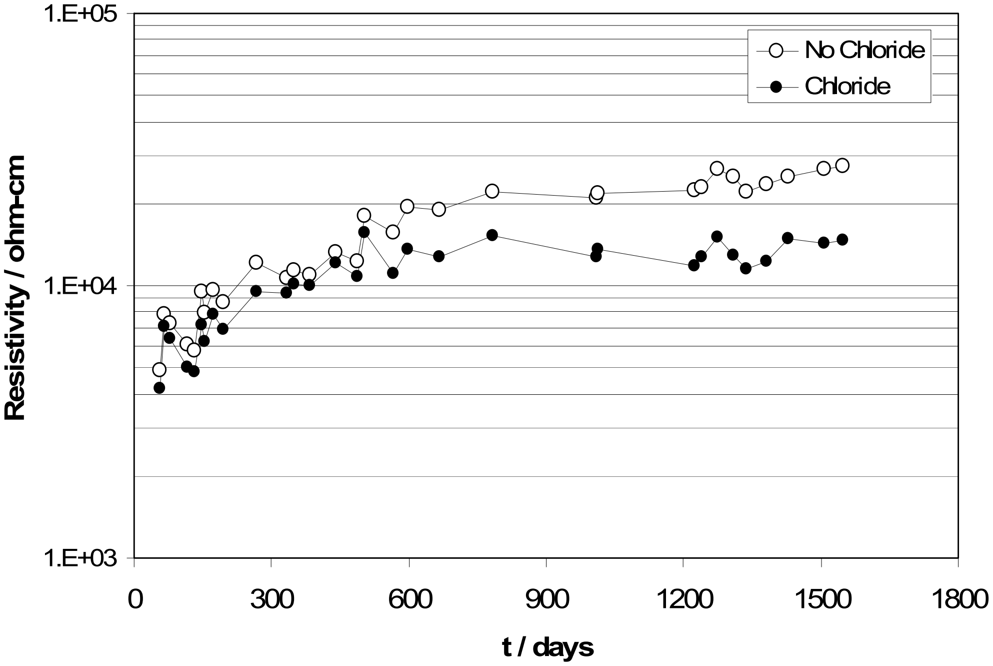

Figure 36 - Concrete resistivity of the zones with and without admixed chloride of all slabs as function of time since casting the concrete. Average values of the 6 slabs.

3.3 Results, Field Installations

3.3.1 Test Site 1

Results of physical condition surveys of the test locations are listed in Table 2. Electric resistance of the combined anode assemblies to the rebar at the wired test locations was measured with a soil resistivity meter similar to the one use for the test yard slabs. Results were affected by uncertainty in that the resistance reported for the initial condition was one order of magnitude or greater than the values reported in subsequent visits. The values measured at 189 days after anode energizing for the Type C anode locations 10-3 and 11-5 were 7.8 Ω and 4.2 Ω respectively. For the Type W anode locations 10-1 and 10-4 the values were 1.6 Ω and 0.3 Ω respectively. Individual anode resistance measurements suggested that at least two short circuits between individual anodes and the rebar assembly occurred at each of the Type W anode locations.

At this site parts of most patches were at or near the tidal zone. Thus, potentials before as well as after repair and anode energizing tended to span a range from values typical of submerged concrete at low elevations, to those of drier concrete at higher elevations. This is illustrated in Figure 37 for Type C anode location 10-3.

The combined anode current was divided by the number of anodes at each location. The result is reported in Figure 38 as average anode current, I_{AVGE}, as function of time since repair patching. It is recalled that at this site the anodes were not connected to the rebar assembly until a period ranging from 53 days to 111 days had elapsed from the day of repair patching. In Figure 38 and those following, t=0 corresponds to the day of repair patching. The first I_{AVGE} datum corresponds to the moment of energizing the anodes. For both Type C anode locations I_{AVGE} started at values in the order of 1-2 mA and dropped by about one order of magnitude after 1200 days. The measured current for the W anodes started at values comparable to that of the C anodes but dropped very fast afterwards, reaching values 2 orders of magnitude smaller after about 2 years.

Figure 39 shows steel potentials values averaged for positions 3, 6 and 12 inches (7.6, 15 and 30 cm) away from the patch, as well as anode Instant-Off potentials averaged for the test positions on top of the anodes. The results are presented for each of the anode test locations as function of time elapsed from the day of repair patching. Solid symbols for steel potentials indicate the pre-patching condition. The first open symbol of each steel series corresponds to the moment just before the anode assembly was energized; all subsequent values are Instant-Off measurements. Anode potentials were available only for the times indicated. Figure 40 shows results for the control locations (no anodes installed) presented otherwise similarly to those in Figure 39.

The results of the steel depolarization tests performed at various ages of the installations are presented in Figures 41 to 44 (one for each of the anode test locations) in the form of cumulative distribution curves. The rightmost point of each curve represents the largest value measured around the perimeter of the patch, at the indicated distance from the patch edge, at the time of the test. That depolarization amount is assigned a cumulative fraction n/(n+1), where n is the number of test points around the patch perimeter at the indicated distance. The other values are assigned fractions = j/(n+1), where j =1 for the smallest value, 2 for the next, and so on. The cumulative fraction so obtained is an estimate of the probability that all similar measurements will yield an equal or smaller depolarization value [Mac Berthouex, 2002]. Thus, the value for which the cumulative fraction equals 0.5 corresponds to the median of the distribution. Positive potential decay values indicate that the steel potential increased above its Instant-Off value over the depolarization interval (usually ~1 day), showing that the steel was being cathodically polarized. It is noted that in several instances many of the values were negative, suggesting that part of the steel was effectively anodic to the rest of the system including the point anode.

Individual cumulative distributions showed often a wide range of depolarization values. Preliminary analysis could not clearly determine if some of that spread reflected a dependence of polarization conditions with elevation (as manifested for steady state values in Figure 37). More detailed examination of this issue is left for future investigation. With some exceptions the distribution curves were roughly symmetric around the median point. Consequently he results were on first approximation treated as normal distributions; average and standard deviation values were calculated for each curve and are reported in Tables 4 and 5 for locations with anode Types C and W respectively.

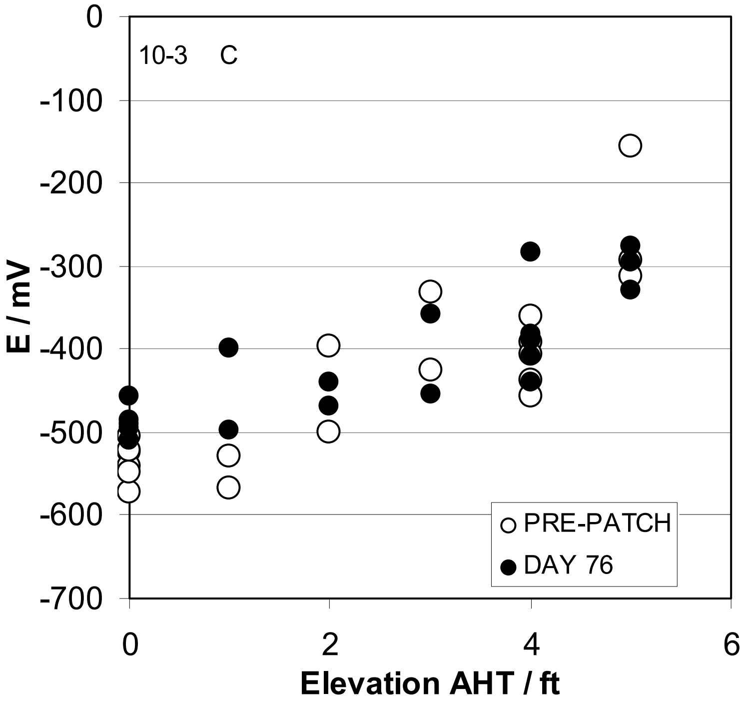

Figure 37 - Field Site 1. Potential measured at a distance 3 in from the patch zone edge just before (PRE-PATCH) the location was repaired by concrete removal and patching at 0 days, and 76 days later (DAY 76, Instant-Off measurements). The anodes were energized at t=70 days. The results are shown as function of elevation above the high tide (AHT) level. Location 10-3, furnished with Type C anodes.

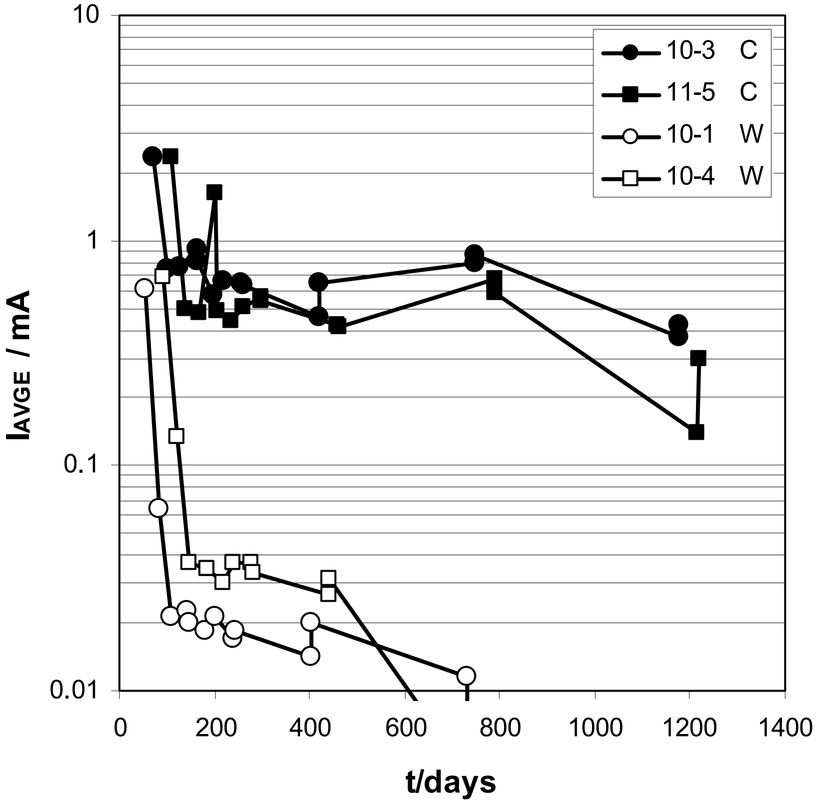

Figure 38 - Field Site 1. Average anode current for each wired site as function of time elapsed since repair and patching. Legend details test location and type of anode. First datum corresponds to the moment of anode energizing.

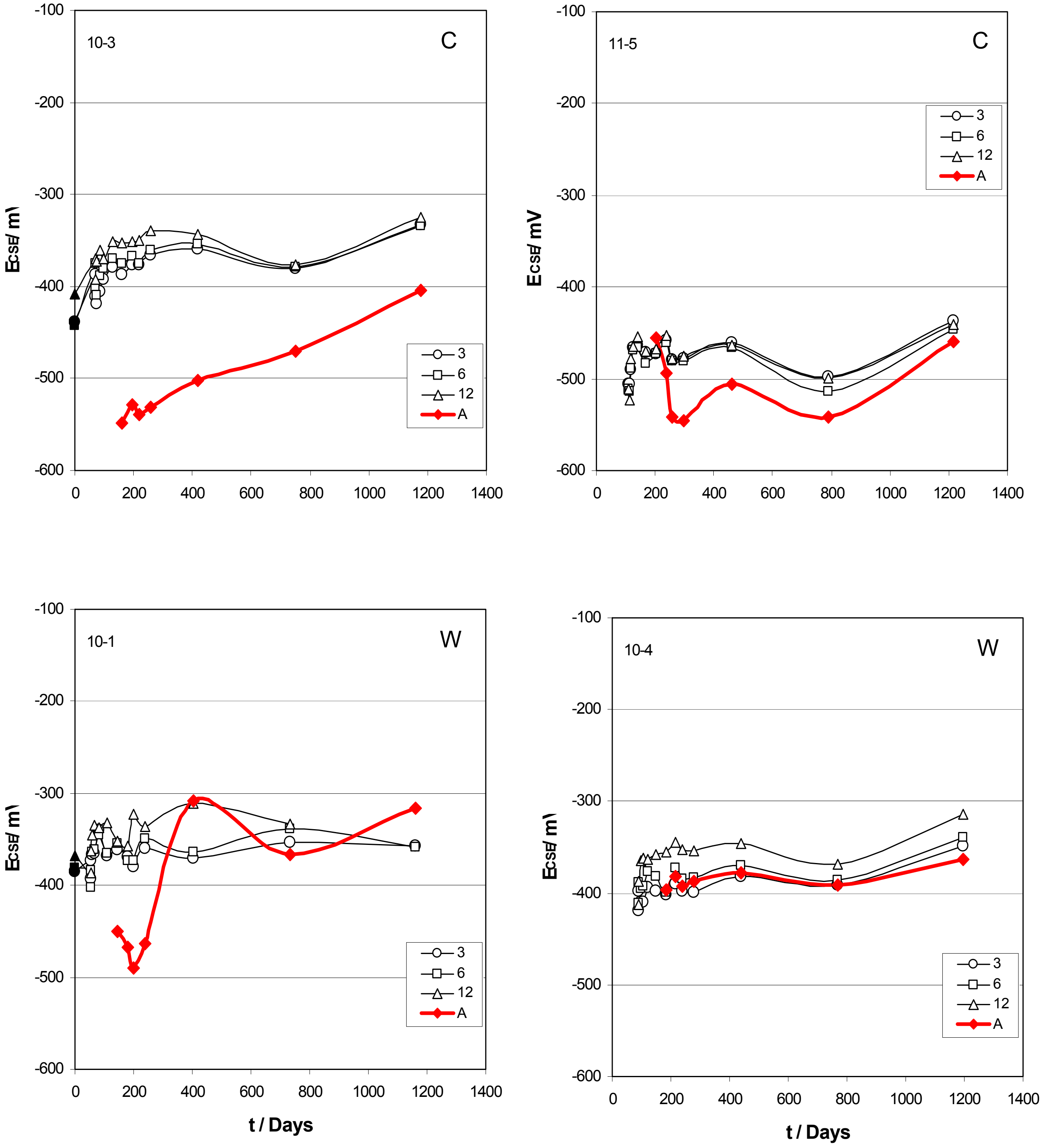

Figure 39 - Field Site 1. Anode test locations. Open symbols: Steel potential averaged for the indicated distance (inches) from the patch perimeter. First datum corresponds to value just before anode energizing; all others are Instant-Off measurements. Filled symbols at t=0 denote, if data available, steel potential just before repair and patching. Series A indicates anode Instant-Off potential, whenever available.

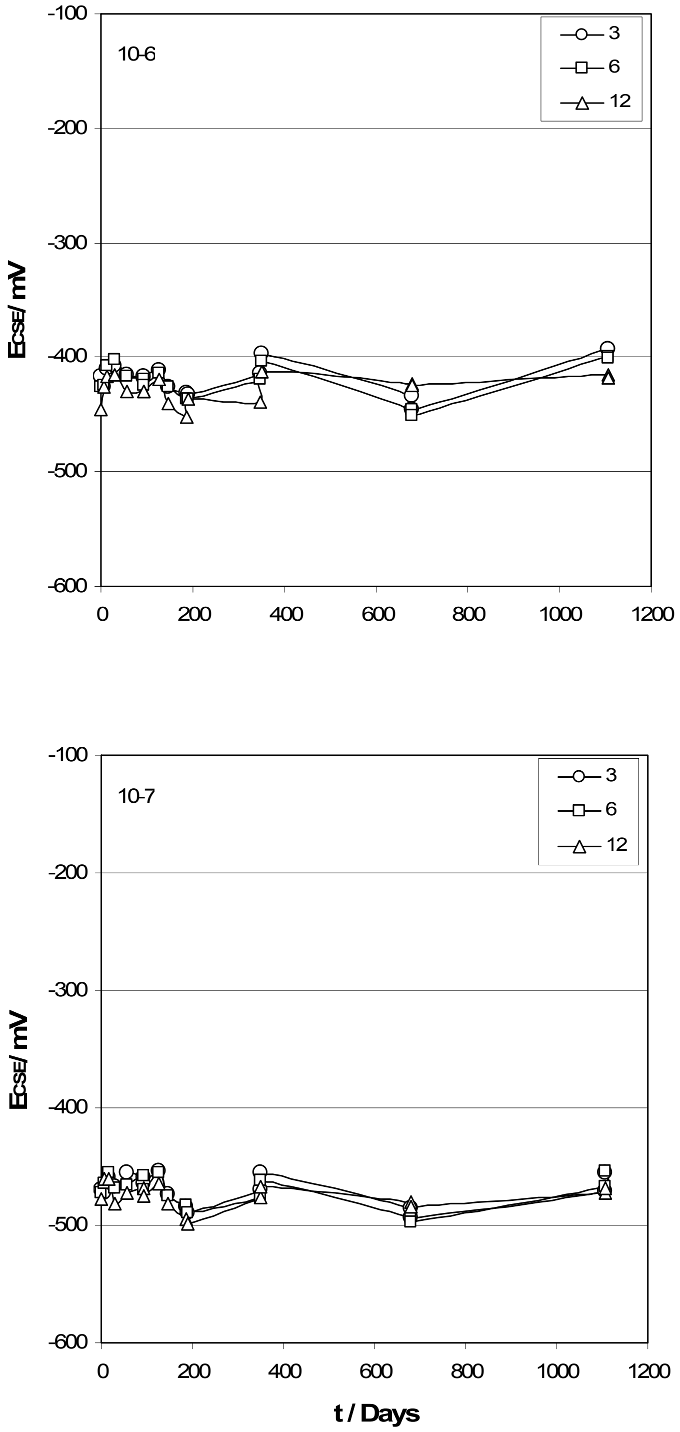

Figure 40 - Field Site 1. Control test locations with no anodes. Open symbols: Steel potential averaged for the indicated distance (inches) from the patch perimeter. Patching took place at 0 days.

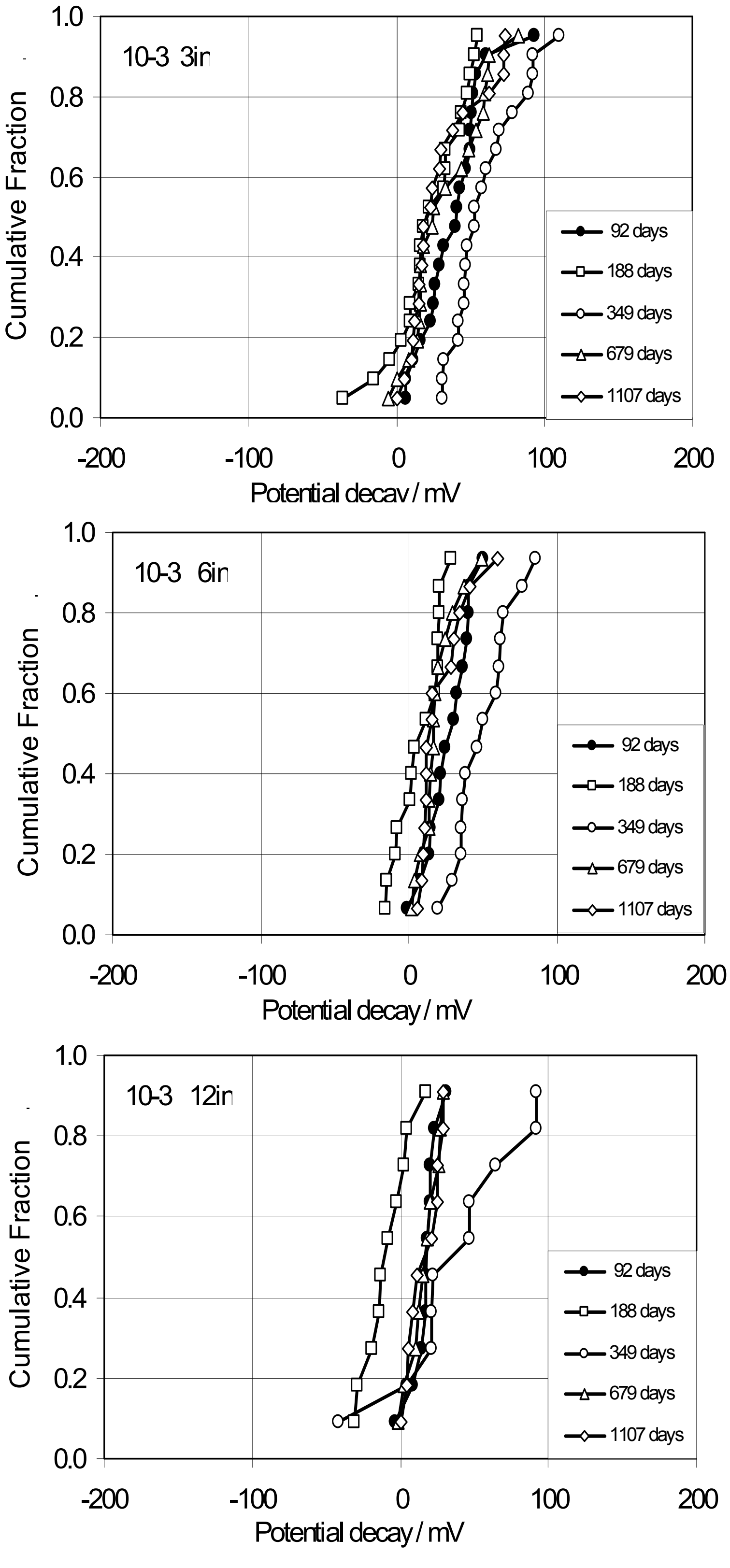

Figure 41 - Field Site 1, location 10-3 (Type C anodes). Cumulative distribution of steel depolarization decay values for test points at the indicated distance from the patch edge at various times since energizing the anodes. Positive values indicate steel was polarized cathodically.

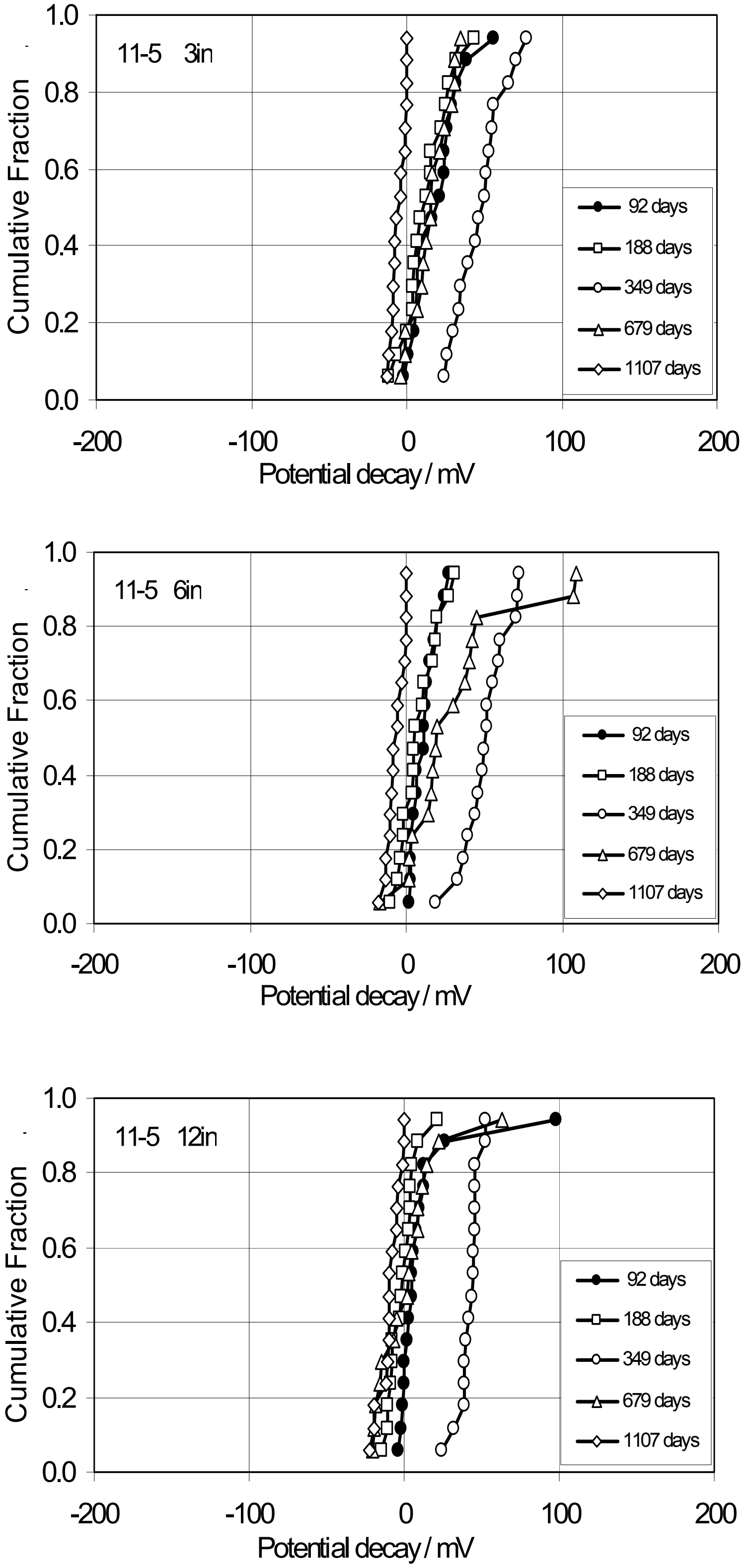

Figure 42 - Field Site 1, location 11-5 (Type C anodes). Cumulative distribution of steel depolarization decay values for test points at the indicated distance from the patch edge at various times since energizing the anodes. Positive values indicate steel was polarized cathodically.

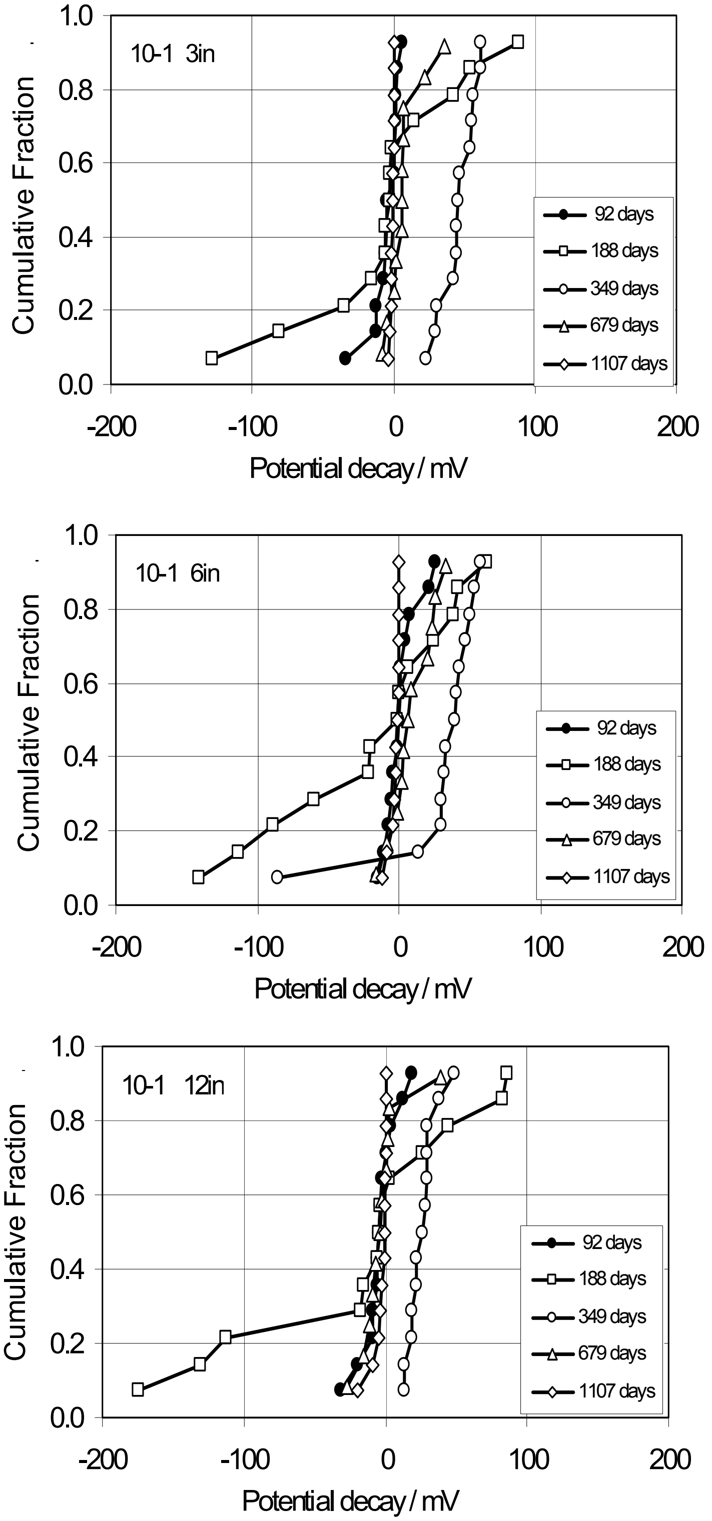

Figure 43 - Field Site 1, location 10-1 (Type W anodes). Cumulative distribution of steel depolarization decay values for test points at the indicated distance from the patch edge at various times since energizing the anodes. Positive values indicate steel was polarized cathodically.

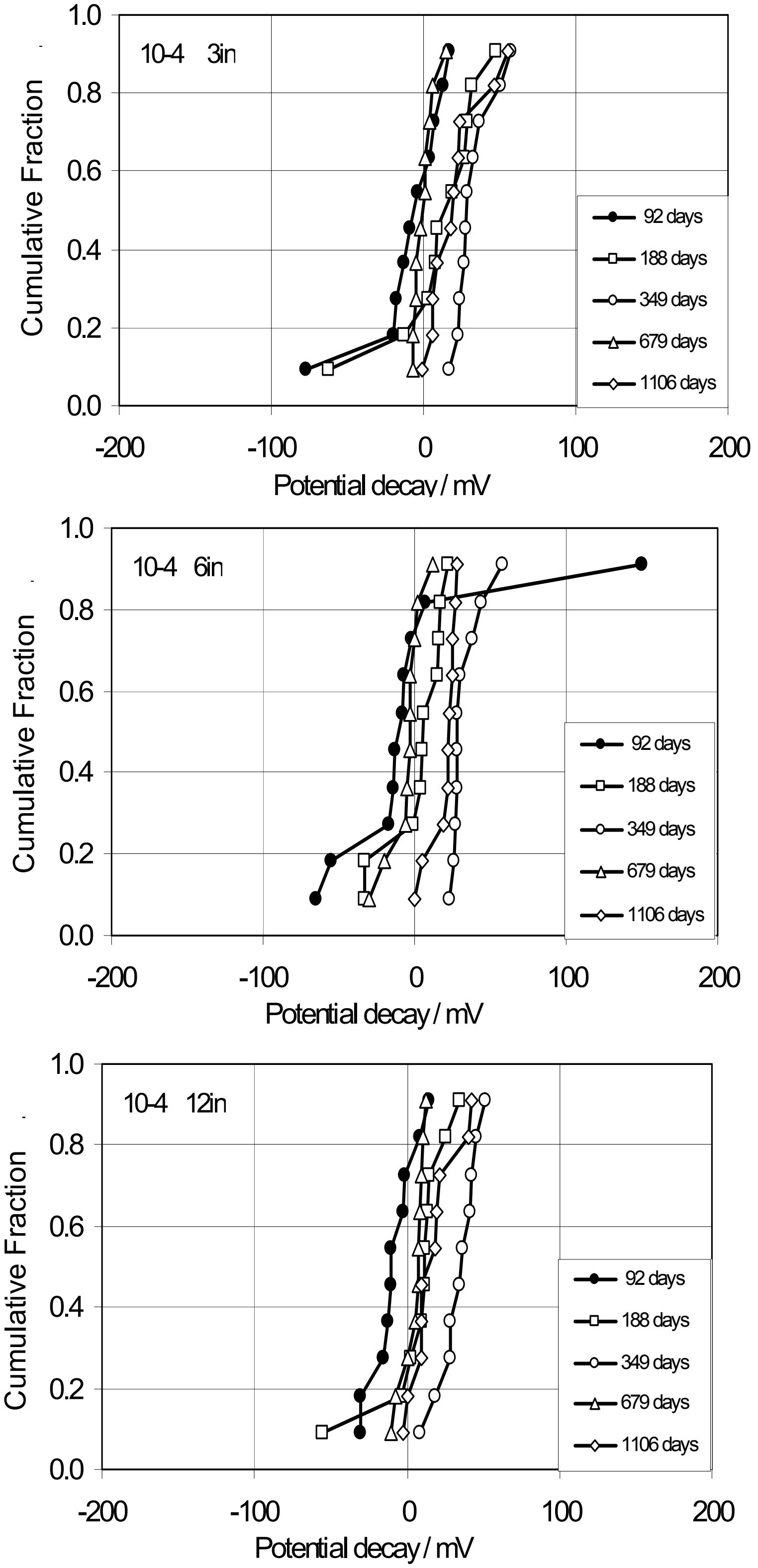

Figure 44 - Field Site 1, location 10-4 (Type W anodes). Cumulative distribution of steel depolarization decay values for test points at the indicated distance from the patch edge at various times since energizing the anodes. Positive values indicate steel was polarized cathodically.

Table 4 - Field Site 1. Summary of depolarization observations for Type C anode test locations.

Location and distance from patch edge / in		Age (days)	Average Decay / mV	Standard deviation / mV	Type of anode	Number of anodes
10-3	3	92	27	14	C	10
		188	22	24		
		349	45	10		
		679	33	25		
		1107	15	8		
	6	92	27	14		
		188	7	15		
		349	50	19		
		679	19	13		
		1107	21	16		
	12	92	17	9		
		188	-9	15		
		349	37	41		
		679	16	10		
		1107	16	11		

Location and distance from patch edge / in		Age (days)	Average Decay / mV	Standard deviation / mV	Type of anode	Number of anodes
11-5	3	92	13	10	C	10
		188	13	15		
		349	42	11		
		679	16	12		
		1107	-7	4		
	6	92	11	8		
		188	8	12		
		349	51	14		
		679	31	35		
		1107	-7	6		
	12	92	11	24		
		188	-1	9		
		349	42	7		
		679	3	21		
		1107	-9	7		

Table 5 - Field Site 1. Summary of depolarization observations for Type W anode test locations

Location and distance from patch edge / in		Age (days)	Average Decay / mV	Standard deviation / mV	Type of anode	Number of anodes
10-1	3	92	-5	10	W	7
		188	-6	55		
		349	46	12		
		679	7	12		
		1107	-1	1		
	6	92	1	12		
		188	-21	63		
		349	30	37		
		679	9	15		
		1107	-3	4		
	12	92	-5	13		
		188	-17	78		
		349	26	10		
		679	-3	16		
		1107	-3	6		

Location and distance from patch edge / in		Age (days)	Average Decay / mV	Standard deviation / mV	Type of anode	Number of anodes
10-4	3	92	-10	27	W	6
		188	10	31		
		349	33	12		
		679	0	7		
		1106	21	18		
	6	92	-2	58		
		188	2	20		
		349	33	11		
		679	-6	12		
		1106	20	9		
	12	92	-9	14		
		188	6	24		
		349	33	13		
		679	4	7		
		1106	17	15		

.

3.3.1 Test Site 2

Results of physical condition surveys of the test locations are listed in Table 3. Combined electric resistance to the rebar assembly for the Type C and Type W locations measured initially, were 1.5 Ω and 7.8 Ω respectively. Later measurements showed comparable results.

It is recalled that at this site the anodes and test points tend to span a relatively narrow elevation range so variation of results with elevation was limited. Results are presented in a manner similar to that for Site 1 to which reference is made for explanation of the variables reported.

Average anode current, I_{AVGE}, as function of time since repair patching is shown in Figure 45 for the two wired locations in this site. The water level at the time of each measurement is also indicated, as the distance from the water line to the bottom of the footer. In that scale, mean high tide is at approximately 24 in. Unlike at Site 1, the anodes at the wired locations were energized within one week of the day of repair patching. Both types of anodes showed high initial currents, comparable to those of Type C anodes in Site 1. The reported current of the Type C anodes dropped only moderately over the ~ 600 day test period. Some of the variation between consecutive measurements reflects tidal levels. Unlike at Site 1, the current for the W anodes did not drop precipitously early on. Instead, the data available so far indicates that it maintained a trend, relative to its initial value, comparable to that of the Type C anodes after allowing for temporary differences induced by tidal level.

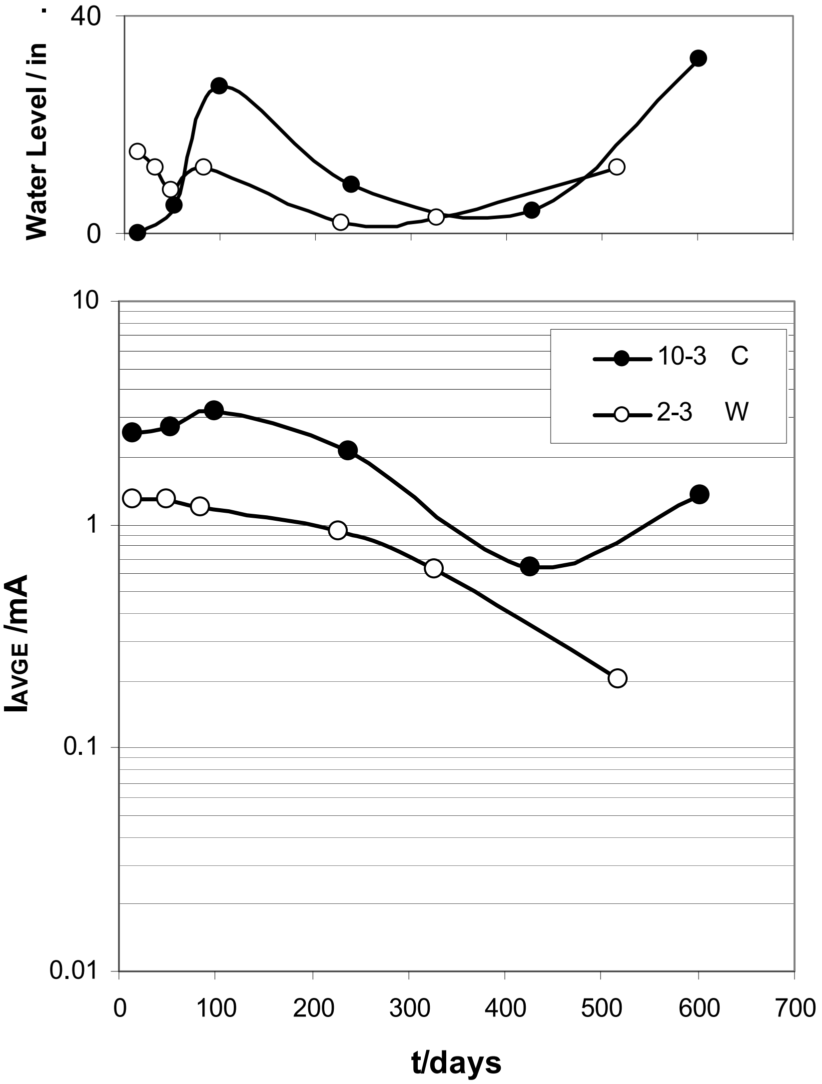

Figure 45 - Field Site 2. Average anode current for each wired site, and water level at the time of the measurement, as function of time elapsed since repair and patching. Legend details test location and type of anode. First datum corresponds to the moment of anode energizing. Water level is measured from water line to bottom of the footer.

Figure 46 shows steel potentials values averaged for positions away from the patch, as well as anode Instant-Off potentials averaged for the test positions on top of the anodes. Presentation follows the pattern used for Site 1, Figure 39. Steel potentials in the pre-patching condition were available only for locations 10-1 and 10-3. Anode potentials were available only for the times indicated.

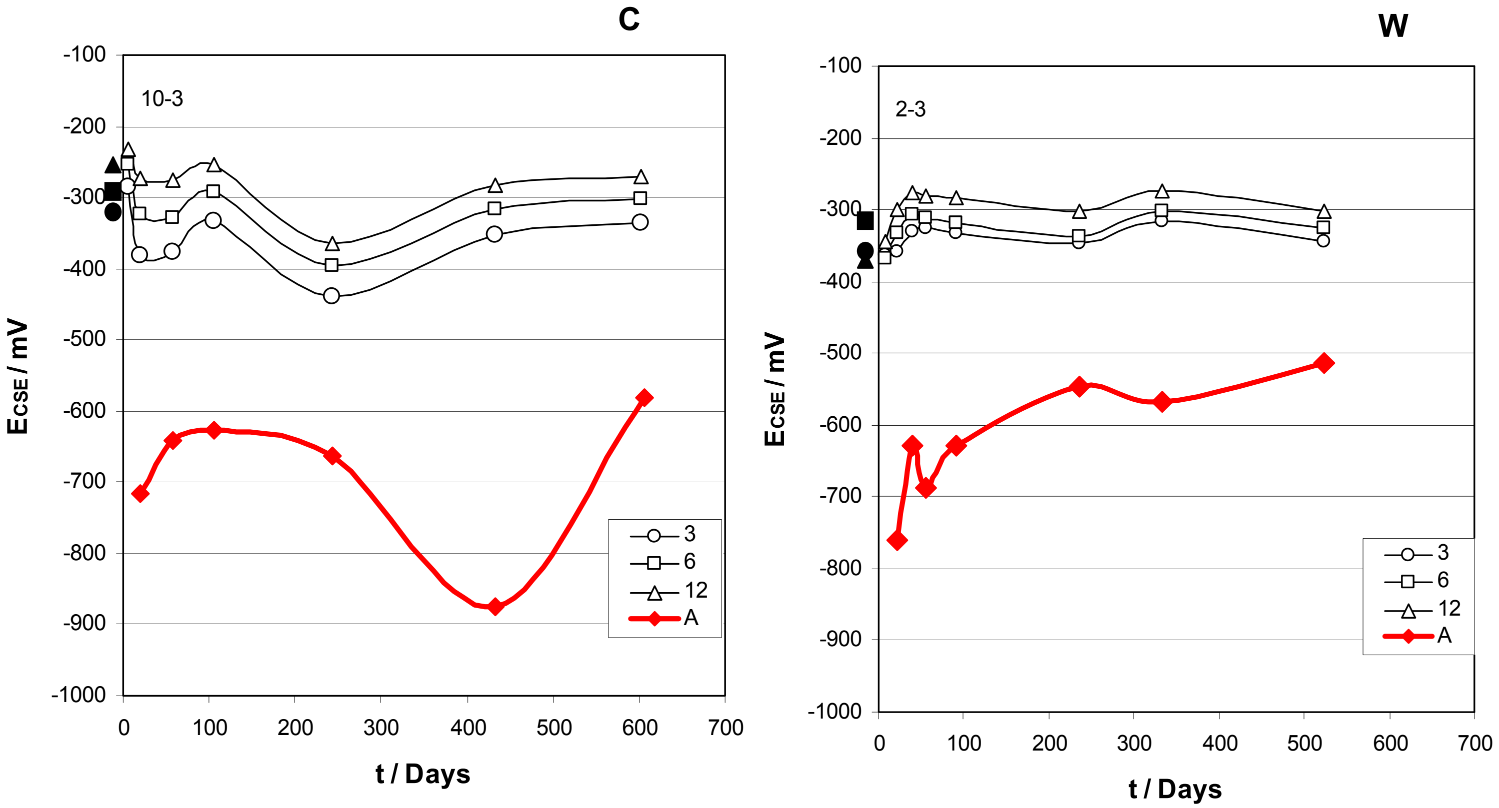

Figure 46 - Field Site 2. Anode test locations. Open symbols: Steel potential averaged for the indicated distance (inches) from the patch perimeter. First datum corresponds to value just before anode energizing; all others are Instant-Off measurements. Filled symbols at t=0 denote steel potential just before repair and patching. Series A indicates anode Instant-Off potential, whenever available.

Figure 47 shows the average Current-On steel potentials for the wired Type C anode location 10-3. Figure 48 presents the Current-On average steel potentials for the wired Type W anode location 2-3 as well as the averaged steel potentials for the three permanently connected Type W anode locations. Figure 49 shows the average steel potentials for the four control locations with no anodes. The Current-On potential data for the wired locations is shown to permit direct comparison with the results from the permanently connected and control locations.

Steel depolarization results were available for only two and one test times in the wired Type C and Type W anode locations respectively. Results are presented in Figures 50 and 51 in the manner detailed in the Field Site 1 section. Unlike in Site 1, the depolarization values were nearly all in the expected positive direction and subject to less variability. A summary of depolarization results is presented in Table 6.

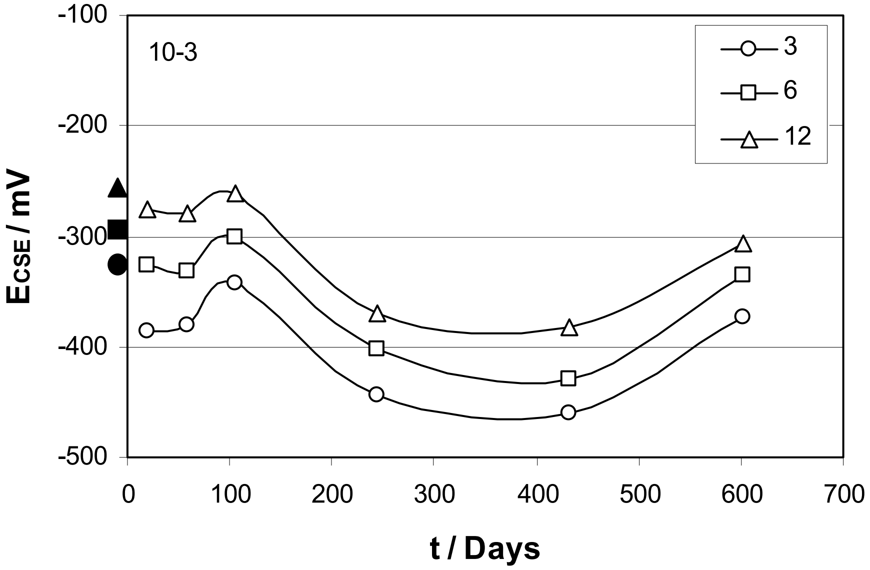

Figure 47 - Field Site 2. Current-On steel potential evolution of the wired location with C anodes. Potential is averaged for the indicated distance (inches) from the patch perimeter. Filled symbols at t=0 denote steel potential just before repair and patching. Patching took place at 0 days.

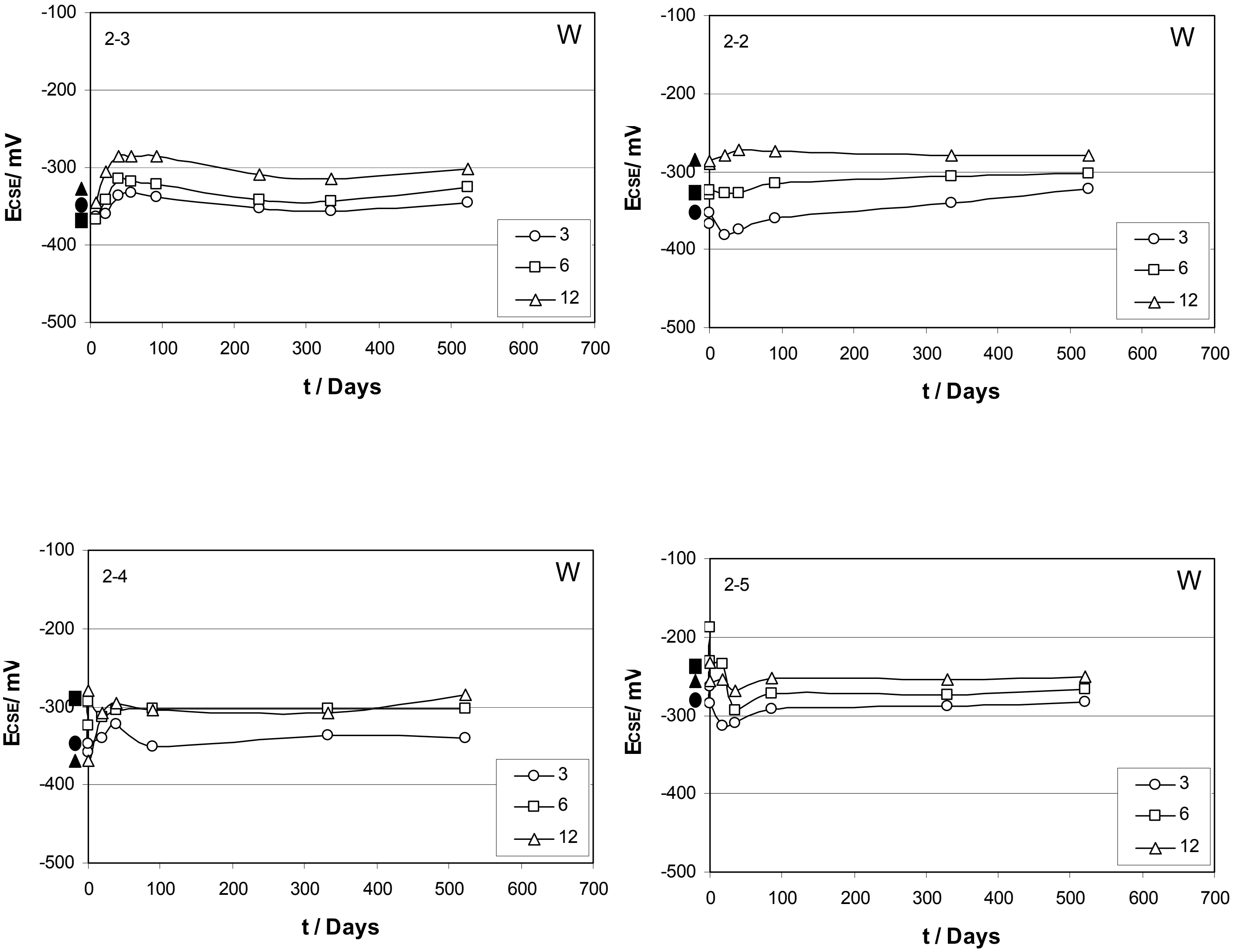

Figure 48 - Field Site 2. Steel potential evolution of all locations with W anodes. Location 2-3 is instrumented and potentials reported are Current-On. The other 3 locations have anodes permanently connected to the rebar assembly. Potential is averaged for the indicated distance (inches) from the patch perimeter. Filled symbols at t=0 denote steel potential just before repair and patching. Patching took place at 0 days.

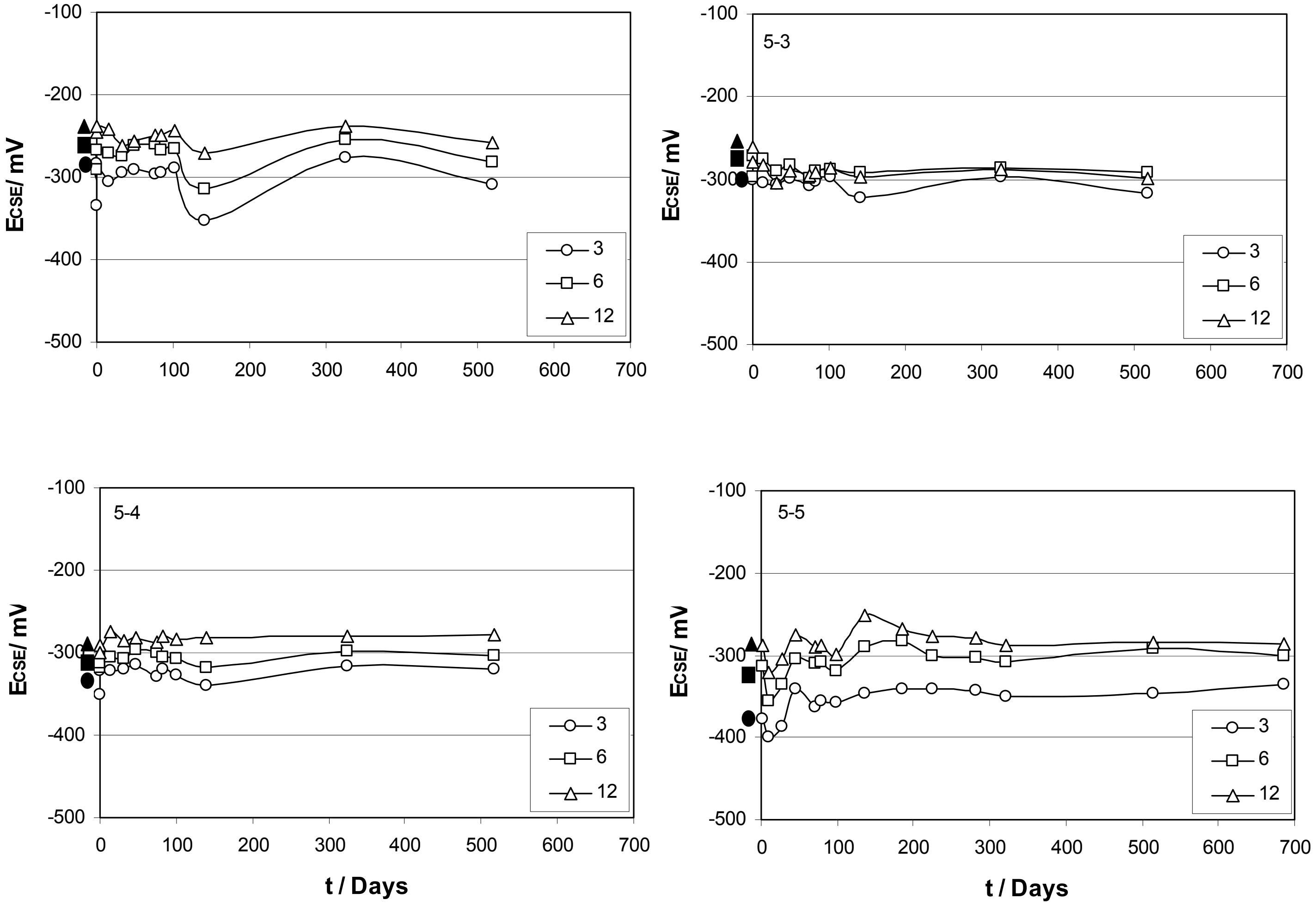

Figure 49 - Field Site 2. Control test locations with no anodes. Control test locations with no anodes. Open symbols: Steel potential averaged for the indicated distance (inches) from the patch perimeter. Filled symbols at t=0 denote steel potential just before repair and patching. Patching took place at 0 days.

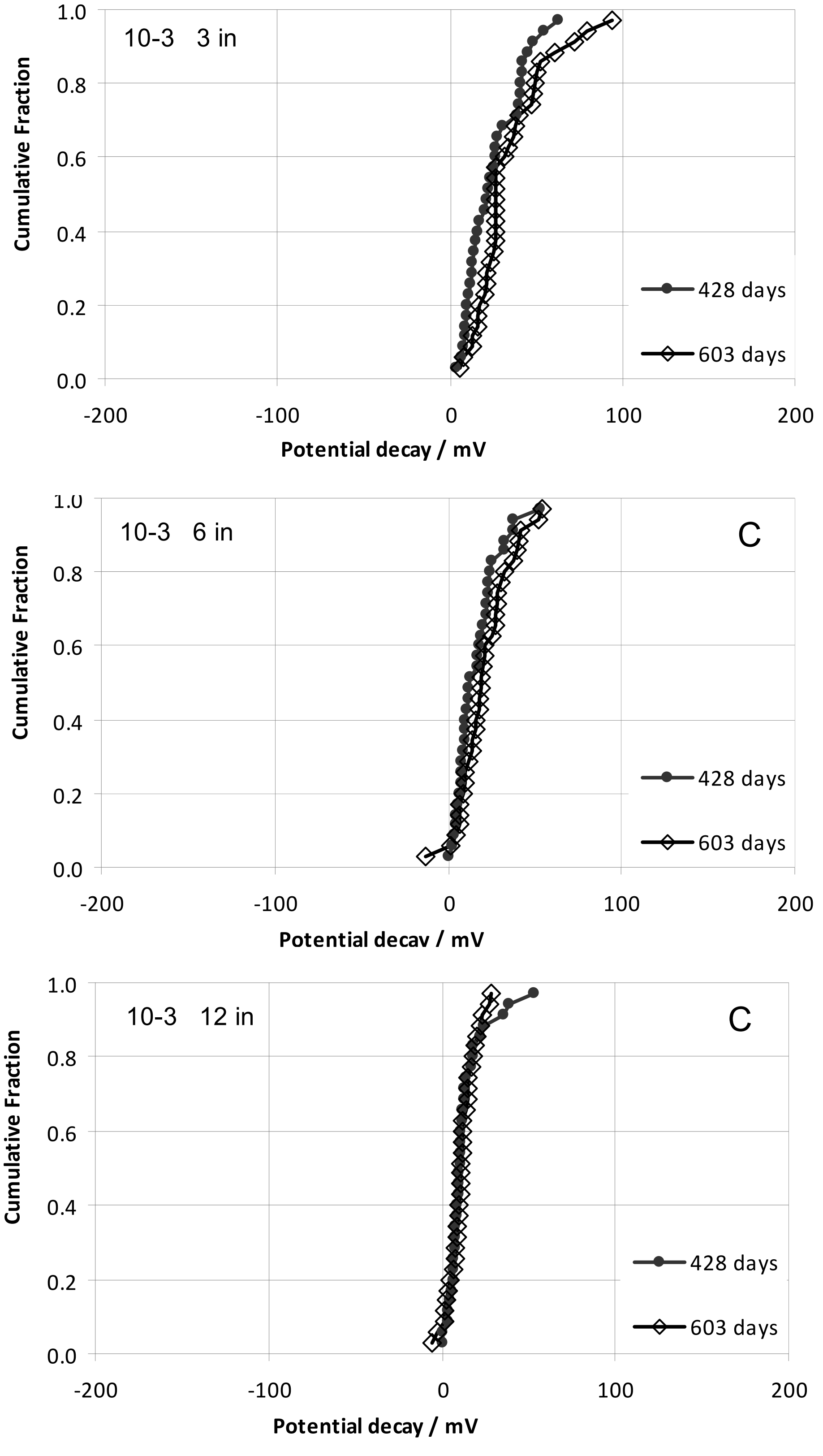

Figure 50 - Field Site 2, location 10-3 (Type C anodes). Cumulative distribution of steel depolarization decay values for test points at the indicated distance from the patch edge at various times since energizing the anodes. Positive values indicate steel was polarized cathodically.

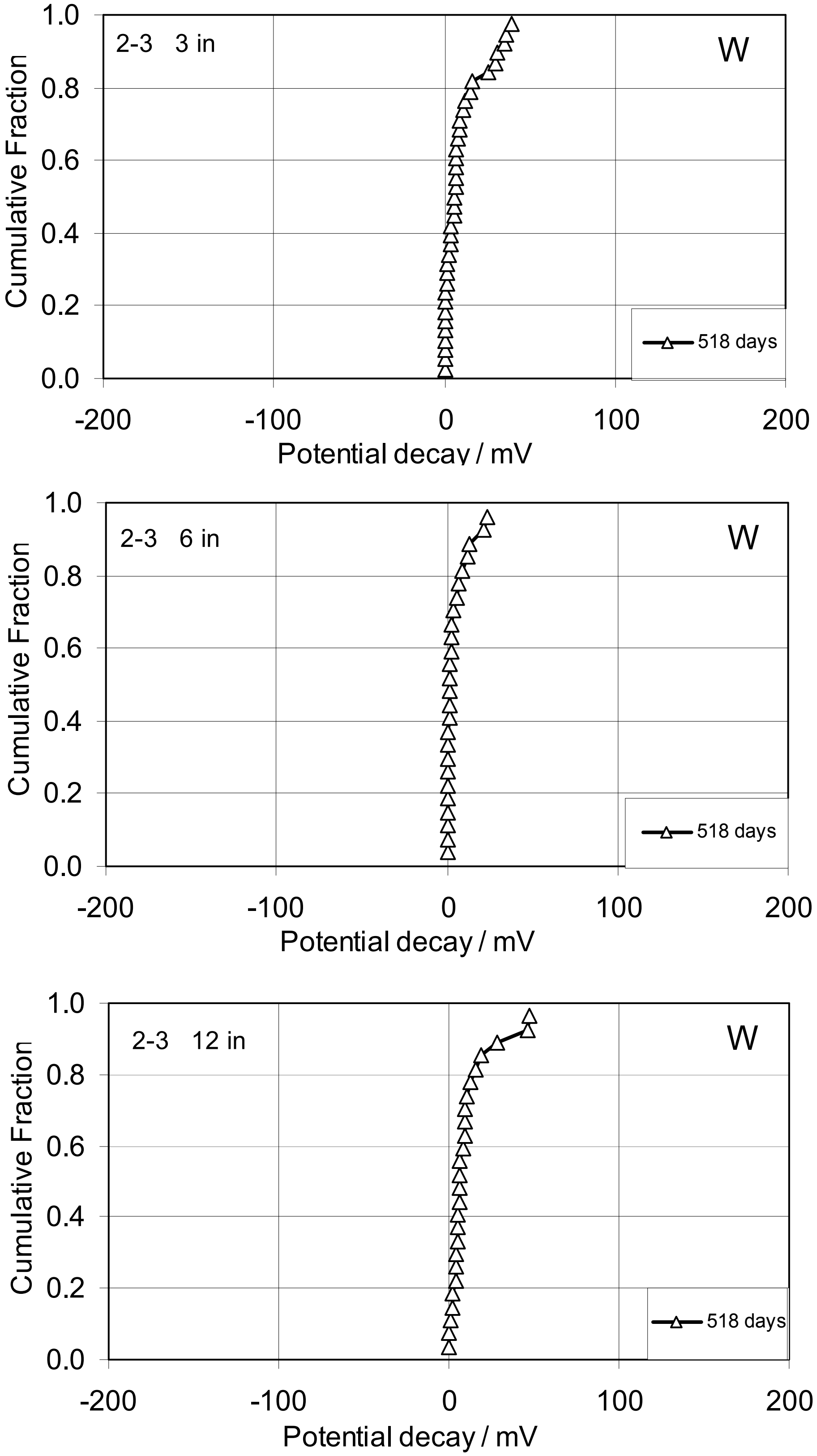

Figure 51 - Field Site 2, location 2-3 (Type W anodes). Cumulative distribution of steel depolarization decay values for test points at the indicated distance from the patch edge at various times since energizing the anodes. Positive values indicate steel was polarized cathodically.

Table 6 - Field Site 2. Summary of depolarization test results for Type C and W anode locations.

Location / Pier / Pile cap	Distance from patch / in	Age (days)	Average Decay / mV	Standard deviation / mV	Type of anode	Number of anodes
10-3	3	428	25	15	C	33
		603	34	20		
	6	428	17	12		
		603	21	15		
	12	428	13	11		
		603	12	8		

Location	Distance from patch / in	Age (days)	Average Decay / mV	Standard deviation / mV	Type of anode	Number of anodes
2-3	3	518	10	11	W	42
	6	518	5	6		
	12	518	10	12		

3.4 Discussion of Experimental and Field Results

3.4.1 Anode potential-current functions (PCFs)

Both the galvanostatic RH chamber and the test yard slab revealed, for both types of anodes, comparably shaped PCFs. The functions showed at low current levels relatively little anodic polarization away from the open circuit potential, followed by an abrupt (in terms of a logarithmic current scale) increase in polarization as the current approached an apparent terminal value. The curves resemble the behavior expected from a system that is approaching a transport-controlled limiting current density, or alternatively, the presence of a sizable ohmic resistance [Jones 1996]. As the curves were constructed using Instant-Off potentials, it could be argued that the presence of an ohmic solution resistance component would have been cancelled by the test method used. However, as noted elsewhere [Sagüés 1994] an Instant-Off (or a high frequency EIS) procedure may not completely cancel out all ohmic polarization components if the corrosion is localized to small parts of the metallic anode surface. That localization may affect various parts of the anode surface as time progresses, so this effect could not be completely ruled out even if autopsy tests were to show a cumulative, near uniform corrosion wastage of the metallic anode. A transport-limited polarization component could occur due to dynamic accumulation of anode corrosion products on its surface, which would effectively shift the equilibrium potential of the anode toward a more positive value as observed. These issues merit attention in continuation research.

For a given test condition and anode service history, the PCFs showed notable variability among anodes of the same type in the 1st set of anodes tested. Thus, in the aged condition two of the three type C 1st set anodes in the replicate test yard slabs had relatively elevated E_{OC} values and low apparent terminal currents, while the remaining anode showed much greater activity. Significant variability, although at much lower performance levels, existed also for the aged type W 1st set of anodes. Unit-to-unit performance variability among each type was much less for the 2nd set of anodes. In the test yard slab the 1st set of W anodes showed notably inconsistent behavior with that of the 2nd set, even though both sets were nominally the same product. The 1st set, as a group, performed much worse than the 2nd suggesting a production problem in the former. Consequently, in the following the discussion of the PCFs of type W anodes will address principally the functions determined for the 2nd set, with the qualification that production uniformity may be an issue.

In general and at moderate aging levels and humid conditions, the C anodes tended to have more negative open circuit potentials, and faster polarization upon current delivery, than the W anodes. Nevertheless, both anodes tended to reach roughly the same operating point when coupled with passive steel in the test yard slabs. Similar behavior was observed in the galvanostatic tests at 95% RH. Initial trends in the 60% RH chamber (1st set of anodes only tested there) showed for both anode types comparable relative PCF features to those seen in the other environments, but it should be recalled that early in that exposure the embedding medium likely still retained much of the initial free water. Later behavior in the 60% RH chamber was obscured by data scatter.

Aging of the anodes by delivering current in service was manifested in the test yard slab, for both types and sets of anodes, by the continually decreasing current output. Increasing ohmic resistance as concrete aged is expected to have been only a minor factor in this decay, since resistivity roughly stabilized in value after the first year, as shown in Figure 36. There was no indication either of any important change in the polarizability of the steel bars that would have resulted in a strong decrease in cathodic current demand as time progressed. As implied by the slow cyclic polarization test results, the current decreases most likely reflect primarily an evolution of the PCF generally toward more positive open circuit potentials and, more importantly, to the onset of elevated polarized potentials at increasingly lower current levels. That situation is explained in Figure 52 where idealized PCF curves are shown for a fresh anode (t=0) and for increasingly aged conditions (t_1, t_2). The anode is coupled to a rebar assembly that creates a cathodic current demand as indicated. For each condition the operating point of the anode is denoted by the open circle. The effective ohmic drop between the steel and the anode is given by the vertical space between the open and filled circles. As the anode ages, the operating point describes the trajectory indicated by the arrowed red line, with corresponding decrease in current delivery and increase in anode potential denoted also by red arrows. That interpretation is supported by the observation of such trajectories for both types and both sets of anodes in Figures 19 and 20.

The evolution of anode potential with time toward more positive values was much faster for the 1st set of anodes than for the 2nd (Figures 15, 19 and 20). This behavior is explained in the following as a consequence of the steel bars in the chloride contaminated zone having been connected to the anode for the first half of the evaluation period of the 1st set of anodes. Moreover, the Type C 1st set anode for Slab 1 (C1) showed anomalous behavior in that its potential elevation trend was reversed at later exposure times (Figure 16). That anomalous behavior will be considered next as well.

The chloride contaminated zone contained 1.5% Cl^- ion by weight of cement, about 4 times the value of commonly assumed critical threshold values for corrosion initiation [Li 2001]. The steel bars there were externally connected to the anode already during casting and curing of each slab, and were kept so over the first 477 days of testing. That coupling was however not sufficient to prevent corrosion initiation of the four rebars in that zone, which were found to be in the active condition from the start. Active rebar has low polarizability, and given the quite low concrete resistivity during the first year of operation (~7 to 10 k Ω-cm, Figure 36) and the large steel surface area involved, that group of four rebars was an important contributor in determining the potential over much of the system. Indeed, as shown in Figure 25, some of those rebars were net anodes even though they were only about 15 cm (6 in) from the point anode. Thus,

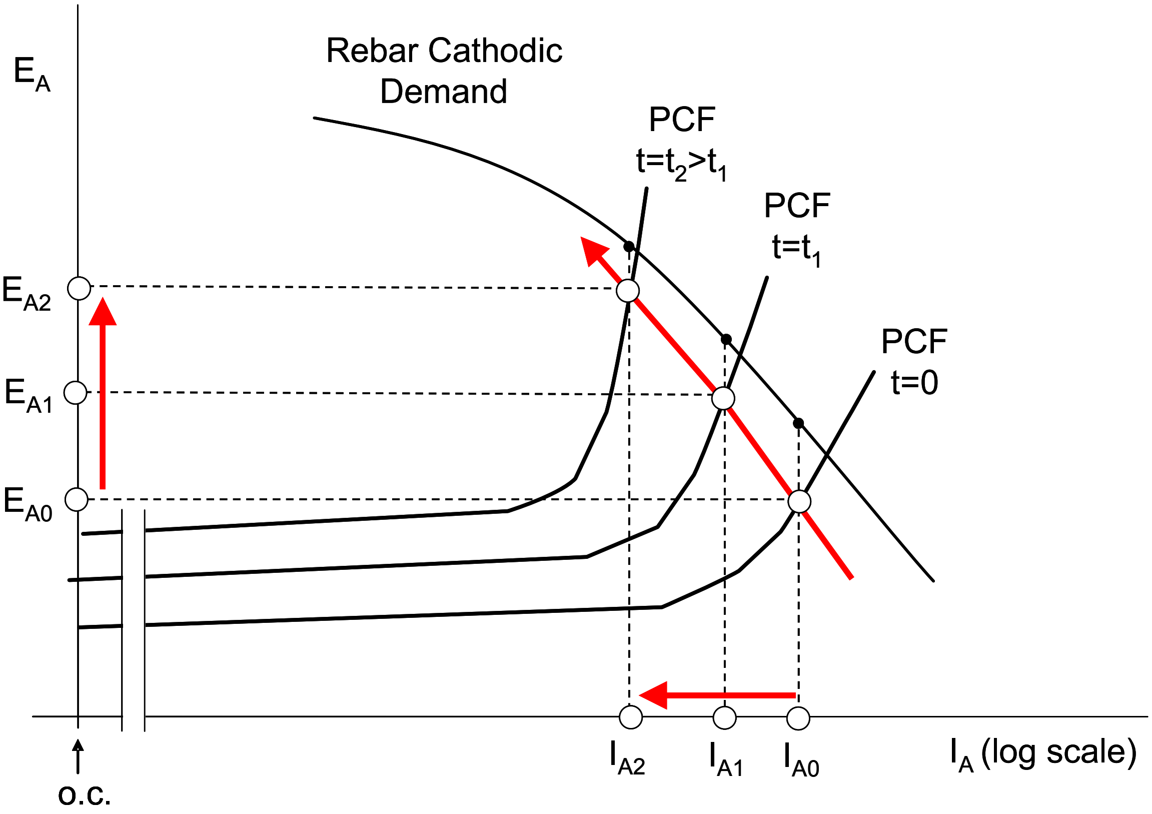

Figure 52 - Idealized evolution of anode PCF with aging and effect on operating conditions. E_A, I_A: anode potential and current; o.c.: open circuit condition. Open circles indicate the polarization condition of the anode. Filled circles correspond to the effective rebar polarization condition, at a potential equal to that of the anode plus an ohmic drop difference (see Figure 3). Arrows indicate trends as aging time increases.

except for a very short initial period (Figure 15), for much of the initial year or so of evaluation of the 1st set of anodes the anode potential was more or less stabilized at a value not much below that of active reinforcing steel in chloride-contaminated concrete (e.g. ~-400 mV CSE). Consequently the potential-current trajectory for the first set normally spanned a shorter potential range than if the anode would have been in contact with a more polarizable (i.e. passive) assembly. That latter scenario applied to the second anode set, for which the rebars in the chloride zone were never connected. Accordingly, the potential-current trajectories for the 2nd set anodes were found to span a wider potential range (Figure 20) more fitting to the outcome described in Figure 52.

The auxiliary anodes did not have a galvanic current load so in principle their potential history should be indicative of the effects of self corrosion plus any changes in the composition of the proprietary mortar in the pellet surrounding the metallic core. With the exception of the auxiliary C anode in Slab 1, the potential changes were significant over time (hundreds of mV) and in the positive direction suggesting degradation. A possible cause for that evolution is diffusion into the surrounding concrete of the substances in the anode pellet that were responsible for zinc activation. For young concrete with the mixture proportions of the ORC in the humid outdoors environment used, diffusivity of ionic species typified by that of chloride ions is in the order of 10^{-8} to 10^{-7} cm^2/sec [Sagüés 1994], and likely nearer to the high end of the range based on the low values of resistivity observed [Berke 1992]. Consequently characteristic diffusion distances of ionic species into the surrounding concrete after a year or so could amply exceed 1cm. That distance is in the order of the pellet thickness so substantial dissipation of anode activators with the test time interval would not be surprising. That dissipation could be an important contributor to anode performance derating over time, above and beyond any detrimental effects from galvanic current delivery.

The more straightforward anode degradation effect expected from current delivery is loss of anode mass. Based on the measurements reported in Section 2.1, rounded-off values of 110g and 45 g will be assigned in the following to the initial anode metallic mass of Type C and W anodes respectively. Those masses correspond respectively to 1.68 and 0.69 mol of Zn, based on the atomic weight of Zn = 65.39 g/mol. Assuming dissolution as Zn^{+2} ions the maximum (also called the "theoretical") amount of galvanic charge Q_T that could be delivered can be calculated. The amount, equal to 2 F n_M, where F=96.49 k Coul/equivalent is Faraday's constant and n_M is the number of moles, is then Q_T=324 k Coul and =133 k Coul for C and W anodes respectively. Anode self corrosion and loss of physical continuity between parts of the anode or with the connecting wires often lower significantly the practical amount of possible charge delivery by actual cathodic protection anodes, e.g. to ~0.5 Q_T. Thus, even if other factors have not already had significant derating consequences, by the time the anodes evaluated here deliver about 160 k Coul (C) or 65 k Coul (W), they would be expected to be approaching the end of their effective service life.

As shown in Figure 17, all type W anodes in the 1st set tested in the yard slabs showed substantial loss of the ability to provide galvanic current after having delivered only 10 to 22 kCoul, or only ~7% to 15% of Q_T. Two of the C anodes in the 1st set experienced faster current derating at Q~ 10% of Q_T, but anode C1 in that set still retained appreciable current capacity at Q~20% of Q_T. Performance of the W anodes in the 2nd set showed considerable improvement over the 1st, as current remained at substantial levels for all three anodes with Q approaching 25% of Q_T. The 2nd set of C anodes performed, up to the final data acquired at Q~10% of Q_T, similarly to the earlier stages of the1st set when only moderate current decay was taking place.

The potential trends as function of Q shown in Figure 18 correlate well with the current trends only for the 2nd set of anodes, likely because of the obscuring effect of coupling to the active bars during the first part of the evaluation of the 1st set. The 2nd set potential and current trends, if they were to be sustained over later aging stages, would suggest that current delivery for these test conditions would reach values well below 100 μA, and potentials approach ~-200 mV (thus providing little beneficial effect), at Q ~¼ to ⅓ Q_T for the Type C and W anodes respectively. Such projection would be somewhat, but not extraordinarily less than the behavior expected for many galvanic anode systems as indicated earlier. This issue will be revisited in Section 3.4.3 by comparison with the anodic efficiency encountered in the field installations.

The energized and the auxiliary 1st set Type C anodes in Slab 1 showed anomalous active behavior, as suggested by the highly negative potential of both anodes late in the test period, and by the high current and total charge delivery of the energized anode. This behavior is suggestive of anode activation beyond that expected from the effect of the anode pellet mortar and the initially chloride-free ORC medium. Such activation is likely to have occurred because of chloride transport from the chloride contaminated zone into the nearby concrete surrounding the anode. As indicated earlier, the characteristic chloride diffusion distance in the sound concrete could easily be >> 1 cm after 1year, and it may have been even higher locally due to the instances of poor consolidation noted earlier. Also as indicated earlier, there were also signs of incipient activation of rebars No. 5 and No. 10, (immediately on either side of the chloride zone) in some of the slabs during the last stages of testing. Those observations are further indication of substantial chloride diffusion into the previously chloride free concrete. Consequently, the behavior of the 1st set of C anodes in Slab 1 may be explained by that slab being the first where chloride intrusion into the previously chloride-free concrete reached a sufficient level to promote enhanced activation of that anode. This explanation will be further examined in continuation testing of the auxiliary and disconnected 1st set anodes of the other slabs to ascertain if signs of activation develop there as well in the future. It is noted that the 2nd set anodes were intentionally placed one extra rebar step further than the 1st set from the chloride transition line, to minimize the chances of extraneous activation from Cl^- ions diffused in from the chloride-rich zone.

3.4.2 Rebar Polarization

The poor rebar polarization levels achieved by the 1st set of anodes while all rebars in the yard slab were connected can be ascribed to the low polarizability of the active rebars, as discussed earlier. The rebar current distribution patterns along the slab main direction showed that, before their disconnection, rebars in the chloride-contaminated zone were often net anodes, contributing at times a total anodic current comparable to or exceeding the current supplied by the point anode. During that period, the rebar potential distribution along the slab main direction showed clearly that the rebars in the chloride contaminated zone, which exhibited potentials typical of actively corroding steel, were a substantial polarizing source for the rest of the system. The steel in the chloride zone of the slabs had potentials similar to, or even more negative than, the typical potential of the main anode, which in turn was more negative than that of the bars in the chloride-free concrete zones. When conducting depolarization tests, the overall potentials relaxed relatively little, toward terminal values influenced by those of the active rebars. Consequently, the overall depolarization levels were poor. These results indicate also that point anodes of this size and at the placement density used, and for the amount of steel present in the slabs, are not likely to provide substantial levels of conventional cathodic protection of an already corroding rebar assembly.

After disconnection of the active rebars in the 1st set tests, the anodes were indeed the most negative elements in the system, and the only source of cathodic polarization of the remaining, passive, bars. The steel depolarization levels for the Type C anodes, which were still quite active at that time, improved accordingly to average levels in excess of 100 mV for the rebar group closest to the anode. The 1st set of Type W anodes had already degraded considerably by that time and failed to achieve appreciable levels of polarization even for only the passive rebars.

For the 2nd set of anodes polarization involved always only the passive rebars, and overall rebar polarization was consequently improved from the beginning compared with that of the 1st set. Furthermore, the 2nd set of Type W anodes did not show the deficiency affecting the 1st set and steel polarization for those anodes improved accordingly.

The composite cathodic rebar polarization curve shown in Figure 35 shows features well establish by previous work, including an apparent Tafel region at low polarization levels followed by incipient indications of the establishment of a diffusion control regime at greater polarization levels. The main cathodic reaction has the characteristics of oxygen reduction, and the polarization/current function parameters match approximately those reported elsewhere for steel in moderately humid concrete [Sagüés 2003]. Further analysis of this curve is presented in the Modeling section.

3.4.3 Field Installations

It is noted that analysis of field installation results and monitoring at one of the sites is expected to continue in the future, so the present findings describe work in progress.

The average anode current trends in the field paralleled the test yard slab observations. In both conditions the anodes delivered initial currents in the order of 1 to 3 mA which continually decayed with anode age. The much faster decay of Type W anode current in Field Site 1 matched that observed in the test yard slabs for the 1st set of W anodes (roughly contemporary with those in Site 1), suggesting a common production deficiency. It is noted however that anode to steel resistance measurements for the Type W anode locations in Site 1, and the discussion in the next paragraph, indicate the presence of anode to rebar short circuits for some of the individual anodes. Short circuits would strongly limit the applicability of the current and depolarization data for the W anodes at Site 1.

The average ohmic resistance for individual anodes may be estimated by assuming a simple parallel configuration and multiplying the combined resistance by the number of anodes. The resulting amount for Type C anodes is ~60 Ω and 50 Ω for Sites 1 and 2 respectively, values mutually consistent and generally consistent as well with those obtained in individual anode measurement in those sites, as well as in the order of values obtained in the test yard slabs. In contrast, for Type W anodes the result was ~6 Ω for Site 1 while it was ~300 Ω for Site 2. The latter value is more representative of those observed for individual anodes in the field (including most individual Type W anodes in Site 1) and of values estimated for the test yard slabs. These results indicate the presence of short-circuits in the Type W anode Site 1 locations, although caution is in order in view of the uncertainty concerning the initial resistance measurements at that site.

The anode current values and trends for Site 2, for which there is no evidence of short circuits, are comparable to those obtained for the 2nd set of anodes in the test yard slabs where the Type W anodes did not show deficient performance. That observation is also consistent with Site 2 likely having W anodes manufactured at about the same time as the 2nd set tested in the slabs.

The shorter term variations in current levels for the Type C anodes in Site 2 track well the relatively large changes in tidal level recorded at that test location. Thus, the apparent surge in current at ~600 days likely reflects the particularly high tide present at that time. The tidal levels at the time of the measurements for the Type W anode location varied less, consistent with an apparently smoother long term current trend for those anodes.

At both sites, but especially at Site 2, many of the anodes were close to or often below the waterline. When below the water line, the anode would be coupled electrolytically to highly conductive estuary water path through a relatively short path of moist concrete. Thus, at high tide the anode current could increase significantly (as indicated by Figure 45) and further dispersed toward reinforcement in other parts of the bridge footer and piling depending on overall continuity. At lower tides the coupling should be less efficient, but it is likely still important given the cyclic tidal wetting of the footer. These considerations suggest that the anodes at these sites experience current demand from a relatively large steel area, with consequently diminished polarization effects on the steel. As shown in the following, the potential and potential decay measurements showed generally small or nil steel polarization effects.

In Site 1 the steel Instant-Off potentials at locations 10-3 (C anodes) and 10-1 (W anodes) showed values that varied little from or were actually more positive than the pre-repair readings. Long term potential trends did not deviate significantly form those encountered in the control locations with no installed anodes (Figure 40). Steel depolarization values for the Type C anode locations were overall quite modest at location 10-3. With one exception for one value at day 349, individual position values at 3-in from the patch were never reached 100 mV. Average values at 3-in started at 27 mV and decayed to only 15 mV after about 3 years. The effect was not too different at 6-in and 12-in from the patch, in keeping with predictions for behavior under relatively good electrolytic coupling as detailed in the Modeling section. Polarization levels were on average even smaller at type C anode location 11-5. The anodes appeared to have experienced significant polarization themselves. That is manifested in Figure 39 for the C anodes, showing instant-Off anode potential values that either tracked those of the steel early on, or approached them near the end of the test period.

The interpretation of the data for the Type W anodes in Site 1 is obscured by the indications of anode shorting mentioned earlier. The anode instant-Off potentials seem to be similar to those of the steel (consistent with the presence of a short circuit) at all times except for a few instances early on at location 10-1. The cumulative distributions of potential decay in Figures 43 and 44 show generally inconsistent behavior, with average values that are mostly either negative or very small. The appearance of negative depolarization values for a fraction of the readings would be consistent with the present of short circuits to some of the anodes, if any of those were to remain more active than the rest. Overall, the depolarization and galvanic data for the W anodes at this site may remain largely inconclusive.

At Site 2 both types of anodes delivered appreciable amounts of current, but the polarizing effect on the steel remained modest at best. Only at Type C anode location there was an appreciable effect on the Current-On anode potential relative to the control test locations with no anodes (Figures 47 and 49). However, the effect was smaller in the Instant-Off values and seems to have dissipated by the end of the test period. The potential decay readings had least variability than for Site 1, but the results were equally modest for Type C anodes (34 mV as the highest average value at 3-in) and very small for Type W anodes (only 10 mV at 3-in).

It is noted that in this site the steel potentials for the 3-in test points were consistently more negative than those at 6-in and those in turn more negative than the 12-in values. That was the case in nearly all conditions, whether Current-On or Instant-Off, or at control or anode test locations. Because of the patch placement, the 3-, 6- and 12-in locations are in increasing elevation order, thus increasingly less wet. The potential differences then are likely to reflect less efficient oxygen transport to the steel surface at the lower elevations, with consequently greater polarization of the cathodic reaction and a more negative mixed potential there. The same phenomenon, on a larger distance scale, is expected to account for the potential profile shown in Figure 37 for Site 1. The depolarization data for the Type C anode location in Site 2 suggest a greater effect for the 3-in than for the higher elevation test points, possibly as a result of easier polarizability of the cathodic reaction at lower elevations. As indicated earlier this effect, if present, is obscured for Site 1 due to other sources for experimental scatter including variable alignment of the test spots around the patch perimeter.

The Type C anode polarization at Site 2 appeared to respond to tidal variations as well. The current increase at day ~ 600 was matched by an elevation of anode Instant-Off potential. Such correlation is to be expected from the shape of the PCF discussed in the previous sections. The long term evolution of that function in the field sites may become more apparent upon continuing monitoring.

Additional insight on the anode aging trends may be derived from expressing performance as function of total charge delivered, as it was done in Section 3.4.1. Figure 53 shows the current evolution of the anodes from the field installations as a function of the cumulative amount of galvanic charge, Q. The values are averaged per anode for each pier tested. For each type of anode the value of Q_T, as calculated in Section 3.4.1, is designated by vertical lines. The graphs show for comparison also the current/charge trends from the test yard slab for the 2nd set of anodes. For clarity, only the average currents for each group of triplicate slabs are displayed and a logarithmic horizontal scale is used to accommodate the variety of behavior observed.

For the Type C anodes the current-charge behavior in Site 1 was comparable to that observed in the test yard slabs, again showing a noticeable decrease in current output as Q reached ~ 25 k to 35 k Coul. In contrast, substantial current delivery in Site 2 persisted toward Q values about 2 to 3 times higher than in Site 1. Since the Type C anodes of both the 1st and the 2nd set performed similarly in the test slabs, the enhanced performance on Site 2 (expected to have anodes contemporary with those of the 2nd Set) may be reflective of other factors. Likely factors responsible for the longer lasting current and activity at Site 2 are the use there of a high conductivity embedding medium for the Type C anodes at Site 2, and the exposure to a saltwater tidal regime that both reduced circuit resistance and may have promoted sustained activity of the zinc alloy surface.

The performance of the W anodes in Site 1 showed drastic deterioration at Q values that were even much smaller than those recorded for the 1st set of anodes (expected to be contemporary) in the test yard slabs (Figure 17). As noted earlier however the W anode installations in Site 1 had signs of short circuits that may have created misleading performance indications. The W anodes in Site 2 (expected to be contemporary with the 2nd set of anodes in the test yard slabs) showed comparable evolution of current delivery with Q to those in the test yard slab. The trends suggest that currents would decay to ~ 100 μA when Q reached ~ 35 k to 45k Coul for test yard slabs and field installations respectively. The apparent absolute Q values for the onset of significant decay are smaller than those for the C anodes. However, the overall trends for both yard tests and field sites (considering 2nd set anodes only) do not seem too different when considering Q as a fraction of the respective theoretical limits (i.e. distance in the logarithmic Q axis to the respective limits indicated by the vertical lines).

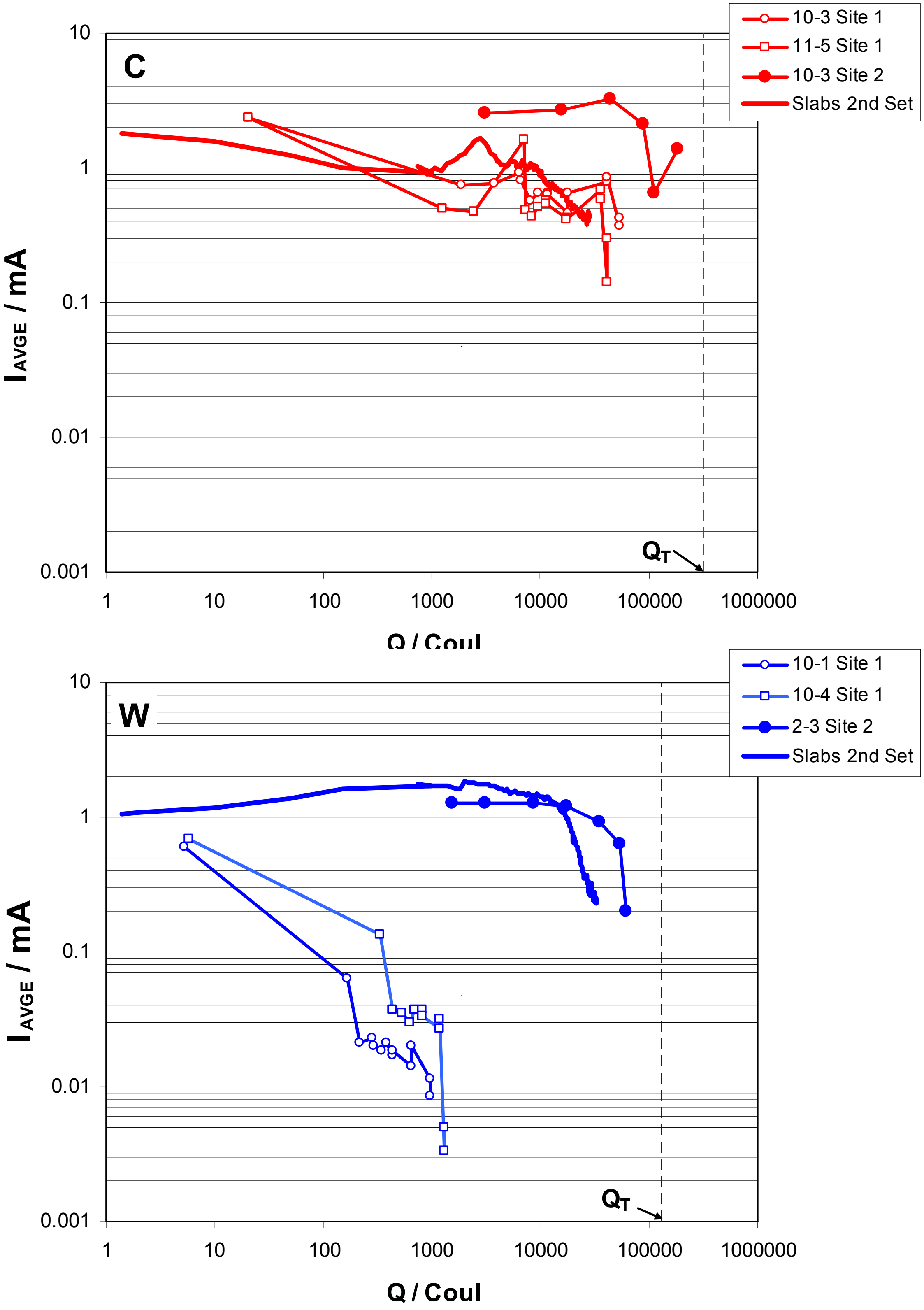

Figure 53. Anode current as function of integrated anodic charge delivered for both sets of anodes in the test yard slabs and field installations. The dashed lines indicate the theoretical alloy consumption limit.

4 MODELING

4.1 Principles and assumptions

This section addresses projecting the performance of point anodes for patch repairs as function of service time (or, alternatively, total electric charge delivered) and operating conditions. The anode performance is measured by how far away from the patch perimeter (the "throwing distance" x_T) an amount of cathodic polarization meeting or exceeding a required minimum (the "prevention criterion" C_P) can be provided to the passive rebar surrounding the patch[2]. Calling E_{SU} the steady state potential that the passive rebar in the surrounding zone would achieve in the absence of any galvanic coupling with the rebar in the patch, and $E_S(x,t)$ the rebar potential at service time t and a distance x away from the patch perimeter, then the performance condition is given by

$$E_{SU} - E_S(x_T,t) = C_P \tag{1}$$

All electrode potentials are given in the CSE scale.

As discussed earlier, within certain limits, anode aging may sometimes be better described not in terms of service time but rather by the total amount Q of charge delivered since the moment of placement in service. In such case the performance condition can be alternatively given as

$$E_{SU} - E_S(x_T,Q) = C_P \tag{2}$$

In the following, a formalism on Q will be presented for completeness alongside equations based on time as the aging parameter. However, calculations and examples will be limited for brevity to the case of time as the aging parameter.

The desired projection model output is therefore the value of x_T , for the chosen values of C_P and t (or Q), as function of the other system conditions which serve as model inputs. The simplified system chosen for implementation of the model consists of a reinforced concrete slab (which may represent a bridge deck, parking structure floor, or a part of a wall) having a patch zone in which all the concrete has been replaced. The patch is assumed to be roughly circular with anodes placed at uniform intervals just inside the patch perimeter. It is assumed for simplicity that x_T is not large compared with the dimensions of the patch, so radial spread of the galvanic current is modest. The rebar mat (or mats) in the slab is treated as roughly corresponding to a uniform amount of steel surface to be polarized per unit area of the external concrete footprint. Thus, the problem can be considered on first approximation as a one-dimensional current

---

[2] The value of C_P is an input to the model, to be chosen based on the extent of chloride contamination in the concrete around the patch and how the chloride threshold depends on potential. This issue is discussed separately later on.

distribution calculation. Further simplifications involve assuming uniform concrete resistivity, concrete thickness and rebar polarization properties. The latter include time-and potential-independent anodic passive dissolution current density and a time independent cathodic reaction (oxygen reduction) current density equal to that measured on the rebars in the test yard slabs, but constricted by a limiting current density of fixed value. The polarization function (and its dependence on t or Q) of the point anode correspond to that observed experimentally for each of the two types of anode investigated, and is expressed in closed mathematical form by the abstraction process described below. In the derivation presented below, the current needed to polarize the region of steel inside the patch area is neglected for simplicity. A variation of that treatment was conducted as well to take into account for the presence of that steel.

The base conditions outlined above then correspond to an anode placed at the end of a linear concrete beam, with the galvanic current running lengthwise and a distributed sink current density on the steel given by the local concrete potential and the polarization function of the steel. At the anode end of the beam the potential is a function of the end potential and the polarization function of the anode. The nomenclature to be used is listed in Table 5.

Following the treatment described elsewhere [Presuel-Moreno 2005B] for similar conditions, at any given distance x charge conservation under the above assumptions requires that the concrete potential satisfies:

$$d^2E_C/dx^2 = -\rho\ S_F\ t_C^{-1}\ i_S \qquad (3)$$

The following boundary conditions apply:

At the patch perimeter (anodes placed there), by Ohm's law:

$$I_A = w\ t_C\ \rho^{-1}\ dE_C/dx\ |_{x=0} \qquad (4)$$

At the outer slab edge (no current leaving the slab):

$$dE_C/dx = 0|_{x=L} \qquad (5)$$

The net steel current is assumed to depend only on potential, $i_S(E_S)$. It is noted that given $i_S(E_S)$, setting $i_S=0$ yields the value of E_{SU}. The anode current is assumed to depend on both potential and aging condition , $I_A(E_A, t)$ (or $I_A(E_A,Q)$).

Accounting for the presence of the current constriction resistances, and by using the configuration parameters $k_1= \rho\ S_F\ t_C^{-1}$and $k_2= S_F\ w$, the ruling equation and anode-end boundary condition become:

$$d^2E_C/dx^2 = -\ k_1\ i_S\ (E_C-R_S\ i_S) \qquad (6)$$

$$I_A(E_C+R_A\ I_A)= k_2\ k_1^{-1}\ dE_C/dx\ |_{x=0} \qquad (7)$$

Thus, giving as inputs k_1, k_2, L, R_S and R_A as well as the functional relationships $i_S(E_S)$ and $I_A(E_A, t)$ (or $I_A(E_A,Q)$), solution of Equation (6) with the boundary conditions in Eqs. (5,7) yields $E_C(x, t)$ (or $E_C(x, Q)$) as output. The use of the parameters k_1 and k_2 permits obtaining solutions that are roughly scalable for all systems having the same values of those parameters, and the same anode and steel polarization properties. Generality is precluded however if, for example, the factors that determine local resistance vary sufficiently from system to system. Post-processing of that output then yields the value of the throwing power x_T for any chosen criterion C_P at the specified anode aging condition, therefore achieving the objective of the performance projection model.

The sign convention used in writing the system equations is to declare $i_S < 0$ when i_S is a net cathodic current. That choice permits keeping the customary polarity designation when evaluating the results, with electrode potentials referred to the electrolyte and absolute values of activation-polarized anodic/cathodic current densities respectively increasing/decreasing with potential. Interpretation of the findings is thus facilitated compared with other alternatives [Kranc 1994].

4.2 Implementation of the model

4.2.2 Model inputs

Overall dimensions and global concrete properties

The ranges of values for model inputs $k_1$and k_2 were chosen to bracket typical dimensional and concrete resistivity conditions that may be encountered in the field. L was fixed at 200 cm which approaches a semi-infinite condition compared with the throwing power values that may be usually expected; the solution is in that case conservatively evaluated and with low sensitivity to the precise value of L.

Local resistance

The following are rough estimates of the current constriction resistances of rebar and anode, intended to refine to some extent the throwing power calculations. More accurate solutions would necessitate use of a multidimensional model, but such step may be premature considering the limited extent of the performance data base available at present.

Model inputs R_S and R_A were estimated from geometric considerations and from the input values of k_1 and k_2. For R_S the approach corresponding to the current flow between two concentric cylinders was assumed to apply on first approximation. In such case the length-specific current constriction resistance R_{SUL} is given by [Sagüés 1994]:

$$R_{SUL}=\rho\ (2\pi)^{-1}\ \ln\ (t_C/\Phi_S) \qquad (8)$$

where Φ_S is the rebar diameter (diameter of the inner cylinder) and t_C is an approximation to the diameter of the outer cylinder, in this case taken to be in the order of the characteristic thickness of the system. Taking into account the problem scaling, the term R_S in Eq. (6) is then

$$R_S=\pi \ \Phi_S \ R_{SUL} \tag{8a}$$

Complications in estimating R_A stem from the metallic anode being surrounded by consecutive shells corresponding to corrosion products, proprietary anode pellet mortar, anode placement mortar/concrete if different from the slab concrete, and finally the slab concrete itself. Moreover, current distribution can be highly complicated if the metallic surface of the anode is not uniformly activated. In such case the polarization function $I_A(E_A, t)$, even if determined by instant-Off measurements, may itself contain a considerable ohmic component per arguments described in detail by Sagüés [1994] and as discussed elsewhere in this report. Assuming that only the uniform part of the current constriction effect needs to be considered, the value of R_A may be estimated on first approximation as corresponding to that for the space between a sphere of effective diameter Φ_A in an spherical medium of diameter in the order of t_C and resistivity equal to that of the slab concrete [Landolt 2007], so that

$$R_A \sim ½ \ \rho \ \pi^{-1} \ [(\Phi_A)^{-1} - t_C^{-1}] \tag{9}$$

Assuming that the anode pellet mortar is highly conductive and that any ohmic effects due to corrosion product accumulation are already built into $I_A(E_A, t)$, then the effective anode diameter Φ_A is considered to be in the order of the characteristic outer dimension of the anode mortar pellet, $\Phi_A \sim ½$ (pellet width + pellet thickness). A rounded-off value representative of both anode types evaluated was used.

Polarization function - steel

The function $i_S(E_S)$ for the model realizations explored below is chosen to be representative of the behavior of the steel used in the test yard slabs. The function is abstracted starting from the combined data set of instant-Off potential measurements as function of rebar current given earlier in Figure 35. The abstraction consists of assuming for the cathodic reaction an increasing current density with decreasing potential following simple Tafel kinetics, until a nominal limiting current density value i_L is reached. For more negative potentials the current is fixed at i_L thus creating a simplified combined activation-concentration limited cathodic polarization curve. The anodic reaction on the rebar is assumed to correspond to a potential-independent passive dissolution current density i_P. Thus when i_{0S} 10^((E_S-E_{0S})/β_{CS}) <= i_L :

$$i_S = i_{0S} \ 10\hat{}((E_S-E_{0S})/\beta_{CS}) - i_P \tag{10}$$

and when otherwise:

$$i_S = i_L - i_P \tag{11}$$

Where i_{0S}, E_{0S} and β_{CS} are the nominal exchange current density, nominal equilibrium potential and nominal Tafel slope respectively for the species undergoing the cathodic reaction. The values of i_P, i_{0S} , E_{0S} [3] and β_{CS} were determined by least square fitting to the data shown in Figure 35, treating the portion of the polarization diagram spanned by the data as if the cathodic reaction were simply activation-polarized. The resulting abstracted function is shown by the solid line in Figure 35. Application of the chosen parameter set resulted in a visually plausible fit function. However, it is cautioned that the fit procedure is prone to produce alternative parameter sets with nearly similar fit quality, so the set chosen for these calculations should be viewed only as a representative example of the steel polarization function parameters.

The value of i_L is a preset parameter. A comparatively large value (i_L = 2 μA/cm^2) was chosen to represent cases where cathodic diffusional limitation was unlikely (e.g. concrete atmospherically exposed at moderate relative humidity regimes [Sagüés 2003]). Smaller i_L values were chosen based on previous findings [Sagüés 2003] to represent moist conditions.

Polarization function - anode (PCF)

As indicated earlier, the following application is limited to the use of time as the anode aging parameter. The functions $I_A(E_A, t)$ from instant-Off measurements for individual anodes at various t have been shown when presenting the PCF results in Section 3. Tests with various abstraction representations showed that a function of the form shown in Eq.(12) yielded a reasonably fit to the experimental potential-current curves of individual anodes under nearly all circumstances. Eq.(12) is written with service time as the age parameter, but it is expected that on first approximation a comparable form could be used with Q as the aging parameter.

$$E_A(I_A,t)\ V^{-1} = E_{A0}(t)\ V^{-1} + (I_A/I_{A0}(t))^{n(t)} \tag{12}$$

Here E_{A0} is the unpolarized potential of the anode, and I_{A0} is the anode current that, when delivered, results in 1V of anode polarization over E_{A0} (effectively corresponding to an anode potential close to that of isolated passive rebar, where the anode provides essentially no protection). The exponent n indicates how steeply the anode output approaches that level as current demand approaches that limit. It is emphasized that Eq.(12) is a convenient empirical fit function and no relationship with fundamental causes is implied. The parameters E_{A0}, I_{A0} and n were obtained by least square fit from the polarization curve of each individual anode at various ages. Those parameters exhibited significant variability for the replicate specimens of a given type of anode at a given age, reflecting the unit-to-unit variability in behavior noted earlier. For the purposes of

---

[3] The values of i_{0S} , E_{0S} are not independent for the purposes of these calculations [Kranc 1992] so E_{0S} was specified arbitrarily.

obtaining a generic age-dependent anode performance curve, the combined trends of E_{A0}, I_{A0} and n with age for all anode specimens of a given type were displayed graphically and a representative simplified variation function with age was abstracted in each case. Convenient empirical relationships thus found, again not necessarily reflecting basic issues were:

$$E_{A0}(t) = E_B + a\ (t/t_u) \tag{13}$$

$$I_{A0}(t) = I_B\ (t/\ t_u)^{\ b} \tag{14}$$

$$n(t) = n_B\ (t/t_u)^{\ c} \tag{15}$$

Where t_u is the time unit (e.g. months).

Those relationships reflect the observation that the unpolarized potential tended to increase roughly linearly with time, while both the limit condition current and the steepness of approach to it tended to increase with time, but at a rate that decayed as time progressed (which resulted in parameters b and c being significantly <1).

4.2.3 Implementation of the model - computational procedure

Numeric solutions of the ruling equation with boundary conditions were obtained by the finite differences method using a 20-element array and an iterative Jacobi technique with a relaxation factor between consecutive calculations chosen to achieve stability and prompt convergence of the solution. Separate calculations were performed for each value of time t . The functions $i_S(E_S)$ and $I_A(E_A, t)$ were entered as numeric arrays, which permitted manipulation to obtain reciprocal functions by lookup and interpolation as well as easily obtaining values of expressions such as $i_S\ (E_C-R_S\ i_S)$ or $I_A(E_C+R_A\ I_A)$. Entry by numeric array also provided flexibility to accommodate if desired functions other than the analytical expressions given in the previous section.

4.2.4 Model application scope

The model is not intended for precise design purposes, but rather as an exploratory tool to obtain insight and identify broad operating conditions. As such sweeping simplifications were made such as the use of a one-dimensional representation, an approach that could be vastly improved if sufficiently accurate data on component properties became available. The x_T model output is obtained by interpolation between consecutive spatial nodes, so reported values should be viewed as only approximate estimates with only marked changes meriting note. In these calculations the spatial node array is not intended to replicate the placing of individual rebars. Thus values of x_T are reported nominally with cm resolution for comparison purposes, with the understanding that in an actual rebar grid the polarization pattern would be strongly influenced by the local geometry. Further model development is expected in continuation work (Dugarte 2009).

Table 5 - Nomenclature of model variables and parameters.

t (s)	amount of time since anode placement and energizing
Q (coul)	integrated electric charge delivered by the anode since placement and energizing
x (cm)	distance away from perimeter of the patch (where anodes are placed)
x_T (cm)	throwing power
C_P (V)	cathodic prevention criterion value
L (cm)	distance from perimeter of the patch to outer edge of the concrete slab.
t_C (cm)	concrete slab thickness
w (cm)	anode center-to-center placement distance along patch perimeter
$S_F(cm^2\text{-}cm^{-2})$	steel placement density (amount of steel surface area per surface area of concrete slab footprint)
Φ_S (cm)	rebar diameter
Φ_A (cm)	effective anode diameter
ρ (Ω-cm)	concrete resistivity
i_S (A-cm^{-2})	net current density on steel surface
i_P (A-cm^{-2})	anodic passive current density on steel surface
i_C (A-cm^{-2})	cathodic current density at the steel surface
I_A (A)	galvanic current delivered by anode
E_C (V)	potential of the concrete away from the immediate proximity of the steel surface or the metallic surface of the anode.
E_S (V)	potential of the concrete at a point immediately adjacent to the steel surface
E_{SU} (V)	unpolarized steel potential
E_A (V)	potential of the mortar at a point immediately adjacent to the metallic surface of the anode
R_{SUL} (Ω-cm)	effective length-specific current constriction resistance of concrete at the steel surface
R_S (Ω-cm^2)	effective area-specific current constriction resistance of concrete at the steel surface
R_A (Ω)	effective current constriction resistance of concrete around the active zone(s) of the metallic portion of the anode.
k_1 (Ω)	configuration parameter: $k_1 = \rho\ S_F\ t_C^{-1}$
k_2 (cm)	configuration parameter: $k_2 = S_F\ w$
i_{0S} (A-cm^{-2})	nominal exchange current density, cathodic reaction on steel
E_{0S} (V)	nominal equilibrium potential, cathodic reaction on steel
β_{CS} (V)	nominal Tafel slope, cathodic reaction on steel
i_L (A-cm^{-2})	nominal limiting current density, cathodic reaction on steel
E_{A0} (V)	unpolarized anode potential
E_B, a(V)	E_{A0} time dependence parameters
E'_B, a'(V)	E_{A0} Q dependence parameters
I_{A0} (A)	anode current demand resulting in 1V polarization
I_B (A), b	I_{A0} time dependence parameters
I'_B (A), b'	I_{A0} Q dependence parameters
n	anode potential steepness of variation with current demand

n_B, c	n time dependence parameters
n'_B, c'	n Q dependence parameters
t_u (e.g. mo)	time unit for parameter abstraction
Q_u (e.g. Coul)	charge unit for parameter abstraction

Table 6 – PCF, Steel and Other Parameters for Model Cases

Anode	**E_B (V)**	**a (V)**	**I_B (A)**	**b**	**n_B**	**c**
C	-1.16	0.0057	2.0E-03	-0.43	2.7	-0.03
W	-0.85	0.0085	5.4E-02	-1.7	0.81	0.33

Steel:	Parameters used as base for k_1, k_2 cases and for constriction resistances
i_{0S} = 2.03 E-9 A-cm^{-2} E_{0S} = -0.00 V_{CSE} * β_{CS} = 0.138 V i_P = 2.59 E-8 A-cm^{-2} i_L = 2 E-6 A-cm^{-2} E_{SU}= -0.153 V_{CSE} ** Φ_S = 2.2 cm *Nominal value **Value resulting from the other inputs	Φ_A = 5 cm tc = 20 cm L = 200 cm S_F = 1

Table 7 –General Model Parameters for Calculated Cases

k_1 (kΩ)	3.33 , 1.00, 3.00
k_2 (cm)	25, 50, 75
C_P (V)	0.10, 0.15, 0.20
T (months)	1, 4 , 10, 13
Anode Current to Steel in Patch	0, ½

4.3 Results and Discussion

Figure 54 presents model results for the C anodes, showing the throwing distance x_T as function of k_1 and using the cathodic prevention criterion value C_P as a secondary parameter, for a fixed value of k_2=50 cm and for anode ages of 1, 4, 10 and 13 months respectively. Those ages were chosen to correspond to the times for which PCF data were collected in the yard slabs. Also for the C anodes Figure 55 shows as a function of time, and for a fixed value of k_1=1kΩ, the effect of variations in the value of k_2 on the throwing distance. Figures 56 and 57 show similarly displayed results for the W anodes. In all cases, the polarization amount can be converted into steel current density by reference to Figure 35; the results are i_S = 0.11, 0.29 and 0.70 $\mu A/cm^2$ for C_P = 100, 150 and 200 mV respectively. It is noted that for these model calculations the area of steel inside the patch was considered to be relatively small, and the current needed to polarize this area was neglected. The resulting projections are consequently somewhat optimistic, and the derating effect of current flowing into the patch is discussed afterwards.

The results can be best interpreted by recalling that a value of k_1=1kΩ , at the center of the horizontal axis in Figures 54 and 56, corresponds to a reinforced concrete slab of thickness t_C=20 cm (8 in), a steel density factor S_F=1 and a concrete resistivity ρ = 20 kΩ-cm, baseline conditions that may be considered typical of many bridge deck or parking structure conditions. The other k_1 values for which results are given, 0.33 and 3.3 kΩ correspond for the same T_C and S_F combination to concrete resistivities of 6.7 and 60 kΩ-cm, or severe and mild corrosion propensity conditions respectively. Since S_F was chosen as unity for theses examples, the parameter value k_2= 50 cm corresponds to a placement density of one anode for every 50 cm of patch perimeter, which may be considered to be a reasonable practical value. Finally, C_P values of 0.1, 0.15 and 0.2 V represent depolarization criteria for cathodic prevention that are increasingly more conservative [Presuel-Moreno 2005B]. In Figures 55 and 57 and for the above combinations, variations of k_2 to values of 25 cm and 75 cm represent anode spacing near the tighter or wider extremes respectively of expected practical applications.

Using the C anode cases as an example, and for the above assumed baseline conditions, the 1-month projections indicate an appreciable throwing distance, 33 cm for a 100 mV polarization criterion. For that polarization level reducing the anode spacing to 25 cm elevated x_T to 40 cm, while it still reached 29 cm even for the 75 cm wide anode placement case. The projected throwing distance for k_2=50 cm however degraded to less than 10cm when the wide anode spacing and a more conservative polarization criterion (200 mV) was used. A throwing distance of less than 10 cm may be considered to be quite ineffectual as it is in the order of rebar spacing in many applications. The other scenarios in the same figures can be similarly evaluated for insight.

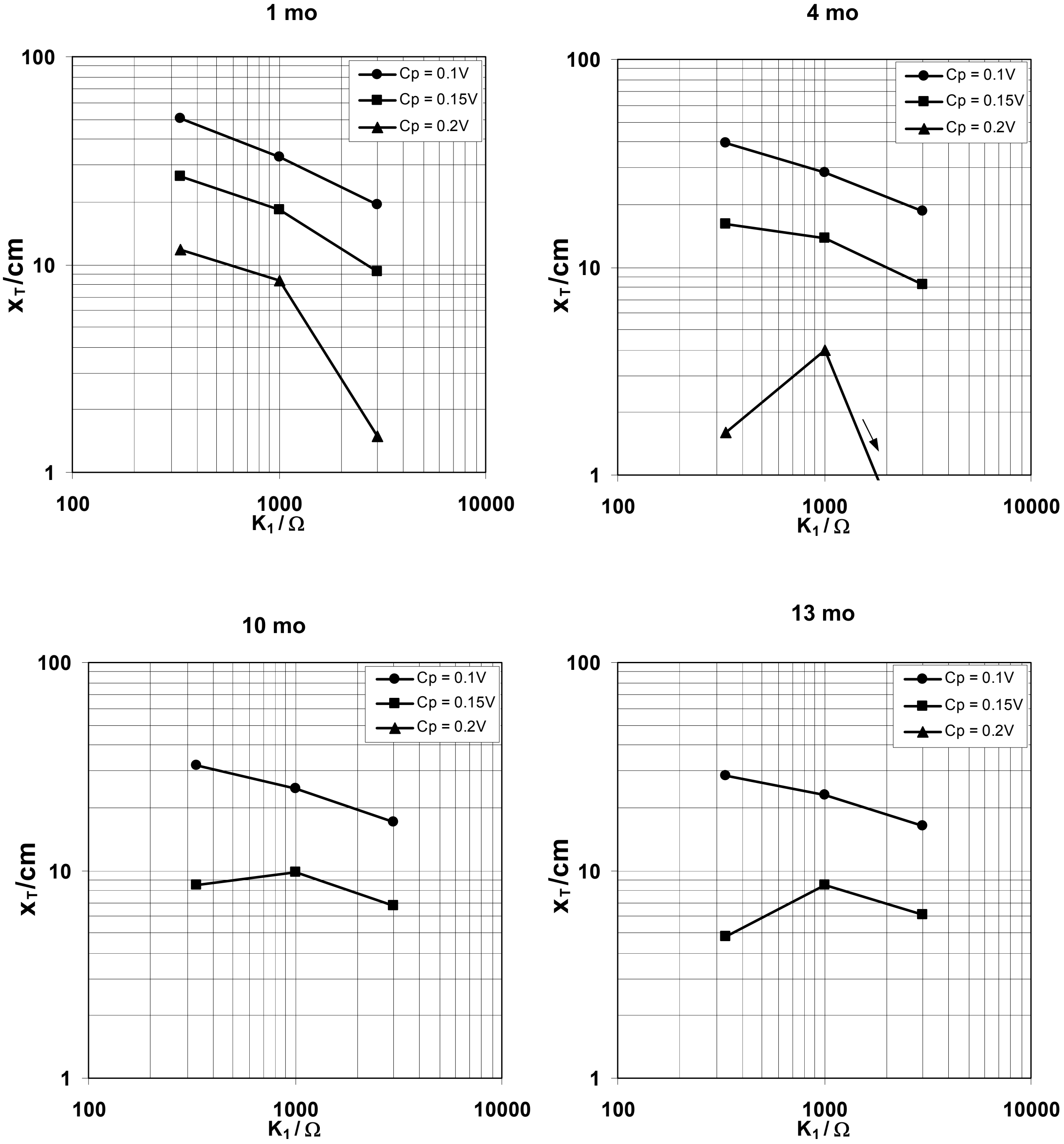

Figure 54 - Model projections of throwing distance for C anodes at the indicated service times. All graphs are for k_2 = 50 cm, C_P as shown. Absent symbol/line: polarization not achievable or x_T < 1 cm.

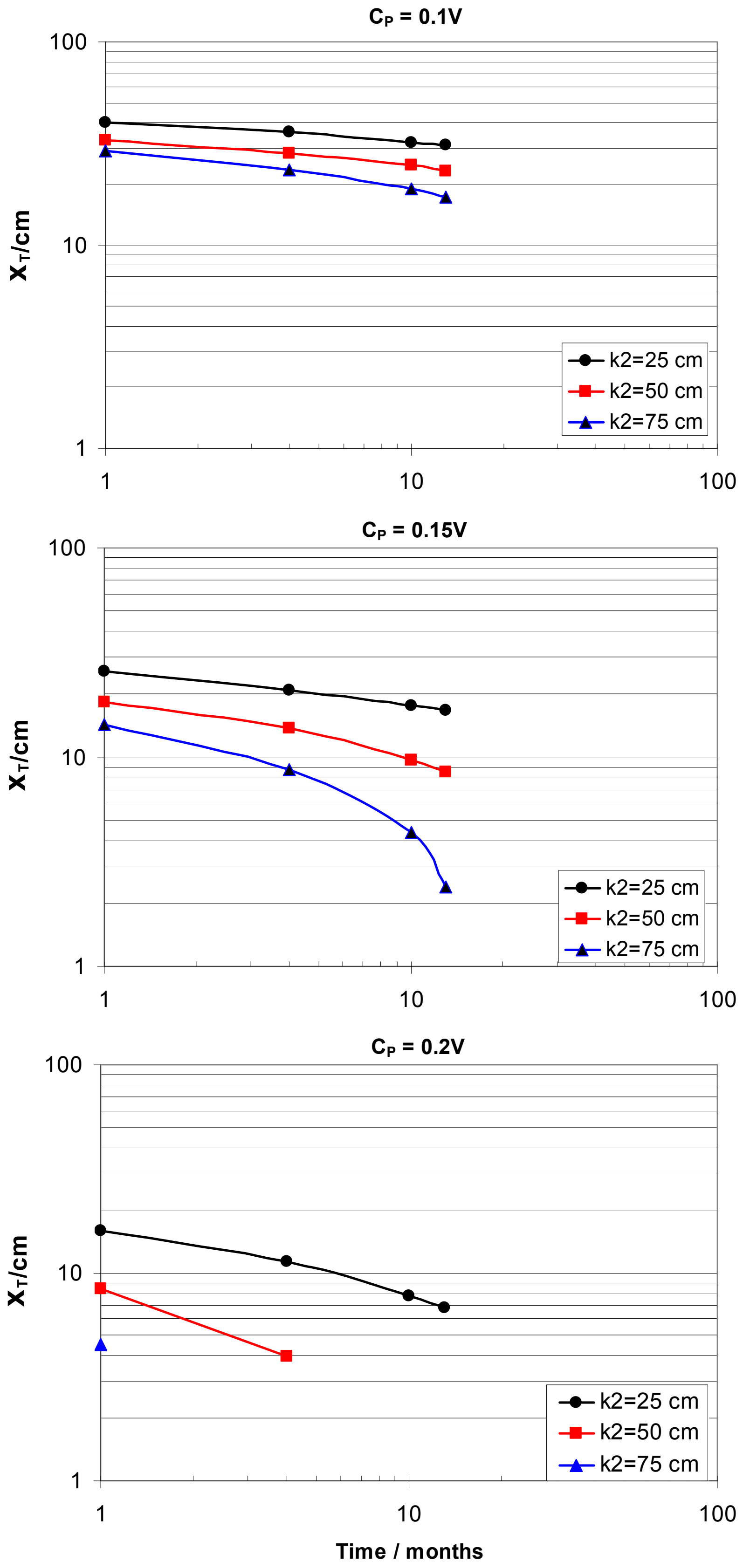

Figure 55 - Model projections of throwing distance for C anodes, as a function of service time. Legends indicate values of k_2 (cm). Absent symbol/line: polarization not achievable or x_T < 1 cm.

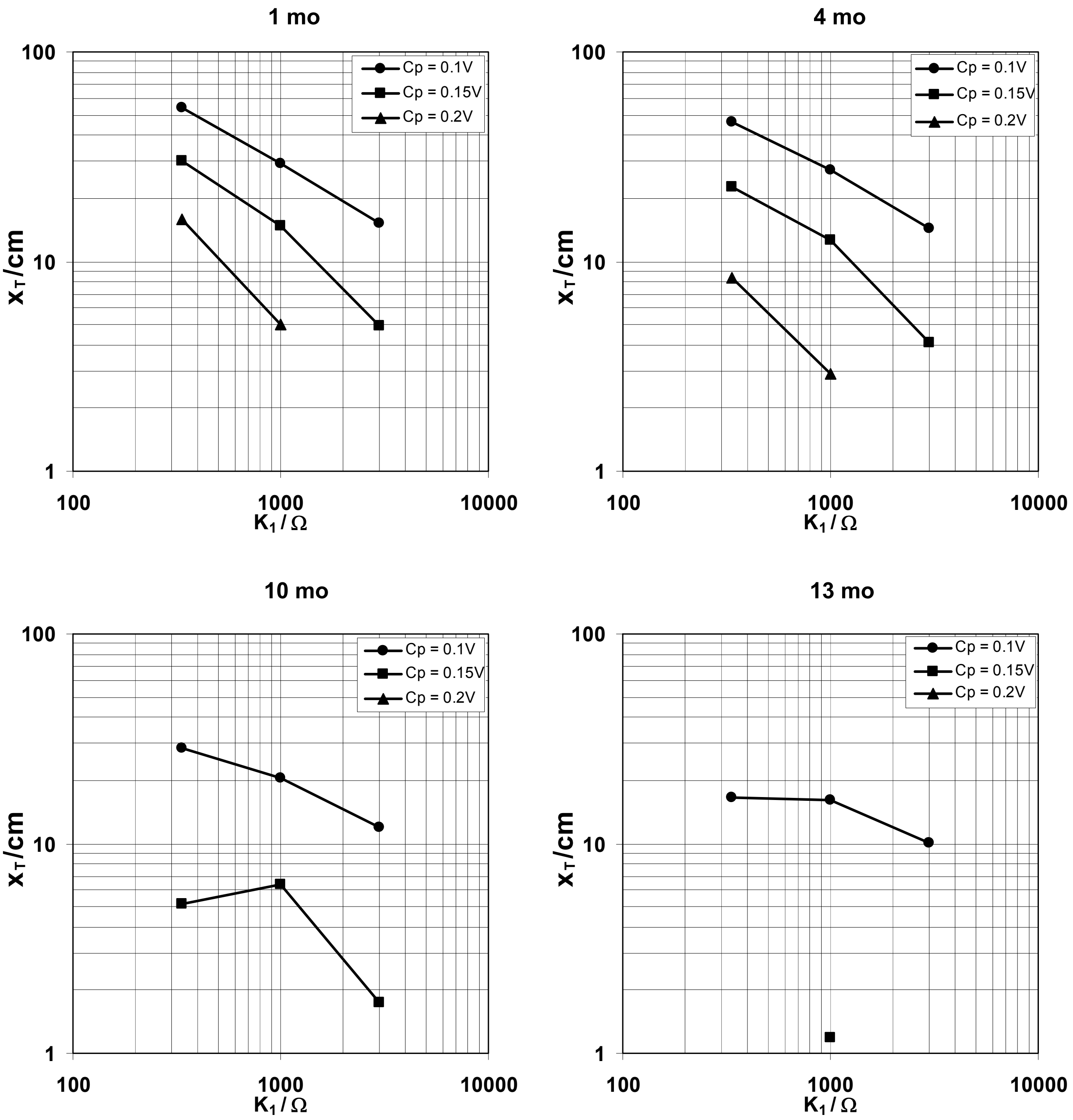

Figure 56 - Model projections of throwing distance for W anodes at the indicated service times. All graphs are for k_2 = 50 cm, C_P as shown. Absent symbol/line: polarization not achievable or x_T < 1 cm.

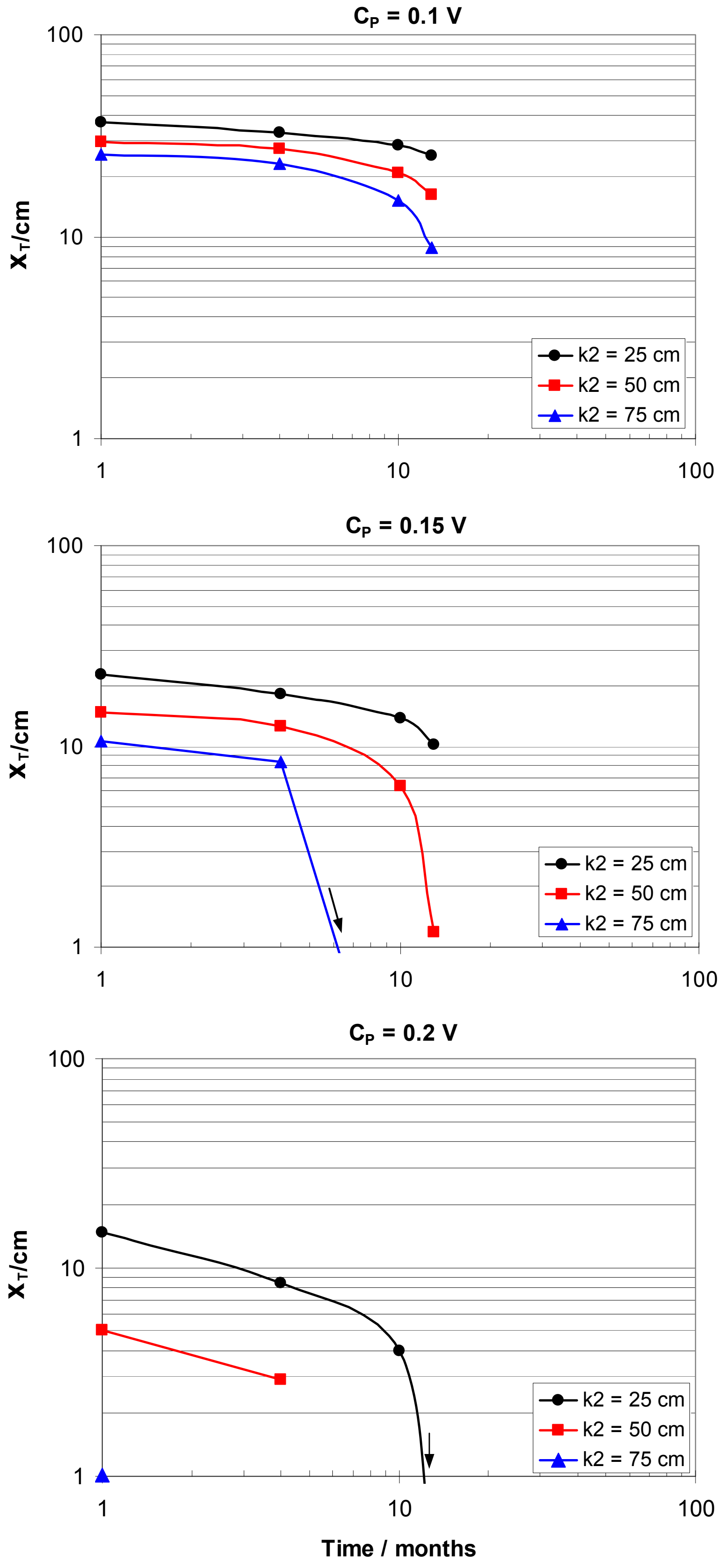

Figure 57 - Model projections of throwing distance for W anodes, as a function of service time. Legends indicate values of k_2 (cm). Absent symbol/line: polarization not achievable or $x_T < 1$ cm.

The projected throwing distance decreased with service time to various extents as shown in figures 55 and 57, depending strongly on the polarization prevention criterion used. Thus, continuing with the above example, for baseline conditions and 13 mo age the projected 100 mV throwing distance for the 50 cm anode spacing was reduced to 23 cm. For the same anode spacing Increasing the polarization criterion to 150 mV lowered the projected throwing distance to less that 10 cm, and the model projected that the 200 mV criterion was no longer reachable. The 200 mV criterion could be met at 13 mo by reducing the anode spacing to 25 cm, but the projected throwing distance was poor (<10 cm).

The projections for the W anodes (Figures 56 and 57) resulted in x_T values that were comparable to those of the C anodes at early ages, but generally smaller later on, in keeping with the relative anode polarization behavior of the anodes in the yard slab tests as noted earlier. Otherwise, the same general trends and observations noted for the C anodes apply here as well.

As indicated earlier, the projections would become more pessimistic when current demand by the steel in the patch area is considered. The extent of this effect was addressed by evaluating model projections for the case where the region inside the patch required half of the galvanic current from the anode, so that the anode current is distributed equally between the patch area and the surrounding concrete. The results are presented in Table 8 for the baseline condition with k_1=1kΩ and a 50 cm anode spacing. As expected the projected performance degraded compared to the cases where the entire anode current flowed outside the patch. The extent of degradation depended particularly on the polarizability of the anode. Thus the projected effect was relatively small early on when the added current demand caused only a relatively small shift of the anode potential toward more positive values. However, the shift would be more pronounced as later anode ages are considered, where a consequently steeper polarization curve applies. At age 13 months the projections indicated a substantial reduction in the throwing distance to about ⅓ to ½ of the value obtained when no current to the patch was assumed depending on anode type. In an actual system the patch zone may be small compared to its surroundings, so the galvanic current partition and resulting effect in polarization would be somewhat in between the two extreme situations (no current vs. ½ of the current going to the patch) considered in Table 8.

A sensitivity analysis was performed to establish how model results may be affected by variations in the choice of assumed steel polarization parameters. The parameters selected for this analysis were the nominal Tafel slope for cathodic reaction on steel (β_{CS}), and the anodic passive current density on steel surface (i_P), both of which may be affected by considerable uncertainty. As a slave variable, the nominal exchange current density for the cathodic reaction of steel (i_{0S}) was chosen coupled to the variations in i_P and β_{CS} so that the value of E_{SU} always remained fixed at the same value used for the baseline model computations. That way the calculations evaluated sensitivity to the polarizability of the steel without the added complication of changes in the unpolarized steel potential. The value of β_{CS} was varied from its central scenario conditions value of 138 mV downwards to 100 mV (an approximate low end of commonly reported values (Glass 2000, Sagüés 2003)), and in to opposite direction, but by the same amount, to 176 mV to span a plausible range of conditions. The parameter i_P was varied from its central scenario choice of 2.6 E-08 A/cm^2 to ½ and 2 times that value (1.3 E-08 and 5.2E-08 A/cm^2 respectively) to account for an appreciable uncertainty range. All calculations were performed with k_1=1kΩ and k_2 =50 cm, for 10 mo age of both types of anode. Only cases with zero current to the patch region were explored.

Table 8 – Effect of current demand by the patch zone

C Anode		**Base Cases (No current to patch)**	**Alternative (½ current to patch)**
Age	**C_P / V**	**X_T /cm**	**X_T /cm**
1 mo	0.1	33	26
	0.15	18	11
	0.2	8	1
4 mo	0.1	28	19
	0.15	14	5
	0.2	4	–
10 mo	0.1	25	14
	0.15	10	–
	0.2	–	–
13 mo	0.1	23	12
	0.15	8	–
	0.2	–	–

W Anode		**Base Cases (No current to patch)**	**Alternative (½ current to patch)**
Age	**C_P / V**	**X_T /cm**	**X_T /cm**
1 mo	0.1	29	22
	0.15	15	8
	0.2	5	–
4 mo	0.1	27	19
	0.15	13	5
	0.2	3	–
10 mo	0.1	21	10
	0.15	6	–
	0.2	–	–
13 mo	0.1	16	3
	0.15	1	–
	0.2	–	–

Figure 58 presents the results from the sensitivity analysis. Changes in β_{CS} in either direction from the central scenario resulted in moderate relative changes (by about a factor of 2 or less) in the value of the projected throwing distance for the 100 mV polarization criterion. The effect was comparably moderate for the 150 mV criterion when the excursion was toward greater values of β_{CS}, but if β_{CS} was reduced to 100 mV the resulting lower rebar polarizability became effectively prohibitive. For the most demanding criterion, 200 mV, excursion of β_{CS} toward 176mV increased x_T above the zero or nearly zero values at the central scenario, but not enough to exceed 10 cm. Analogous to the effect of variations in β_{CS}, changes in i_P had moderate impact on the 100 mV criterion throwing distance, and stronger relative effect for the cases of the more demanding criterion values. Overall, the sensitivity calculations showed that relatively wide changes in key steel polarization parameters induced no dramatic change in the highest projected values of x_T for the age condition examined. Large relative changes in x_T were projected for the more demanding polarization criteria cases, but the absolute values in those cases tended not to be large.

Projections over periods of time longer than 13 months are subject to considerable uncertainty as those would be beyond the testing period that yielded the PCF data used as input to these model calculations. However, the trends from Figure 23 and the performance derating information as function of total charge in Figures 17 and 18 suggest that both types of anodes may settle, under conditions resembling those in the test yard slabs, into quasi-steady state operating currents in the order of ~0.1 mA after another year or two of operation. The corresponding charge delivery would be~3.2 k Coul/year. Barring the effects of any other aging mechanism (such as dissipation of pellet activator compound into the surrounding concrete), and based on the arguments made in Section 3.4.1, anode operation at that rate might continue over about a decade of years range before approaching excessive consumption levels. Due to the relative shape of the anode and rebar polarization curves, under the conditions modeled here the anodes tend to operate near the limit current condition defined by the upward leg of the PCF. As shown in Figure 23, at age 13 months that current for both C and W anodes is in the order of ⅓ to ½ mA. As noted before, by 13 months age the projected throwing distance had begun to shorten considerably especially for the more demanding polarization criteria. The effect on x_T of further lowering the anode current by twofold or more toward ~0.1 mA may be inferred from the projected decrease of x_T as anode spacing increased in comparable proportions (effectively lowering the anode current available per unit of patch perimeter) and also from the results of halving the anode current shown in Table 8. Such comparison suggests that as anode currents decay into the order of 0.1 mA the throwing distance for satisfying the 100 mV polarization criterion would become two or more times smaller than those projected for 13 mo, yielding quite poor projected performance. By the same argument, the more demanding polarization criteria (150 mV, 200 mV) would result in even poorer or nil projected long performance.

C Anodes, 10 mo

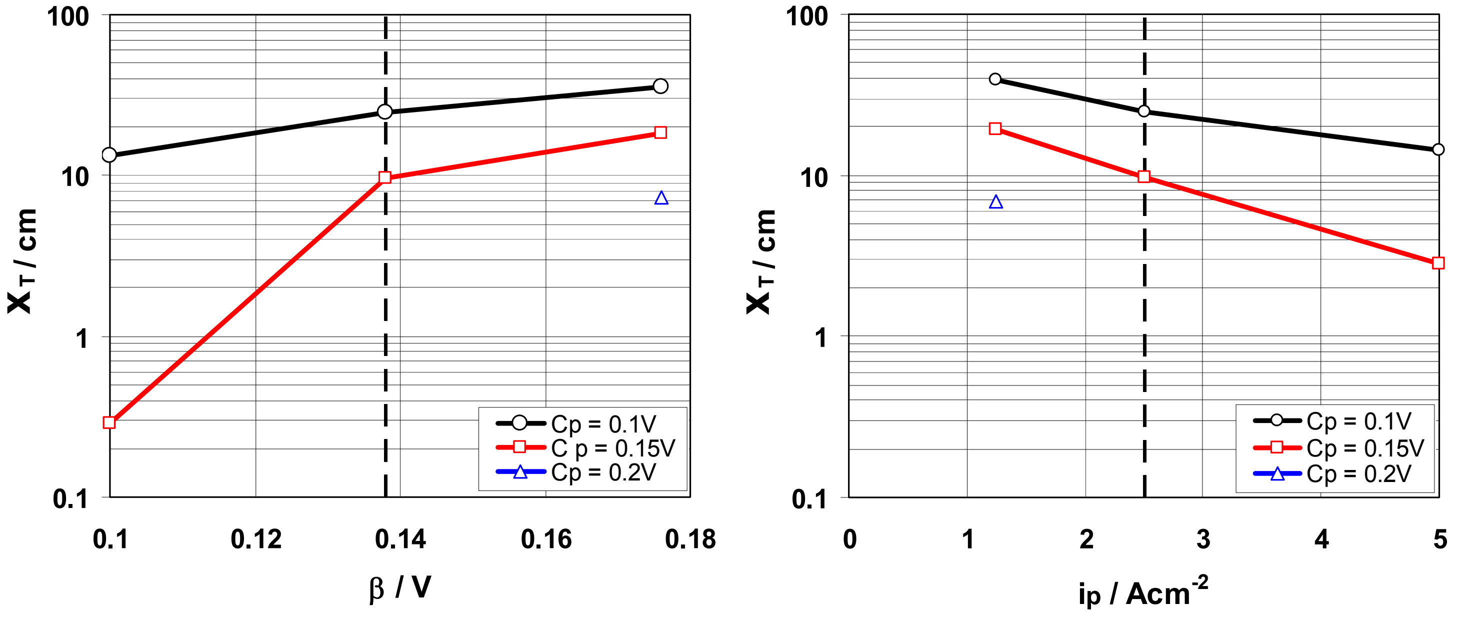

W Anodes, 10 mo

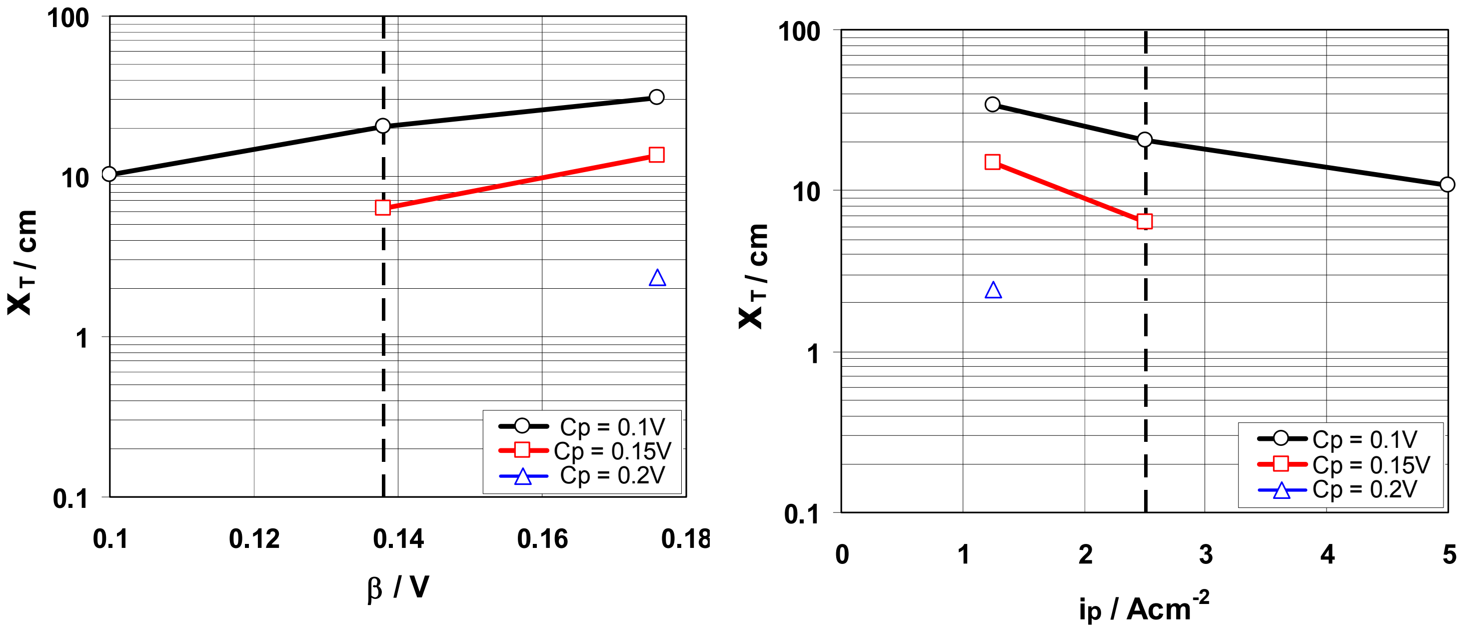

Figure 58 - Sensitivity analysis of model projections to the choice of β_{CS} and i_P , for 10 mo anode age. Dashed lines denote the central scenario. Absent symbol/line: polarization not achievable or x_T < 0.1 cm

In summary, the model projections together with the aging information detailed in Section 3 suggest that anode performance in the likely scenarios discussed above, as measured by the throwing distance, may seriously degrade after only a few years of operation even if a 100 mV corrosion prevention criterion were assumed.

It has been proposed in the technical literature that, even with small polarization levels, significant corrosion control benefits can accrue from sustaining cathodic current densities with low values ranging from 0.2 $\mu A/cm^2$ to as little as 0.02 $\mu A/cm^2$ on passive steel [Pedeferri 1996, Sergi 2008]. The lower end of that range may not be relevant to atmospherically exposed concrete, for which a low end of 0.05 $\mu A/cm^2$ has been cited instead [Pedeferri 1996]. Those low end values would correspond to polarization levels in the order of only 34 to 65 mV for 0.02 and 0.05 $\mu A/cm^2$ respectively (Figure 35), with consequently greater throwing distances than those obtained for the 100 mV cases. It is noted however that the 0.2 $\mu A/cm^2$ high end of the range does not improve prognosis relative to the situations addressed earlier, as it corresponds in the present model to a C_P value approaching 150 mV (Figure 35). That case has already been addressed above, and yielded generally poor performance projections.

There are indeed benefits from long term application of cathodic currents, in particular from an increase in pH near the surface of the rebar and also a decrease in chloride content if contamination already exists [Glass 1997, 2007]. Those effects are to be expected at substantial cathodic current densities. However, the extent of benefits at the very low polarization levels that correspond to the low end of the current density-based criteria awaits sufficient experimental demonstration. Should future research develop adequate supporting evidence, the less conservative criterion requirements may merit further consideration.

A contrary argument, for a more conservative corrosion prevention criterion, may be made based on the analysis by Presuel-Moreno [2005A] summarized in Figure 59. As indicated there, polarization to as much as 400 mV below the normal open circuit potential (which is some -0.1 V vs SCE, or ~-0.18 V CSE) of passive steel in atmospherically exposed concrete may be required for an order-of- magnitude increase in the chloride corrosion threshold. If that were the case, cathodic polarization in the order of 100 mV would only achieve a marginal threshold increase. In the light of such conservative scenario, the model projections would question the ability of point anodes of the size investigated here to provide a useful corrosion prevention effect. The precise dependence of corrosion threshold on potential of the passive steel is a critical issue in interpreting the results of the present investigation. However, as evidenced from the scatter of available data in Figure 59 there is much uncertainty as to the extent of that effect. The issue is much in need of resolution by development of reliable data in future investigations.

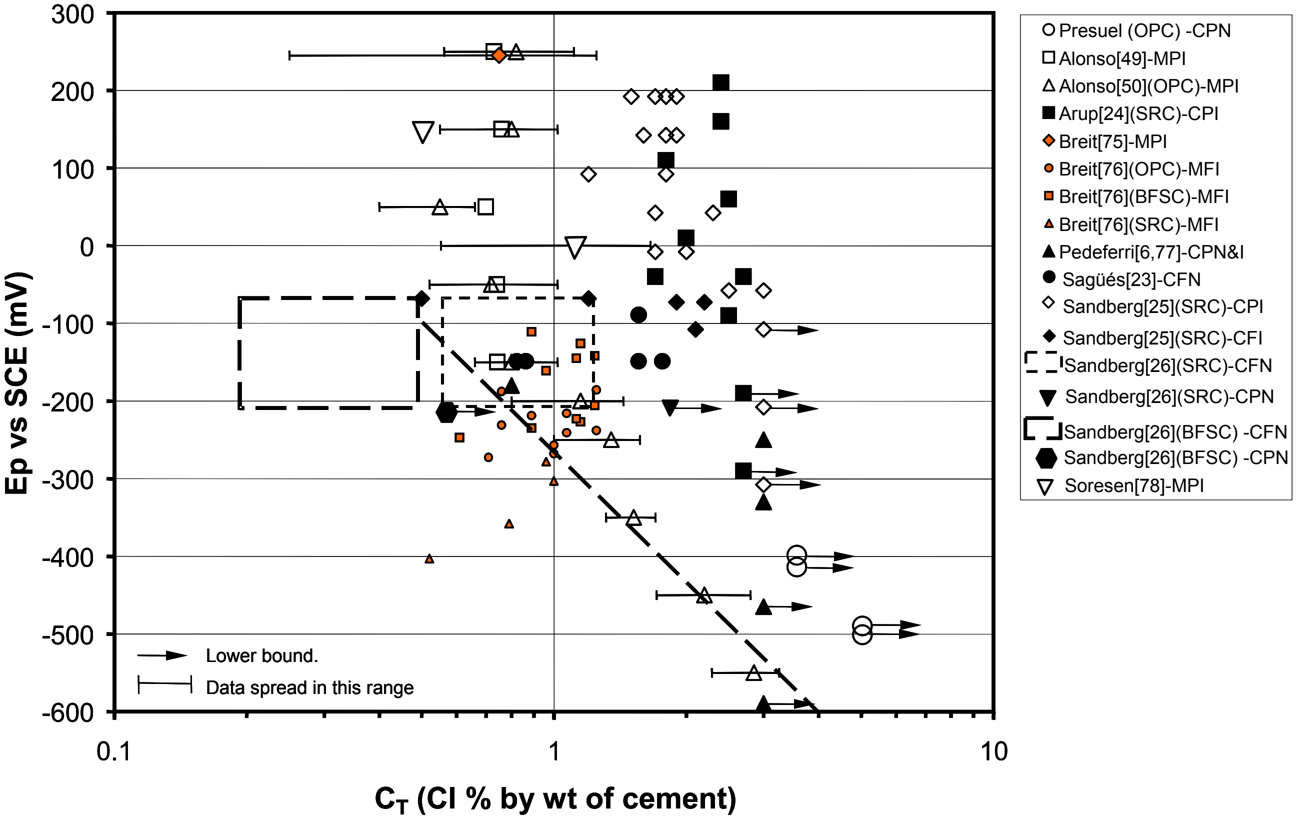

Figure 59 - Summary of information toward establishing a cathodic prevention polarization criterion. Each symbol represents an instance of documented corrosion threshold for passive steel held in concrete at the potential indicated. Arrows indicate that the chloride threshold was equal or higher than the corresponding value. The dashed line yields the proposed cathodic prevention potential for a given level of protection. Potentials are in the saturated calomel electrode scale; potentials vs CSE are 77 mV lower than the value indicated. See Presuel-Moreno [2005A] for the references cited in the figure.

5 CONCLUSIONS

1. A laboratory approach to evaluate candidate anodes for patch repair applications was developed, and its feasibility demonstrated by applying the experimental and analysis methods to actual commercially produced anode samples. Anode polarization was formulated in terms of a Potential-Current Function (PCF) and its evolution with anode service aging. Two types of commercially available point anodes were evaluated.

2. Galvanostatic tests under controlled humidity and test yard slabs with reinforced concrete for both types of anodes revealed PCFs with comparable features. The PCFs showed relatively little anodic polarization from an open circuit potential at low current levels, followed by an abrupt increase in potential as the current approached an apparent terminal value. The curves resemble the behavior expected from a system that is approaching a diffusion-controlled limiting current density, or alternatively having a sizable ohmic resistance polarization component.

3. For a given test condition and anode service history, the PCFs showed significant variability among anodes of the same type within a given set of anodes delivered by the suppliers. For one of the anode types, the first set tested performed notable worse as a group than the second set (delivered 3 years later) suggesting an initial manufacturing problem.

4. Aging of the anodes by delivering current in service was manifested by a continually decreasing current output in the test yard slabs, and by increasingly more positive potentials in the galvanostatic tests. As implied by slow cyclic polarization test results, those changes reflected an evolution of the PCF generally toward more positive open circuit anode potentials and, more importantly, to the onset of elevated polarized potentials at increasingly lower current levels.

5. Coupling of the anodes to rebar at the time of casting in concrete containing 1.5% Cl^- by weight of cement was not sufficient to prevent corrosion initiation of the steel rebars in that zone. Testing for about 480 days in reinforced concrete slabs containing those corroding rebars in addition to passive rebars showed that the point anodes induced only modest to negligible polarization of the steel assembly. That effect was ascribed to the low polarizability of the actively corroding rebars.

6. Upon disconnection of the actively corroding rebars while evaluating the first set of anodes, one of the anode types produced cathodic polarization levels exceeding 100 mV in the passive rebars that were in close proximity to the anode. The other anode type (suspected of deficiency in the first set evaluated) had already exhausted much of its polarizing ability in the preceding interval and produced only negligible effects on the surrounding passive steel.

7. A continuation test with a second set of anodes of each type, coupled with only passive rebar, showed substantial polarization levels (100 mV to 200 mV) of rebar in the proximity of either type of anode. Current delivery decreased with service time but appreciable polarization levels were still achieved in nearby rebars after ~500 days of operation.

8. Most anode units of both types in the first set tested showed on average significant current delivery decrease after delivering a cumulative anodic charge that was only about 10% to 20% of the maximum theoretical amount for complete consumption. Anodes in the second set tested showed less aging effects over the duration of the test, which was conducted until reaching up to about 25% of the theoretical limit. Estimates based on the extent of derating observed in the test interval suggest that in the absence of other degradation effects, anodes of this type may be able to function up to about ¼ to ⅓ of the theoretical consumption limit.

9. Quantitative polarization functions of the steel rebar were found to agree with the results of previous investigations. Those functions were used as input for modeling projections of anode performance in a generic reinforced concrete system.

10. Results of field evaluations of anode performance were evaluated and found to be generally in keeping with those from laboratory and yard tests, with instances of increased current delivery consistent with greater moisture and a chloride rich environment. Decreased performance with aging was noted in the field for both makes of anode.

11. Modeling of a generic patch configuration with a one-dimensional approximation was used to calculate the throwing distance that could be achieved by a given number of anodes per unit perimeter of the patch, concrete thickness, concrete resistivity, amount of steel and amount of polarization needed for cathodic prevention. The model projections together with the aging information determined experimentally suggest that throwing distance in likely application scenarios may seriously degrade within a few years of operation, even if a relatively optimistic 100 mV corrosion prevention criterion were assumed.

12. Less conservative, current density-based corrosion prevention criteria have been proposed in the literature that would result in improved throwing distance projections under some conditions yet to be substantiated. However, other investigations suggest that a significantly more conservative corrosion prevention criterion than 100 mV polarization may be necessary instead. The latter case would question the ability of the point anodes to provide a useful corrosion prevention effect for reinforcement around the patch.

6 REFERENCES

Alonso, C., Castellote, M. and Andrade, C., “Dependence of Chloride Threshold with the Electrical Potential of Reinforcements,” in 2nd Int. RILEM Workshop on Testing and Modeling the Chloride Ingress into Concrete, PRO 19 (Cachan, France: RILEM Publications, (2000), p. 415.

Alonso, C., Castellote, M. and Andrade, C. "Chloride threshold dependence of pitting potential of reinforcements". Electrochim. Acta 47, 21(2002): p. 3,469.

Bennett, J. and Talbot, C., “Extending the Life of Concrete Patch Repair with Chemically Enhanced Zinc Anodes”, Paper No. 02255, Corrosion/2002, NACE International, Houston, (2002).

Bennett, J. and McCord, W., “Performance of Zinc Anodes Used to Extend the Life of Concrete Patch Repairs”, Paper No. 06331, Corrosion/2006, NACE International, Houston, (2006).

Bentur, A., Diamond, S. and Berke, N.S., “Steel Corrosion in Concrete: Fundamental and Civil Engineering Practice” (New York, NY: E&FN SPON, 1997), p. 30.

Berke, N.S. and Hicks, M.C., “ Estimating the Life Cycle of Reinforced Concrete Decks and Marine Piles using Laboratory Diffusion and Corrosion Data”, p. 207 in Corrosion Forms and Control for Infrastructure, ASTM STP 1137, Victor Chaker, Ed., ASTM, Philadelphia, (1992).

Bertolini, L., Esener, B, Pedeferri, P. and Polder, R., “Corrosion of steel in concrete: prevention, diagnosis, and repair”, Wiley-VCH, (2004).

Breit, W., “Critical chloride content – Investigation of steel in alkaline chloride solutions” Mater. Corros. 49 (1998): p. 539.

Broomfield, J.P., “Corrosion of Steel in Concrete: Understanding, Investigation and Repair”, Taylor & Francis, (1997).

Castro, P., Sagüés, A.A., Moreno, E.I., Maldonado, L., and Genescá, J. “Characterization of Activated Titanium Solid Reference Electrodes for Corrosion Testing of Steel in Concrete”, Corrosion 52, 8 (1996): p. 609.

Dugarte, M. and Sagüés, A.A., to be published (2009).

Fontana, M.G. (1986), “Corrosion Engineering”, 3rd edition, McGraw-Hill Inc.

FunahashI M. ; Bushman J. B. , "Technical review of 100 mV polarization shift criterion for reinforcing steel in concrete " Corrosion, (1991), vol. 47, pp. 376-386

Frankel, G.S., "Pitting corrosion of metals : a review of the critical factors", J. Electrochem. Soc. Vol. 145, p. 2186-2198 (1998).

Glass, G. and Chadwick, J., “An Investigation into the Mechanisms of Protection Afforded by a Cathodic Current and the Implication for Advances in The Field of Cathodic Protection”, Corrosion Science, Vol. 36, No. 12, pp. 2193-2209, (1994)

Glass G. K. and Buenfeld N. R., “Theoretical basis for designing reinforced concrete cathodic protection systems”, British Corrosion Journal vol. 32, pp. 179-184 (1997),

Glass, G.K., Hassanein, A. M. and Buenfeld, N. R., “CP Criteria for Reinforced Concrete in Marine Exposure Zones”, Journal of Mat. in Civil Eng., Vol. 12, No. 2, May (2000), pp. 164-171

Glass, G. K., Reddy, B. and Clark, L. A.,"Making concrete immune to chloride induced corrosion", Proceedings of the Institution of Civil Engineers, Construction Materials, 160 (4) (2007) 155-164.

Glass, G., Roberts, A., “Hybrid corrosion protection of chloride-contaminated concrete”, Const. Mat. 161, Issue CM4, pp. 163 -172, (2008).

Gouda, V. K. and Halaka, W.Y., “Corrosion and Corrosion Inhibition of Reinforcing Steel: II. Embedded in Concrete” *Brit. Corros. J.* **5, 9** (1970), p. 198.

Hausmann, D. A., “Steel Corrosion in Concrete. How Does it Occur?” Mater. Prot. 6, 11 (1967): p. 19.

Hurley, M.F. and Scully, J.R., "Threshold chloride concentrations of selected corrosion-resistant rebar materials compared to carbon steel", Corrosion Vol. 62, p. 892 (2006).

Izquierdo, D., Alonso, C., Andrade, C. and Castellote, M., “Potentiostatic determination of chloride threshold values for rebar depassivation: Experimental and statistical study”, Electrochimica Acta, Volume 49, 2004, Pages 2731-2739

Jones, D. A. (1996), “Principles and Prevention of Corrosion”, 2nd edition, Prentice- Hall, Inc.

Kaesche, H. "Corrosion of Metals", Springer, Berlin (2003).

Kranc, S. and Sagüés, A. “Detailed Modeling of Corrosion Macrocells on Steel Reinforcing in Concrete”, Corrosion Science, Vol. 43, p. 1355, (2001)

Kranc, S.C and Sagüés, A.A., "Computation of Reinforcing Steel Corrosion Distribution in Concrete Marine Bridge Substructures", Corrosion, Vol. 50, p.50, (1994).

Landolt, D. "Corrosion and Surface Chemistry of Metals", CRC Press (2007)

Li, L. and. Sagüés, A.A., "Chloride Corrosion Threshold of Reinforcing Steel in Alkaline Solutions - Open-circuit Immersion Tests", Corrosion, Vol. 57, p.19, (2001).

Li, L. and Sagüés, A.A., "Chloride Corrosion Threshold of Reinforcing Steel in Alkaline Solutions – Cyclic Polarization Behavior" Corrosion 58, 4 (2002): p. 305.

Mac-Berthouex, P., Brown, L.C., “Statistics for environmental engineers”, CRC Press, (2002)

Macdonald, D.D., "The point defect model for the passive state", J. Electrochem. Soc. Vol. 139, p3434 (1992)

Myrdal, R., "Phenomena that Disturb the Measurement of Potentials in Concrete", Paper No. 0339, Corrosion/1996, NACE International, Houston, 1996

Page, C.L. and Sergi, G., “Developments in Cathodic Protection Applied to Reinforced Concrete”, Journal of Mat. in Civil Eng., Vol. 12, (2000), pp. 8-15

Pedeferri, P., “Cathodic protection and Cathodic Prevention” Constr. Build. Mater. Vol. 10, No. 5 (1996), p. 391.

Pour-Ghaz, M., Isgor, O.B, Ghods, P., “The effect of temperature on the corrosion of steel in concrete. Part 1: Simulated polarization resistance tests and model development”, Corrosion Science 51, pp.415–425, (2009).

Presuel-Moreno, F.J., Sagüés, A.A. and Kranc, S.C., "Steel Activation in Concrete Following Interruption of Long Term Cathodic Polarization", Corrosion 61, p.428-436. (2005A)

Presuel-Moreno, F.J, Kranc, S.C., and Sagüés, A. A., “Cathodic Prevention Distribution in Partially Submerged Reinforced Concrete”, Corrosion, Vol. 61 p.548-558 (2005B).

Raupach, M., “Chloride-induced macrocell corrosion of steel in concrete-theoretical background and practical consequences”, Cons. and Bldg. Mat., Vol. 10, Issue 5, Durability of Reinforced Concrete Structures, July (1996), PP 329-338.

Sagüés, A.,"Electrochemical Impedance of Corrosion Macrocells on Reinforcing Steel in Concrete", Paper No. 132, pp. 28 , Corrosion/90, National Assoc. of Corr. Engs., Houston, (1990).

Sagüés, A.A. and S.C. Kranc, S.C."Model for a Quantitative Corrosion Damage Function for Reinforced Concrete Marine Substructure", Rehabilitation of Corrosion Damaged Infrastructure, p.268, Proceedings, Symposium 3, 3rd. NACE Latin-American Region Corrosion Congress, NACE International, Houston, (1998).

Sagüés, A.A., Pech-Canul, M.A., and Al-Mansur, A.K.M., "Corrosion macrocell behavior of reinforcing steel in partially submerged concrete columns", Corr. Sci. Vol. 45 p.25-30 (2003).

Sagüés, A.A, Balakrishna, V. and Powers, R.G, "An approach for the evaluation of performance of point anodes for corrosion prevention of reinforcing steel in concrete repairs", Paper 1-083, International Federation for Structural Concrete (FIB) symposium: "Structural concrete and time:, September 28-30, 2005, La Plata, Argentina.

Sagüés, A., Kranc, S. and Lau, K. "Service Life Forecasting for Reinforced Concrete Incorporating Potential-Dependent Chloride Threhslold", Paper No. 09213, pp.22, Corrosion /09, NACE International, Houston, (2009A)

Sagüés, A.A., Kranc S.C. and Lau, K., "Modeling of Corrosion of Steel in Concrete with Potential-Dependent Chloride Threshold", NACE International, Houston, (2009B)

Sergi, G. and Page, C., "Sacrificial anodes for cathodic prevention of reinforcing steel around patch repairs applied to chloride-contaminated concrete". In: Mietz, J. et al (eds.), Corrosion of Reinforcement in Concrete, IOM Communications, London, European Federation of Corrosion Publications, No. 31, p.93-100, 2001.

Sergi, G., Simpson, D. and Potter, J. "Long-term performance and versatility of zinc sacrificial anodes for control of reinforcement corrosion", Proceedings of Eurocorr 2008, The European Corrosion Congress "Managing Corrosion for Sustainability", 7-11 September 2008, Edinburgh .

Szklarska-Smialowska, Z., "The Pitting Corrosion of Metals", Houston, TX: NACE International, (1986), p. 202-212.

Torres-Acosta, A. and Sagüés, A. "Concrete Cracking by Localized Steel Corrosion - Geometric Effects", ACI Materials Journal, Vol. 101, p.501, (2004)

Virmani, Y.P, Clear, K. and Pasko, T., "Time-to-Corrosion of Reinforcing Steel in Concrete Slabs," FHWA-RD-76-70, Federal Highway Administration, Washington, DC (1983).

Whitmore, D. and Abbott, S., "Using Humectants to Enhance the Performance of Embedded Galvanic Anodes", Paper No. 03301, Corrosion/2003, NACE International, Houston, (2003).